NASA Technical Paper 2282

February 1984

Aerodynamic Design for Improved Maneuverability by Use of Three-Dimensional Transonic Theory

Michael J. Mann,
Richard L. Campbell,
and James C. Ferris

NASA

NASA
Technical
Paper
2282

1984

Aerodynamic Design for Improved Maneuverability by Use of Three-Dimensional Transonic Theory

Michael J. Mann,
Richard L. Campbell,
and James C. Ferris

Langley Research Center
Hampton, Virginia

National Aeronautics
and Space Administration

**Scientific and Technical
Information Branch**

SUMMARY

This study has examined improvements in transonic maneuver performance by the use of three-dimensional transonic theory and a transonic design procedure. The FLO-27 code of Jameson and Caughey was used to design a new wing for a fighter configuration with lower drag at transonic maneuver conditions. The wing airfoil sections were altered to reduce the upper-surface shock strength by means of a design procedure which is based on the iterative application of the FLO-27 code.

The planform of the fighter configuration was fixed and had a leading-edge sweep of 45° and an aspect ratio of 3.28. Wind-tunnel tests were conducted on this configuration at Mach numbers from 0.60 to 0.95 and angles of attack from -2° to 17°. The transonic maneuver performance of this configuration was evaluated by comparison with a wing designed by empirical methods and a wing designed primarily by two-dimensional transonic theory. The configuration designed by the use of FLO-27 had the same or lower drag than the empirical wing and, for some conditions, lower drag than the two-dimensional design. For some maneuver conditions, the drag of the two-dimensional design was somewhat lower.

The FLO-27 code generally gave a reasonable estimate of the experimental wing pressure distributions at transonic maneuver conditions in regions of the wings where the flow was attached; however, in some cases, certain features of the flow were not accurately predicted.

INTRODUCTION

Current research on fighter aircraft includes extensive efforts to produce high levels of maneuverability at subsonic and transonic speeds. Studies at the NASA Langley Research Center related to improved maneuver performance have been directed toward two general types of wings. One type includes the slender wings which provide good supersonic performance and which utilize the high levels of vortex lift available to provide subsonic and transonic maneuver capability. Research on the maneuver performance of slender-wing aircraft has resulted in the development of design concepts which reduce drag by the effective recovery of the leading-edge thrust (ref. 1). The other general type of wing under study is the moderately swept wing of higher aspect ratio, which is based on a compromise between optimum subsonic and supersonic performance. The transonic maneuver performance of these wings is strongly influenced by shock-induced boundary-layer separation. This separation causes a rapid drag rise, buffeting, and a general degradation of the aerodynamic characteristics. Therefore, these wings must be designed to develop large regions of supercritical flow with minimum shock-induced flow separation.

The purpose of the present investigation has been to study improvements in the transonic maneuver performance of the second type of wing by the use of three-dimensional transonic theory and a transonic design procedure. A comprehensive discussion of the various transonic methods applicable to the design and analysis of this type of wing is given in references 2 and 3. One design technique involves the combined use of a transonic flow analysis code and a numerical optimization procedure (ref. 2). Another approach is based on an inverse solution for the wing shape which will produce a specified pressure distribution (refs. 4, 5, and 6). The current

study utilizes the FLO-27 wing-fuselage computer code of Jameson and Caughey (ref. 7) to design a new wing with lower drag at transonic maneuver conditions. The wing contour was altered to reduce the upper-surface shock strength by means of a design procedure which is based on the iterative application of the FLO-27 code.

Two supercritical maneuvering wings have been designed by the use of FLO-27 and the design method of reference 8. These wings were tested, and their experimental lift and drag characteristics were compared with the experimental characteristics of two other supercritical maneuver wing designs. One of the comparison wings was developed empirically, and the other comparison wing was designed primarily by the use of two-dimensional transonic theory (ref. 9) and simple sweep theory. To illustrate the application of the three-dimensional transonic theory to improved maneuver performance, pressure distributions at supercritical conditions and high lift have been calculated for all four wings. The calculated pressure gradients and shock waves are then related to the experimental lift and drag performance of each wing at maneuver conditions. Experimental wing pressure distributions are also utilized to help explain the relative performance of the wings.

The current study has focused solely on the warped-wing geometry required at maneuver conditions. It is recognized, of course, that some form of variable geometry would be required to provide the desired maneuver and cruise wing shapes. This type of variable geometry has not been addressed in this study.

The tests for the current study were conducted in the Langley 16-Foot Transonic Tunnel. Results are presented for Mach numbers ranging from 0.60 to 0.95 and for angles of attack from -2° to 17°.

SYMBOLS

All forces are referred to the wind-axis system. Force coefficients for each wing are based on the trapezoidal geometry of each wing extended to the model centerline. (See table I.) Dimensions are given in the International System of Units (SI) with the U.S. Customary Units in parentheses. The measurements and calculations were made in U.S. Customary Units.

b wing span, cm (in.)

C_D drag coefficient, $\frac{\text{Drag}}{qS}$

$C_{D,i}$ internal drag coefficient

$C_{D,th}$ theoretical inviscid drag coefficient of the exposed wing in the presence of an infinite cylinder, calculated by FLO-27 code, $\frac{\text{Theoretical inviscid drag}}{qS}$

C_L total lift coefficient, $\frac{\text{Lift}}{qS}$

$C_{L,th}$ theoretical lift coefficient from the FLO-27 code for exposed wing in the presence of an infinite cylinder, unless specified as an isolated-wing solution, $\frac{\text{Theoretical lift}}{qS}$

C_p pressure coefficient, $\frac{p_\ell - p}{q}$

c local wing chord parallel to plane of symmetry, m (ft)

c_l section lift coefficient of wing, $\frac{\text{Local chord load}}{qc}$

c_r wing root chord of trapezoidal wing, cm (in.)

c_t wing tip chord of trapezoidal wing, cm (in.)

M free-stream Mach number

p free-stream static pressure, N/m^2 (lbf/ft^2)

p_ℓ local static pressure, N/m^2 (lbf/ft^2)

q free-stream dynamic pressure, N/m^2 (lbf/ft^2)

S wing reference area of trapezoidal wing, see table I, m^2 (ft^2)

t/c ratio of maximum section thickness at a given spanwise station to the wing chord parallel to plane of symmetry at that station

x local chordwise distance from wing leading edge, parallel to plane of symmetry, m (ft)

y spanwise distance from plane of symmetry, cm (in.)

α angle of attack referenced to horizontal reference line in figure 1(a), deg

η semispan location, $\frac{y}{b/2}$

Λ sweep angle of wing leading edge, deg

APPARATUS AND TESTS

Model Description

Drawings of the wind-tunnel model are shown in figure 1, and photographs of one configuration are shown in figure 2. The model represents a supercritical maneuvering fighter (SMF). It has been tested with four wing geometries. One wing (W18) has an aspect ratio of 3.36 and a leading-edge sweep of 40°. The other three wings (SMF-1 and configurations A and B of SMF-2) have an aspect ratio of 3.28 and a leading-edge sweep of 45°. Figures 1(b) to 1(d) show the airfoil sections for each of the four wings. The thickness and twist distributions are shown in figures 1(e) and 1(f). The twist distributions shown in figure 1(f) are referenced to the horizontal reference line in figure 1(a). The same fuselage was used for all tests. Some typical cross sections for the fuselage are shown in figure 1(g). This fuselage had been used in prior experimental studies, and no attempt was made in the current study to alter the fuselage area distribution in accordance with the transonic area rule. Tables I and II provide general geometric characteristics of the wings, fuselage, and vertical tail.

Model Design Considerations

Experimental and theoretical results are presented for two supercritical maneuver wings (W18 and SMF-1) developed in prior studies in order to provide a basis for evaluation of the maneuver performance of the wings designed in the current study. Both W18 and SMF-1 were developed during a cooperative study on advanced fighter concepts between NASA Langley Research Center and General Dynamics, Fort Worth (refs. 10 and 11). This cooperative study was undertaken to improve the aerodynamic maneuver technology available in the F-16 lightweight fighter. Extensive wind-tunnel testing was conducted to study the effects of supercritical aerodynamics, variable geometry, and wing planform on transonic maneuver performance. To provide good supersonic performance, W18 was developed from a thin wing with zero camber. The shape of leading- and trailing-edge flap segments was then experimentally contoured to provide good transonic maneuver performance. (See fig. 1(b).)

SMF-1 represents an effort to improve the transonic manuever performance of W18 by the use of the transonic theoretical methods which were available at the time SMF-1 was designed. The wing airfoils for SMF-1 were designed primarily by the iterative use of the two-dimensional analysis theory of Bauer, Garabedian, Korn, and Jameson (ref. 9) and simple sweep theory. Some adjustments for three-dimensional effects in the root and tip regions were made on the basis of computations with the FLO-22 isolated-wing analysis code of Jameson and Caughey (refs. 12 and 13). In contrast to the approach for W18, the entire SMF-1 wing, rather than just the leading- and trailing-edge regions, was shaped for maneuver conditions. The intention was to use leading- and trailing-edge variable geometry to remove camber for supersonic dash conditions. The design point for SMF-1 was $M = 0.90$ and $C_L = 0.9$. Note that SMF-1 has more twist and a somewhat different planform than W18 (figs. 1(f) and 1(a)). The thickness ratios are compared in figure 1(e).

The design, test, and analysis of the W18 and SMF-1 wings have been reported in references 2, 8, 10, and 11. Subsequent to the development of these wings, it was recognized that further improvements in the transonic maneuver performance would most likely be achieved through the use of design procedures based on three-dimensional transonic theory. In the current study, the FLO-27 wing-fuselage computer code of Jameson and Caughey (ref. 7) and the design procedure of reference 8 have been used to design configurations A and B of the SMF-2 wing (fig. 1(d)).[1] The planform for SMF-2 was selected to be the same as for SMF-1.

Configuration A of SMF-2 was designed to have a weak aft shock wave at a Mach number of 0.90 and a lift coefficient of 0.9 (ref. 8). Although the performance at this design condition was good, theoretical calculations indicated the development of strong shock waves for a Mach number of 0.85 and a lift coefficient of 0.9. Experimental results at a Mach number of 0.85 likewise showed that configuration A had high maneuver drag relative to SMF-1. Therefore, a second supercritical wing was developed. The objectives for configuration B were to reduce the shock-induced flow separation and the attendant maneuver drag penalties which occurred for configuration A at a Mach number of 0.85 and to maintain the performance of configuration A at the higher transonic Mach numbers (ref. 14). The wind-tunnel model for configuration B was constructed by the addition of a filler material to the upper surface of

[1] Previous publications of experimental results for SMF-2 have referred to configurations A and B as configurations 1 and 2, respectively.

the configuration A wing panels. This construction technique limited the upper-surface contours which could be used and also resulted in a substantially thicker wing (figs. 1(d) and 1(e)).

Configurations A and B have, of course, the same twist distribution (fig. 1(f)). This twist distribution was designed to straighten the isobars on configuration A at the design condition and to reduce the section lift coefficients at the wing tip (ref. 8).

Tests and Corrections

Configurations A and B of SMF-2 were tested in the Langley 16-Foot Transonic Tunnel (16-Ft TT). A complete description of these tests is given in reference 14.

The W18 and SMF-1 wings were tested in the Langley 8-Foot Transonic Pressure Tunnel (8-Ft TPT). Although the experimental results for these wings have been reported in references 10 and 11, certain items of the experimental apparatus and test procedure have not been published. Therefore, for the sake of completeness, the tests of W18 and SMF-1 are described in the appendix.

Since none of the current configurations have been tested in both the 8-Ft TPT and the 16-Ft TT, it is not possible to make a direct comparison between results from these tunnels for any of these configurations. However, an indirect comparison is possible by the use of tests made on several versions of SMF-2 in the Langley 7- by 10-Foot High-Speed Tunnel (7- by 10-Ft HST). These tests were run at Mach numbers of 0.60 and 0.85 (ref. 15). Figure 3 shows some representative comparisons between results from the 8-Ft TPT and the 7- by 10-Ft HST and between results from the 16-Ft TT and the 7- by 10-Ft HST. The model used for the comparison shown in figure 3(a) is an early version of SMF-2 which has somewhat different airfoils than either of the current configurations. Because drag levels measured in the 8-Ft TPT and in the 16-Ft TT both correlate well with drag levels measured in the 7- by 10-Ft HST (see fig. 3), drag levels measured in the 8-Ft TPT and in the 16-Ft TT should generally be in good agreement with each other.

COMPUTATIONAL PROCEDURES

The FLO-27 wing-fuselage computer code of Jameson and Caughey (ref. 7) has been used for the transonic flow calculations of this study. The FLO-27 code is a three-dimensional transonic computational method which computes the transonic flow over a wing in the presence of an infinitely long circular cylinder. The full potential flow equation is solved by means of a fully conservative finite volume method. The FLO-27 code and the design procedure of reference 8 have been used for the design of configurations A and B of SMF-2.

The final solutions of FLO-27 were computed on a fine grid with 120 chordwise, 12 normal, and 24 spanwise mesh cells. Convergence was assumed only after changes in the pressure distribution and the shock location were reduced to insignificant levels. A converged solution generally corresponded to a maximum residual on the order of 10^{-6}. Angles of attack were selected to give theoretical wing lift coefficients which are representative of transonic maneuver conditions for the type of wing under study. The resulting values of $C_{L,th}$ were generally about 0.8. The $C_{L,th}$ computed for a wing-cylinder solution is the lift coefficient for the exposed wing and does not include any fuselage lift. Experience with the current configurations

has indicated that at maneuver conditions the fuselage contribution to lift coefficient is usually on the order of 0.1. Therefore, the total lift coefficient for the wing plus the fuselage (C_L) would be about 0.9.

Early design efforts and experimental results for SMF-2 showed that the fuselage effects must be included in the theory to obtain an accurate prediction of the presence and strength of shock waves. Wing pressure distributions calculated by FLO-27 with and without the effect of the cylindrical fuselage are compared with experimental results in figure 4. The wing is an early version of SMF-2 (same as fig. 3(a)), and the comparisons are for maneuver conditions at a Mach number of 0.90. The theoretical angles of attack were adjusted to approximately match the section lift coefficients. The calculated wing lift coefficient is lower for the wing-cylinder than for the isolated wing because the exposed wing area of the wing-cylinder is smaller. The experimental angle of attack was adjusted to provide an increment of about 0.1 in the lift coefficient above $C_{L,th}$ for the wing-cylinder solution. The resulting experimental section lift coefficients were in good agreement with the theoretical values. When the effect of the cylindrical fuselage is included in the calculations, the smooth isentropic flow and weak trailing-edge shock on the inboard region of the wing change into a flow with a double-shock pattern. The experimental pressure distributions confirm the existence of this double-shock pattern. Unpublished experimental results indicate that the shock waves caused extensive flow separation and resulted in high drag at transonic maneuver conditions. These results clearly define the need to include the fuselage in the theoretical calculations for this configuration. Fuselage effects have been included in the calculations for the design of configurations A and B of SMF-2 and for the analysis of all four wings examined in this study. The results of figure 4 also illustrate that a two-dimensional design method is not adequate for the present study, since, aside from other approximations, fuselage effects are not accounted for.

The radius of the infinite-cylindrical fuselage was chosen to be 4.3 cm (1.7 in.). This is the radius at the maximum cross-sectional area of the equivalent axisymmetric fuselage. The equivalent axisymmetric fuselage was obtained by removing the effective duct area of the flow-through nacelle from the cross-sectional area distribution of the actual fuselage. The effective duct area was taken to be the product of the duct inlet area and the measured mass-flow ratio for a Mach number of 0.90. No attempt was made to account for the effect of the finite length of the fuselage on the flow-field Mach number distribution (ref. 16).

Each of the wing geometries was modified to account for the effect of the boundary layer by the addition of a boundary-layer displacement thickness. The boundary layers were computed for one transonic maneuver condition and held fixed for other Mach numbers and lift coefficients (ref. 17). The boundary layers for W18 and configurations A and B of SMF-2 were computed in streamwise strips by the use of the two-dimensional method of Nash and Macdonald (ref. 18). FLO-27 was used to obtain the outer potential flow solution for the Nash-Macdonald method. The upper-surface displacement thickness was extrapolated downstream of the shock wave on the basis of an approximation obtained by use of three-dimensional boundary-layer theory. This was necessary because the calculated shock strength and adverse pressure gradients at maneuver conditions caused the boundary layer to separate. This extrapolation also removed a sudden increase in displacement thickness at the shock location, which would be representative of only the particular flow condition for which the calculation was made. The boundary layer for SMF-1 was computed by the use of a two-dimensional pressure distribution as described in reference 10. The boundary-layer calculations of the present study are, of course, only crude estimates of the effects of viscosity.

PRESENTATION OF RESULTS

The theoretical and experimental results of this study are presented in the following figures:

	Figure
Correlation of theoretical and experimental wing pressure distributions for SMF-1 and configurations A and B of SMF-2	5
Comparison of theoretical wing pressure distributions for configurations A and B of SMF-2	6
Comparison of theoretical wing pressure distributions for W18, SMF-1, and configuration B of SMF-2	7
Effect of SMF-1 twist distribution on theoretical wing pressure distribution of W18. M = 0.90	8
Experimental wing pressure distributions on SMF-1 in regions of breaks in the drag polars	9
Experimental wing pressure distributions on configuration B of SMF-2 in regions of breaks in the SMF-1 drag polars	10
Comparison of experimental wing pressure distributions for configurations A and B of SMF-2	11
Comparison of experimental wing pressure distributions for SMF-1 and configuration B of SMF-2	12
Effect of supercritical wing geometry on experimental lift and drag characteristics	13
Effect of supercritical wing geometry on experimental drag variation with Mach number at fixed C_L	14
Experimental lift characteristics of SMF-1 and configuration B of SMF-2	15

RESULTS AND DISCUSSION

The discussion begins with a comparison of the theoretical and experimental wing pressure distributions for SMF-1 and configurations A and B of SMF-2. This comparison is used to establish the capability of FLO-27 to accurately predict wing pressure distributions at transonic maneuver conditions. Next, the performance of configurations A and B of SMF-2 is examined. As mentioned previously, the results for W18 and SMF-1 are used as a basis for evaluation of the maneuver performance of SMF-2. Theoretical wing pressure distributions at supercritical conditions and high lift have been calculated for all four wings. These theoretical pressure distributions and the experimental pressure distributions are related to the experimental performance of each wing at subsonic and transonic maneuver conditions.

Comparison of Theoretical and Experimental Wing Pressure Distributions on SMF-1 and SMF-2

Figure 5 presents a comparison of theoretical and experimental wing pressure distributions for SMF-1 and configurations A and B of SMF-2. The FLO-27 code has been used to calculate the pressure distributions for several transonic high-lift conditions. The comparisons are for Mach numbers of 0.85, 0.90, and 0.95 and experimental lift coefficients between 0.742 and 0.964. Experimental lift coefficients were selected which were approximately 0.1 greater than the theoretical lift coefficient ($C_{L,th}$) to account for lift on the fuselage which is not calculated by FLO-27.

FLO-27 gives a good estimate of the experimental pressure distributions on SMF-1 in the region of the wing where the flow is attached. Significant discrepancies occur at $\eta = 0.80$ for Mach numbers of 0.85 and 0.90, where the flow is separated as indicated by the loss of flow compression near the trailing edge and the forward movement of the shock wave (fig. 5(a)). The correlations at $\eta = 0.31$ and 0.46 for a Mach number of 0.85 illustrate the tendency of the conservative FLO-27 code to predict too great a shock strength (ref. 19).

The tip regions of configurations A and B of SMF-2 also show large discrepancies between the theoretical and experimental pressure distributions at a Mach number of 0.85 (figs. 5(b) and 5(c)). The flow at the wing tips is highly separated. (This separation is evident in photographs of oil-flow patterns and minituft patterns in ref. 15.) The flow at the wing tip of configuration B for a Mach number of 0.90 also appears to be mostly separated. Regions of these wings where the flow is largely attached show only a very rough correlation between the theoretical and experimental wing pressure distributions (figs. 5(b) and 5(c)). The discrepancies in these largely attached-flow regions at a Mach number of 0.85 are again partly the result of the prediction of too great a shock strength by FLO-27. However, for this Mach number, configuration A appears to have a separation bubble at the shock location for $\eta = 0.45$ (ref. 15). It is expected that such a local separation would tend to smear the jump in pressure at the shock wave and help to explain the difference between the theoretical and measured shock strengths at $\eta = 0.45$. Another reason for the discrepancies between theory and experiment in the predominantly attached-flow regions is the failure of the computer code to predict the existence of a weak shock wave which occurs on the inboard region of configurations A and B between the leading edge and the midchord. This shock appears at all three Mach numbers shown in figures 5(b) and 5(c).

It is evident from the results of figure 5 that viscous effects, including separation, are strong at transonic maneuver conditions. These viscous effects have resulted in significant discrepancies between experimental measurements and theoretical predictions based on inviscid theory coupled with a simple boundary-layer displacement effect. The inconsistent prediction of the inboard shock wave may result from the use of an infinite cylinder to model a finite-length fuselage of varying cross section.

Evaluation of Wings Designed by Three-Dimensional Transonic Theory

Comparison of configurations A and B of SMF-2.- Configuration A was designed for a single transonic maneuver point at a Mach number of 0.90 and a lift coefficient of 0.9. An upper-surface target pressure distribution was chosen in which the flow expands rapidly at the leading edge and isentropically compresses as it proceeds towards the trailing edge (ref. 8). This pressure distribution is intended to produce high lift while permitting the flow to compress ahead of the shock wave and thereby reduce the strength of the shock. The theoretical pressure distribution on configuration A near its design point is shown in figure 6(b). There is some expansion of the flow just ahead of the shock wave; this expansion is caused by the upper-surface curvature in the trailing-edge region. Although this expansion somewhat increases the strength of the shock, this small increase in shock strength was accepted as a compromise with the use of trailing-edge camber to reduce the overall adverse pressure gradient.

Although the performance of configuration A at a Mach number of 0.90 was generally acceptable, both theoretical and experimental results indicated the potential

for substantial reductions in shock strength and drag for maneuver conditions at a Mach number of 0.85. Therefore, configuration B was designed in an effort to reduce the shock-induced flow separation and maneuver drag penalties which occurred for configuration A at a Mach number of 0.85 and to maintain the performance of configuration A at the higher transonic Mach numbers. The theoretical pressure distributions of figure 6(a) indicate that at a Mach number of 0.85, the shock wave is weaker on configuration B than on configuration A for $\eta = 0.31$ and 0.48. Similarly, the experimental pressure distributions of figure 11(b) indicate that configuration B has a weaker shock wave than configuration A at $\eta = 0.45$ and 0.90.

The design of configuration B for a reduced shock strength at a Mach number of 0.85 has resulted in significant reductions in drag at maneuver conditions for Mach numbers of 0.60 and 0.85. These drag reductions are seen in the experimental results shown in figures 13 and 14. Figures 13(a) and 13(b) show that for these Mach numbers, configuration B has less drag than configuration A for lift coefficients greater than about 0.6. Figure 14(c) shows that for a lift coefficient of 0.90, configuration B has reduced the drag coefficient by 0.025 (250 counts) at a Mach number of 0.60 and by 0.018 (180 counts) at a Mach number of 0.85.

Figures 6(b) and 6(c) compare the theoretical pressure distributions for configurations A and B at Mach numbers of 0.90 and 0.95, and figures 11(c) and 11(d) compare the experimental pressure distributions at these same Mach numbers. Both the theoretical and the experimental pressure distributions indicate that significant differences in shock strength occur only in the tip region. As suggested by the pressure distributions, the maneuver drag levels of configurations A and B at Mach numbers of 0.90 and 0.95 are essentially equal (figs. 13(c), 13(d), 14(c), and 14(d)). Theoretical calculations not included in the present report show that as the angle of attack on configuration A is reduced somewhat below the value in figure 6(b), the trailing-edge shock shown in figure 6(b) moves forward and is weakened. This apparently explains why configuration A has somewhat less drag than configuration B at $M = 0.90$ for a small range of conditions near $C_L = 0.80$ (fig. (13c)).

Since configuration B has lower maneuver drag than configuration A at $M = 0.85$ and essentially the same maneuver drag as configuration A at the higher Mach numbers, the design objectives for configuration B were achieved. This improvement was accomplished by the use of the three-dimensional transonic theory and illustrates that a reduction in the computed shock strength at maneuver conditions for $M = 0.85$ resulted in less experimental drag for these conditions.

Configuration B of SMF-2 compared with W18.- Since configuration B of SMF-2 represents a significant improvement over configuration A, the configuration B wing has been selected for comparison with the W18 and SMF-1 wings (ref. 20). Figure 7 presents calculated pressure distributions for all three wings at transonic maneuver conditions. A comparison between configuration B of SMF-2 and the empirically developed W18 will be discussed first.

The theoretical pressure distributions over the inboard region of W18 show the presence of a rapid flow acceleration near the trailing edge followed by a strong shock wave. This acceleration is caused by the large upper-surface curvature in the trailing-edge region (fig. 1(b)). Configuration B of SMF-2 does not have this strong trailing-edge shock wave. The pressure distributions of figure 7 would therefore suggest that configuration B of SMF-2 would have less shock-induced flow separation and lower drag than W18 for these maneuver conditions.

Figure 13 shows that configuration B of SMF-2 has essentially the same or lower drag than W18 over the entire range of lift coefficients and Mach numbers studied. Figures 14(c) and 14(d) show that configuration B of SMF-2 has substantially lower drag between Mach numbers of 0.60 and 0.85 for lift coefficients of 0.90 and 1.0. At Mach numbers of 0.90 and 0.95, the drag levels are approximately the same. However, for a Mach number of 0.90 and lift coefficients greater than 1.0, figure 13(c) shows that the drag of W18 is increasing rapidly relative to the drag of configuration B of SMF-2.

The W18 wing does have a slightly different planform and much less twist than SMF-2 or SMF-1 (figs. 1(a) and 1(f)). Although no attempt was made to assess the effect of the planform difference, the effect of the difference in wing twist was examined. The pressure distributions of figure 8 show the effect of increasing the twist on W18 to the level of the SMF-1 twist. The calculation was made for a Mach number of 0.90. Although the increased twist did result in somewhat less theoretical drag, there is no significant overall reduction in shock strength or adverse pressure gradients.

Configuration B of SMF-2 compared with SMF-1.- Figure 14(c) shows that SMF-1 has about 100 counts (0.01 in C_D) less drag than configuration B of SMF-2 for Mach numbers of 0.85 to 0.95 and a lift coefficient of 0.9. These conditions essentially include the design points for SMF-1 and SMF-2. At a Mach number of 0.60, however, configuration B of SMF-2 has 300 counts less drag than SMF-1. The flow at a Mach number of 0.60 is primarily subsonic with supercritical effects confined to the leading-edge region at the higher angles of attack.

A comparison of the experimental pressure distributions of SMF-1 and configuration B of SMF-2 at maneuver conditions is shown in figure 12. Figures 12(b) to 12(d) ($M = 0.85$ to 0.95) are for lift coefficients where SMF-1 has lower drag than configuration B of SMF-2 and can therefore be used to help explain the results of figure 14(c). At a Mach number of 0.85 (fig. 12(b)), the somewhat better compression in the trailing-edge region of SMF-1 compared with configuration B of SMF-2 indicates that SMF-1 has less trailing-edge separation. At all three Mach numbers, SMF-1 has a large drop in pressure over the inboard leading-edge region, followed by a leading-edge shock wave. This drop in pressure, or suction peak, may help to reduce the section drag coefficients on the inboard part of the wing and, therefore, explain the lower drag levels of SMF-1 at these conditions. The theoretical pressure distributions in figure 7 have also predicted the existence of this leading-edge suction peak and shock wave on SMF-1.

As mentioned previously, the method of construction for configuration B of SMF-2 resulted in a wing which was much thicker than SMF-1 (figs. 1(c) and 1(e)). Calculations with FLO-27 have been used to estimate the penalty associated with this increased thickness. The inviscid drag ($C_{D,th}$) was calculated for configuration B of SMF-2 and for configuration B with the lower surface adjusted to approximate the thickness of SMF-1. The results showed that this additional thickness may account for about 25 counts of drag at the transonic maneuver conditions of figure 14(c) (Mach numbers from 0.85 to 0.95 and a lift coefficient of 0.9).

As the lift coefficient is increased to 1.0, however, the relative drag levels of SMF-1 and configuration B of SMF-2 are greatly altered. Figure 14(d) shows that for Mach numbers between 0.60 and 0.85, the drag levels of SMF-1 have become very

high relative to configuration B of SMF-2 (250 to 600 drag counts higher). Furthermore, for a lift coefficient only slightly greater than 1.0 and a Mach number of 0.90, the drag of SMF-1 changes from a value much lower than the drag of configuration B of SMF-2 to a value much higher than the drag of configuration B (fig. 13(c)).

This change in the relative drag levels of SMF-1 and configuration B of SMF-2 can be seen in the drag polars for Mach numbers of 0.85 and 0.90 (figs. 13(b) and 13(c)). The polars for SMF-1 have "breaks" between lift coefficients of 0.9 and 1.0. Breaks are defined as regions where there is a simultaneous loss in lift and increase in drag. The drag polars for configuration B of SMF-2 do not show any significant breaks. Figure 9 shows the experimental pressure distribution on SMF-1 at Mach numbers of 0.85 and 0.90 for lift coefficients just before and just after the breaks in the drag polars. The leading-edge shock merges with the trailing-edge shock in the tip region (η = 0.80) and causes extensive separation in this area. Of equal or greater significance, however, is the increased strength of the leading-edge shock wave over the inboard area of the wing and the resulting additional separation near the trailing edge in this inboard area. (This separation can also be seen in the photographs of the oil-flow patterns in ref. 11.) Apparently, the increasing strength of the leading-edge shock wave on SMF-1 is responsible for the sudden simultaneous loss of lift and increase in drag at Mach numbers of 0.85 and 0.90. For the sake of comparison, figure 10 shows the experimental pressure distributions on configuration B of SMF-2 for lift coefficients on each side of the maximum lift coefficient of SMF-1 in figure 9. Figure 15 compares the lift characteristics for SMF-1 and configuration B of SMF-2 and illustrates the sharp drop in lift for SMF-1 at Mach numbers of 0.85 and 0.90.

The theoretical predictions for SMF-1 have generally given a good estimate of the shock waves present during transonic maneuver conditions (fig. 5(a)). By the use of the three-dimensional transonic theory, it was possible to design SMF-2 without the leading-edge shock wave of SMF-1 (fig. 7). Apparently, the leading-edge suction peak on SMF-1 is beneficial up to a certain angle of attack, beyond which it is detrimental. Therefore, the use of leading- and trailing-edge variable geometry to control the leading-edge pressure may be an effective way to achieve good maneuver performance. The two-dimensional design process used for SMF-1 was intended to produce a smooth isentropic compression ahead of a trailing-edge shock without any leading-edge suction peak or shock wave. Figure 4 suggests that fuselage effects may be largely responsible for the occurrence of the leading-edge suction peak and shock wave on SMF-1.

As the Mach number is increased, the magnitude of the leading-edge suction peak and the strength of the leading-edge shock on SMF-1 are reduced for a given angle of attack. Therefore, as the Mach number is increased, it is possible to go to higher angles of attack and higher lift coefficients without the flow separation caused by the leading-edge shock wave (fig. 9). Thus, at a Mach number of 0.95, SMF-1 may exhibit the inboard flow separation and the accompanying break in the polar for some angle of attack greater than those achieved in the current tests.

CONCLUSIONS

This study has examined improvements in transonic maneuver performance by the use of three-dimensional transonic theory and a transonic design procedure. The FLO-27 code of Jameson and Caughey was used to design a new wing with lower drag at

transonic maneuver conditions. The wing contour was altered to reduce the upper-surface shock strength by means of a design procedure which is based on the iterative application of the FLO-27 code. The results of this study may be summarized as follows:

1. Results at a maneuver condition for a Mach number of 0.90 showed that the fuselage effects must be included in the theory to obtain an accurate prediction of the presence and strength of shock waves.

2. Theoretical and experimental wing pressure distributions for Mach numbers from 0.85 to 0.95 and lift coefficients from about 0.7 to 1.0 were in reasonably good agreement in regions of the wings where the flow was attached. Strong viscous effects caused significant discrepancies in some areas of the wings. A weak forward shock on the inboard region of the wings was not consistently predicted by the theory.

3. A reduction in the computed shock strength at maneuver conditions for a Mach number of 0.85 correlated with lower experimental drag for these conditions.

4. The three-dimensional transonic theory was used to improve the maneuver performance of a wing (configuration A of SMF-2 (supercritical maneuvering fighter)) designed for a single transonic maneuver point of a Mach number of 0.90 and a lift coefficient of 0.9. The improved wing (configuration B of SMF-2) had lower drag at maneuver conditions for Mach numbers of 0.60 and 0.85 and retained the maneuver drag levels of the original wing for Mach numbers of 0.90 and 0.95.

5. Configuration B of SMF-2 had essentially the same or lower drag than an empirically developed, supercritical maneuver wing (W18) for Mach numbers ranging from 0.60 to 0.95 and lift coefficients up to about 1.0.

6. At a lift coefficient of 0.9 and transonic Mach numbers, configuration B of SMF-2 had somewhat higher drag than a maneuver wing designed primarily by the use of two-dimensional transonic theory (SMF-1). At a lift coefficient above about 1.0, configuration B of SMF-2 had substantially lower drag than SMF-1 for Mach numbers ranging from 0.60 to 0.90.

Langley Research Center
National Aeronautics and Space Administration
Hampton, VA 23665
January 13, 1984

APPENDIX

APPARATUS AND TESTS ON W18 AND SMF-1

The Langley 8-Foot Transonic Pressure Tunnel is a continuous-flow, single-return tunnel with a slotted, rectangular test section. This facility has the capability for independent variation of Mach number, density, temperature, and humidity. A description of this facility as configured for these tests is given in reference 21.

Experimental results for W18 and SMF-1 are for Mach numbers ranging from 0.60 to 0.95 and angles of attack from -5° to 18°. The Reynolds number based on wing mean aerodynamic chord was 2.42×10^6 for W18 and 2.56×10^6 for SMF-1.

Boundary-layer transition strips approximately 0.25 cm (0.1 in.) wide were selected for W18 and SMF-1 by use of the method of reference 22. No. 120 carborundum grains were applied 1 cm (0.4 in.) streamwise behind the leading edges of the wings and vertical tail. No. 100 grains were applied 2.8 cm (1.1 in.) behind the apex of the nose, and No. 120 grains were applied 1 cm (0.4 in.) behind the inlet of the nacelle (inside and outside). Essentially the same transition strip width, location, and grit size were used on all four fighter configurations with the exception of the nacelle inlet. On SMF-2, a transition strip of No. 100 grains was applied to the exterior only of the nacelle (same distance from the inlet). However, this difference in transition strip for the nacelle was found to have no effect on the force data.

Aerodynamic forces and moments for W18 and SMF-1 were measured by an internal, six-component, strain-gauge balance. The angle of attack was measured by a pendulous, inertial, single-axis accelerometer (closed-loop type) mounted inside the model. Tunnel flow angularity was measured and found to be negligible. The force data have been corrected to a condition of free-stream static pressure over the fuselage base. The internal drag of the flow-through nacelle was measured and subtracted from the total measured drag. The values of internal drag are given in table III.

The SMF-1 wing was instrumented with flush-surface static pressure orifices distributed in streamwise rows. Orifices were located on the upper right and lower left wing surfaces at $\eta = 0.31$, 0.63, and 0.92. Upper-surface orifices were also located on the left wing at $\eta = 0.46$ and 0.80. All surface pressures were recorded by the use of differential-pressure-scanning valves mounted in the nose section of the model. Wing surface pressures were not measured for W18.

REFERENCES

1. Lamar, John E.; Schemensky, Roy T.; and Reddy, C. Subba: Development of a Vortex-Lift Design Procedure and Application to a Slender Maneuver-Wing Configuration. J. Aircr., vol. 18, no. 4, Apr. 1981, pp. 259-266. (Available as AIAA-80-0327R.)

2. Nixon, David: Transonic Aerodynamics. American Inst. Aeronaut. & Astronaut., Inc., c.1982.

3. Hicks, Raymond M.: Transonic Wing Design Using Potential-Flow Codes - Successes and Failures. SAE Tech. Paper Series 810565, Apr. 1981.

4. Garabedian, Paul; and McFadden, Geoffrey: Design of Supercritical Swept Wings. AIAA J., vol. 20, no. 3, Mar. 1982, pp. 289-291.

5. Shankar, V.: A Full Potential Inverse Method Based on a Density Linearization Scheme for Wing Design. AIAA-81-1234, June 1981.

6. Henne, P. A.: Inverse Transonic Wing Design Method. J. Aircr., vol. 18, no. 2, Feb. 1981, pp. 121-127.

7. Jameson, Antony; and Caughey, D. A.: A Finite Volume Method for Transonic Potential Flow Calculations. A Collection of Technical Papers - AIAA 3rd Computational Fluid Dynamics Conference, June 1977, pp. 35-54. (Available as AIAA Paper 77-635.)

8. Mann, Michael J.: The Design of Supercritical Wings by the Use of Three-Dimensional Transonic Theory. NASA TP-1400, 1979.

9. Bauer, Frances; Garabedian, Paul; Korn, David; and Jameson, Antony: Supercritical Wing Sections II. Volume 108 of Lecture Notes in Economics and Mathematical Systems, Springer-Verlag, 1975.

10. Hadley, S. K.; Lydick, L. N.; and Mann, H. W.: Variable Contour, Supercritical, Thin, Fighter Wing Design for Transonic Maneuverability. Rep. No. ERR-FW-1740, General Dynamics, Dec. 31, 1976.

11. Hadley, S. K.; and Mann, H. W.: Status Report on the Development of a Supercritical Sloped Rooftop Wing. ERR-FW-1940, General Dynamics, Fort Worth Div., Dec. 22, 1978.

12. Jameson, Antony: Transonic Flow Calculations. Numerical Methods in Fluid Dynamics, H. J. Wirz and J. J. Smolderen, eds., Hemisphere Pub. Corp., 1978, pp. 1-87.

13. Jameson, Antony; Caughey, David A.; Newman, Perry A.; and Davis, Ruby M.: A Brief Description of the Jameson-Caughey NYU Transonic Swept-Wing Computer Program - FLO 22. NASA TM X-73996, 1976.

14. Mann, Michael J.; Mercer, Charles E.; and Campbell, Richard L.: Supercritical Maneuvering Fighter Configuration - Wind-Tunnel Investigation at Mach Numbers of 0.60 to 0.95. NASA TM-84513, 1982.

15. Mann, Michael J.; Huffman, Jarrett K.; Fox, Charles H., Jr.; and Campbell, Richard L.: Experimental Study of Wing Leading-Edge Devices for Improved Maneuver Performance of a Supercritical Maneuvering Fighter Configuration. NASA TP-2125, 1983.

16. Caughey, David A.; Newman, Perry A.; and Jameson, Antony: Recent Experiences With Three-Dimensional Transonic Potential Flow Calculations. NASA TM-78733, 1978.

17. Henne, P. A.; and Hicks, R. M.: Wing Analysis Using a Transonic Potential Flow Computational Method. NASA TM-78464, 1978.

18. Nash, J. F.; and Macdonald, A. G. J.: The Calculation of Momentum Thickness in a Turbulent Boundary Layer at Mach Numbers up to Unity. C.P. No. 963, British A.R.C., 1967.

19. Bhateley, I. C.; Mann, M. J.; and Ballhaus, W. F.: Evaluation of Three-Dimensional Transonic Methods for the Analysis of Fighter Configurations. AIAA Paper No. 79-1528, July 1979.

20. Mann, M. J.; Campbell, R. L.; and Ferris, J. C.: Aerodynamic Design for Improved Maneuverability by the Use of Three-Dimensional Transonic Theory. AIAA-83-1859, July 1983.

21. Schaefer, William T., Jr.: Characteristics of Major Active Wind Tunnels at the Langley Research Center. NASA TM X-1130, 1965.

22. Braslow, Albert L.; and Knox, Eugene C.: Simplified Method for Determination of Critical Height of Distributed Roughness Particles for Boundary-Layer Transition at Mach Numbers From 0 to 5. NACA TN 4363, 1958.

TABLE I.- COMPARISON OF SMF-1, SMF-2, AND W18 WINGS

[Planform quantities are for the basic trapezoidal wing extended to the model centerline]

Parameter	W18	SMF-1 and SMF-2
Sweepback of leading edge, deg	40	45
Aspect ratio	3.36	3.28
Taper ratio	0.2936	0.2142
Area, m^2 (ft^2)	0.138 (1.48)	0.139 (1.50)
Span, cm (in.)	68.006 (26.774)	67.686 (26.648)
Mean aerodynamic chord, cm (in.) ...	22.240 (8.756)	23.518 (9.259)
Root chord, cm (in.)	31.278 (12.314)	33.993 (13.383)
Tip chord, cm (in.)	9.185 (3.616)	7.282 (2.867)
Dihedral, deg	0	0

TABLE II.- CHARACTERISTICS OF VERTICAL TAIL AND FUSELAGE

Vertical tail (exposed trapezoid):

Sweepback of leading edge, deg	61
Aspect ratio	0.856
Taper ratio	0.2854
Tail area/Wing area	0.168
Span, cm (in.)	14.145 (5.569)
Root chord, cm (in.)	25.718 (10.125)
Tip chord, cm (in.)	7.341 (2.890)
Airfoil section	4-percent circular-arc biconvex

Fuselage:

Flow-through inlet area, cm^2 (in^2)	23.020 (3.568)
Flow-through exit area, cm^2 (in^2)	18.872 (2.925)
Base area, cm^2 (in^2)	28.852 (4.472)

TABLE III.- INTERNAL DRAG CHARACTERISTICS

α, deg	$C_{D,i}$ for -				
	M = 0.60	M = 0.80	M = 0.85	M = 0.90	M = 0.95
-4.0	0.00242	0.00253	0.00258	0.00247	0.00236
0	.00242	.00253	.00258	.00247	.00236
2.0	.00243	.00254	.00259	.00248	.00235
4.0	.00245	.00258	.00262	.00252	.00239
6.0	.00251	.00264	.00267	.00258	.00246
8.0	.00259	.00273	.00275	.00267	.00257
10.0	.00270	.00285	.00287	.00279	.00267
12.0	.00286	.00299	.00302	.00295	.00278
14.0	.00307	.00318	.00320	.00315	.00298
16.0		.00340	.00340	.00338	.00325

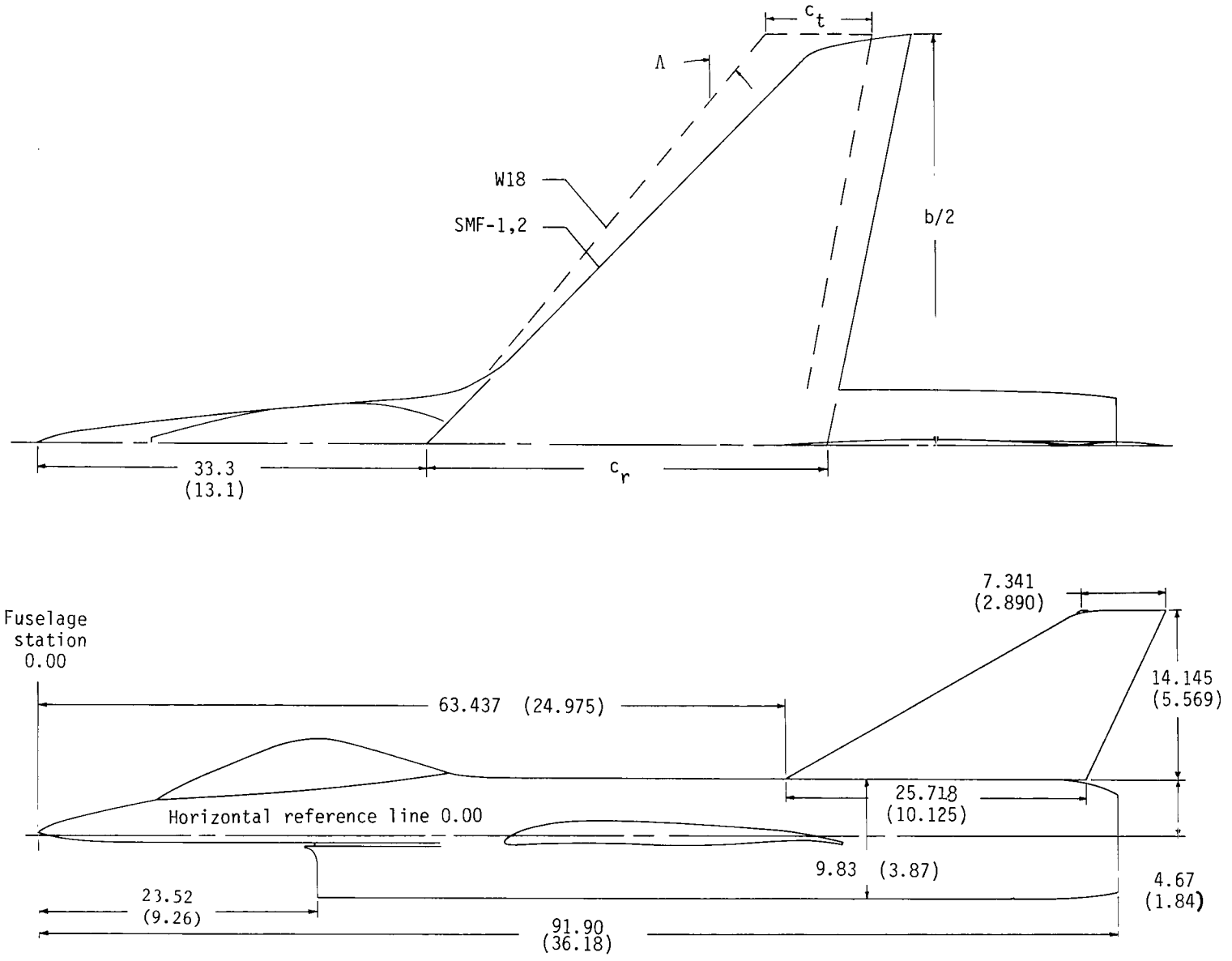

(a) General arrangement of model. Planform dimensions given in table I.

Figure 1.- Details of model geometry. Dimensions are given in centimeters (inches).

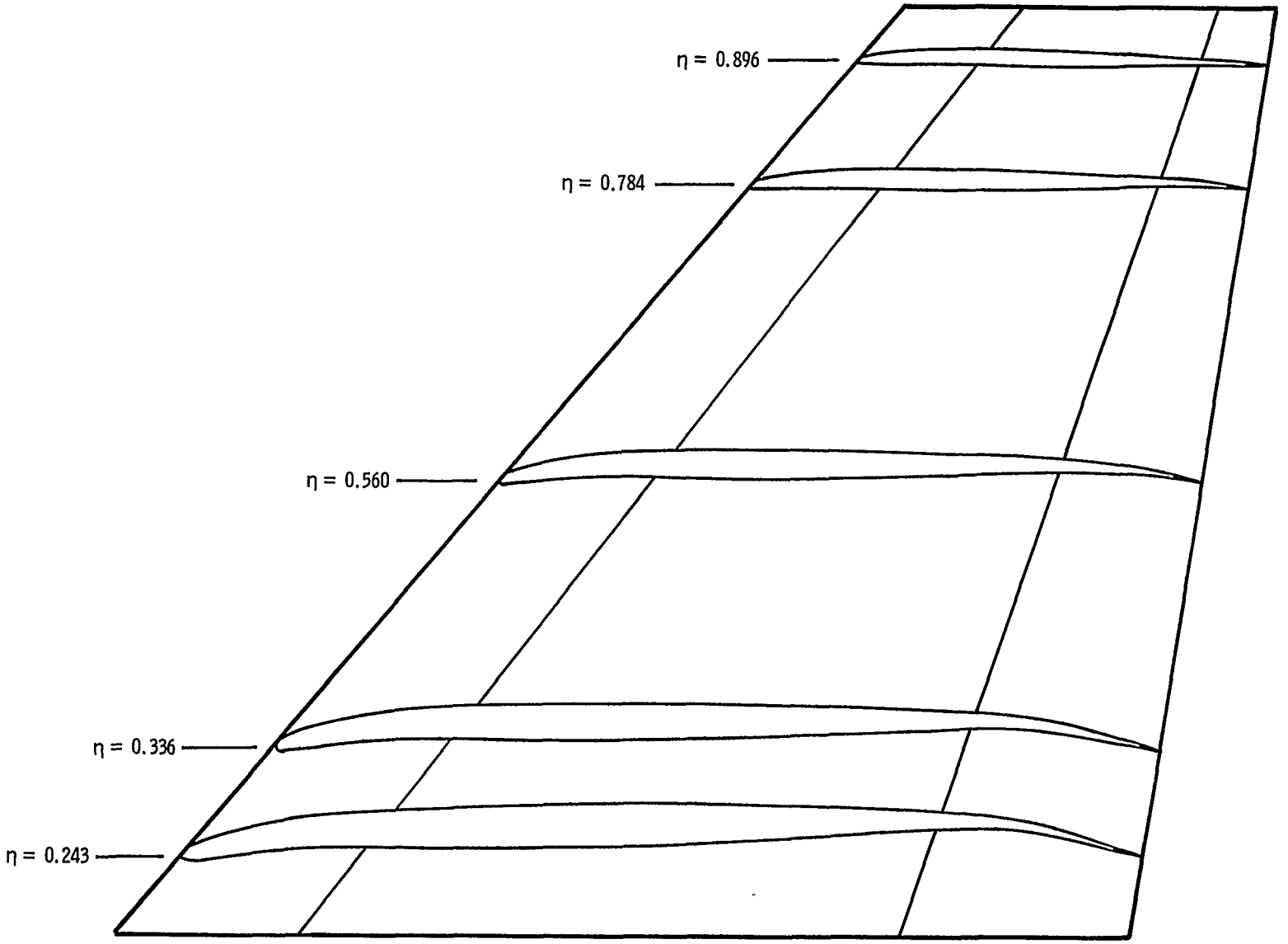

(b) Wing sections and flap locations for W18.

Figure 1.- Continued.

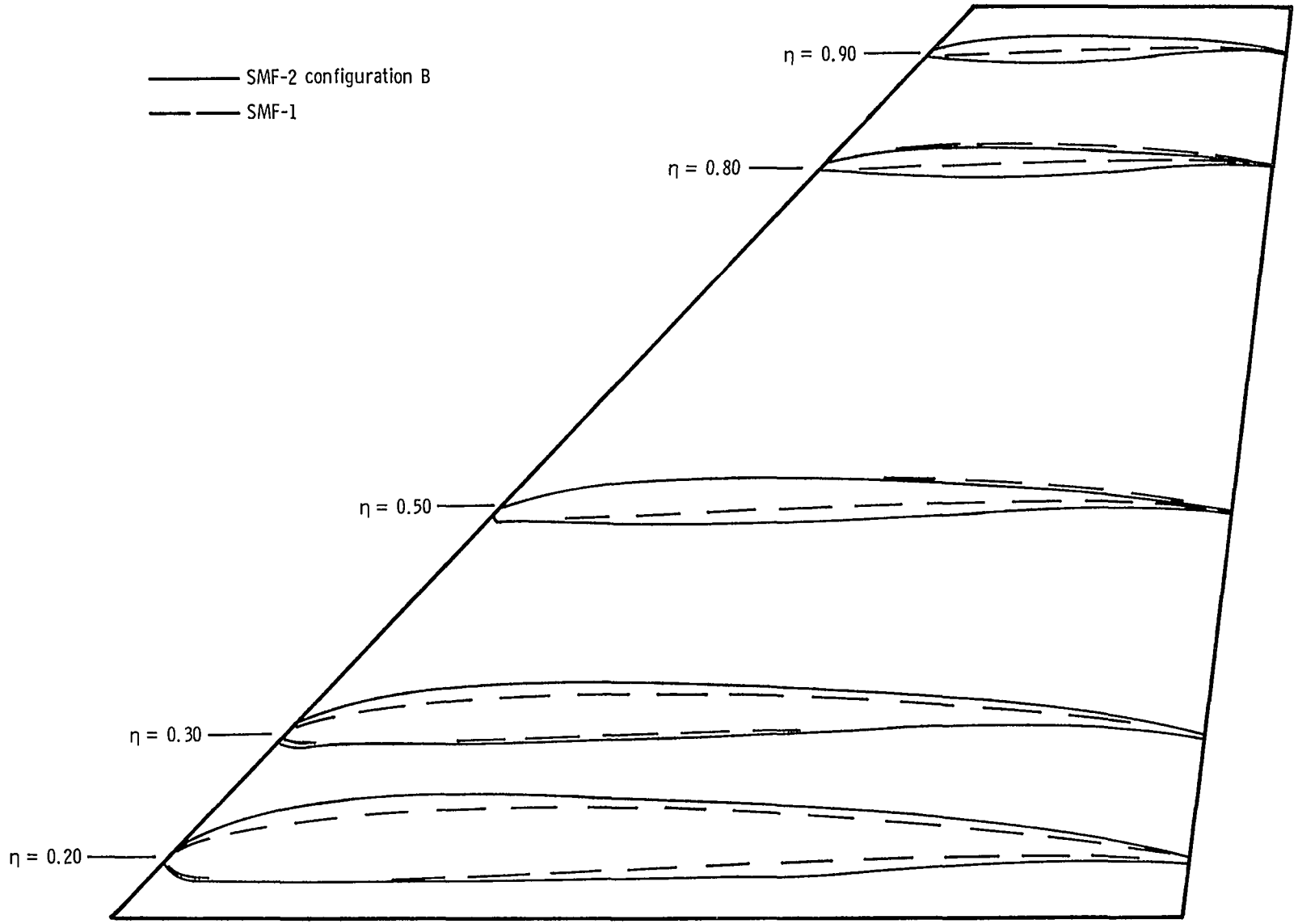

(c) Comparison of wing sections for SMF-1 and configuration B of SMF-2.

Figure 1.- Continued.

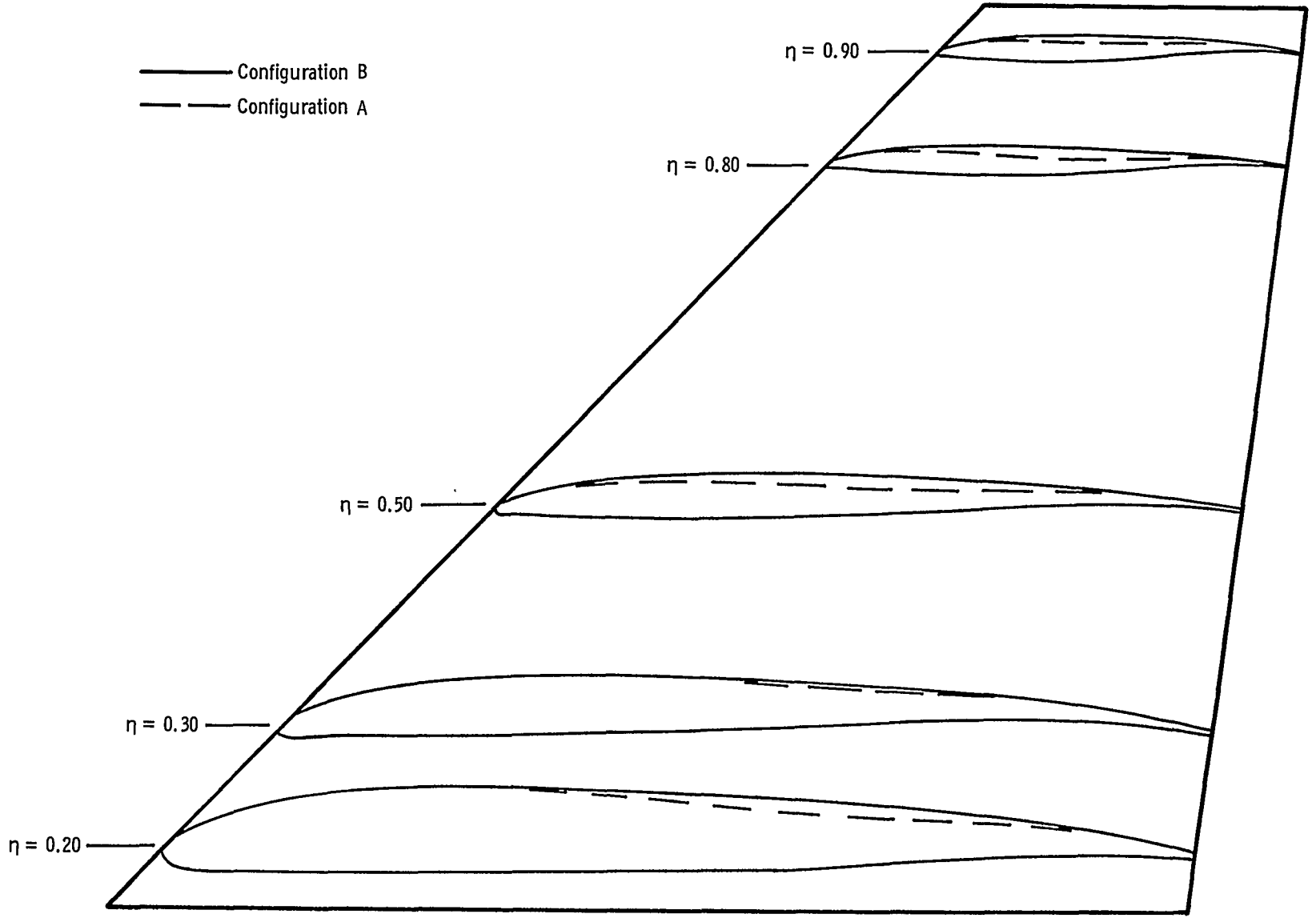

(d) Comparison of wing sections for configurations A and B of SMF-2.

Figure 1.- Continued.

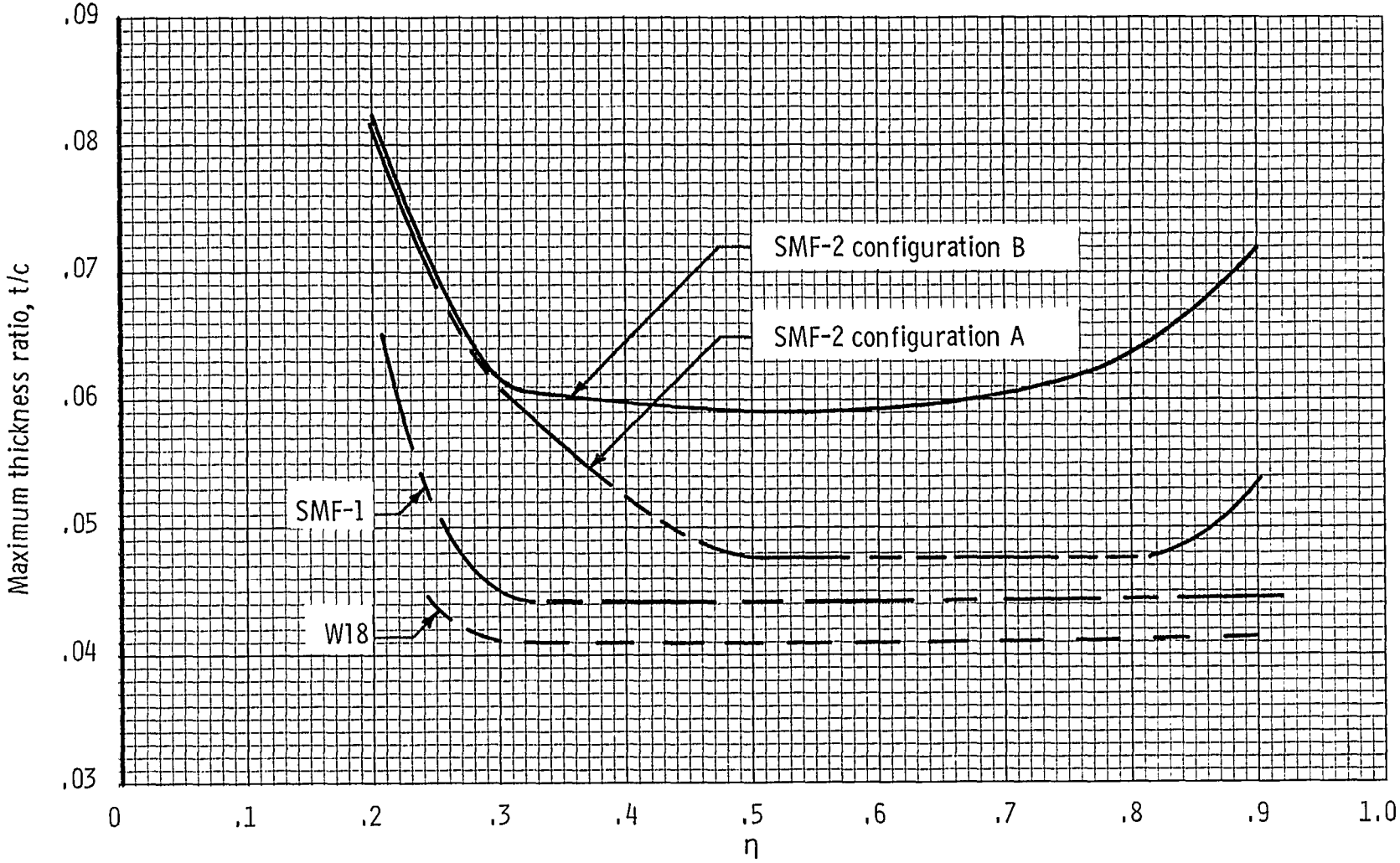

(e) Maximum thickness-ratio distribution for all wings.

Figure 1.- Continued.

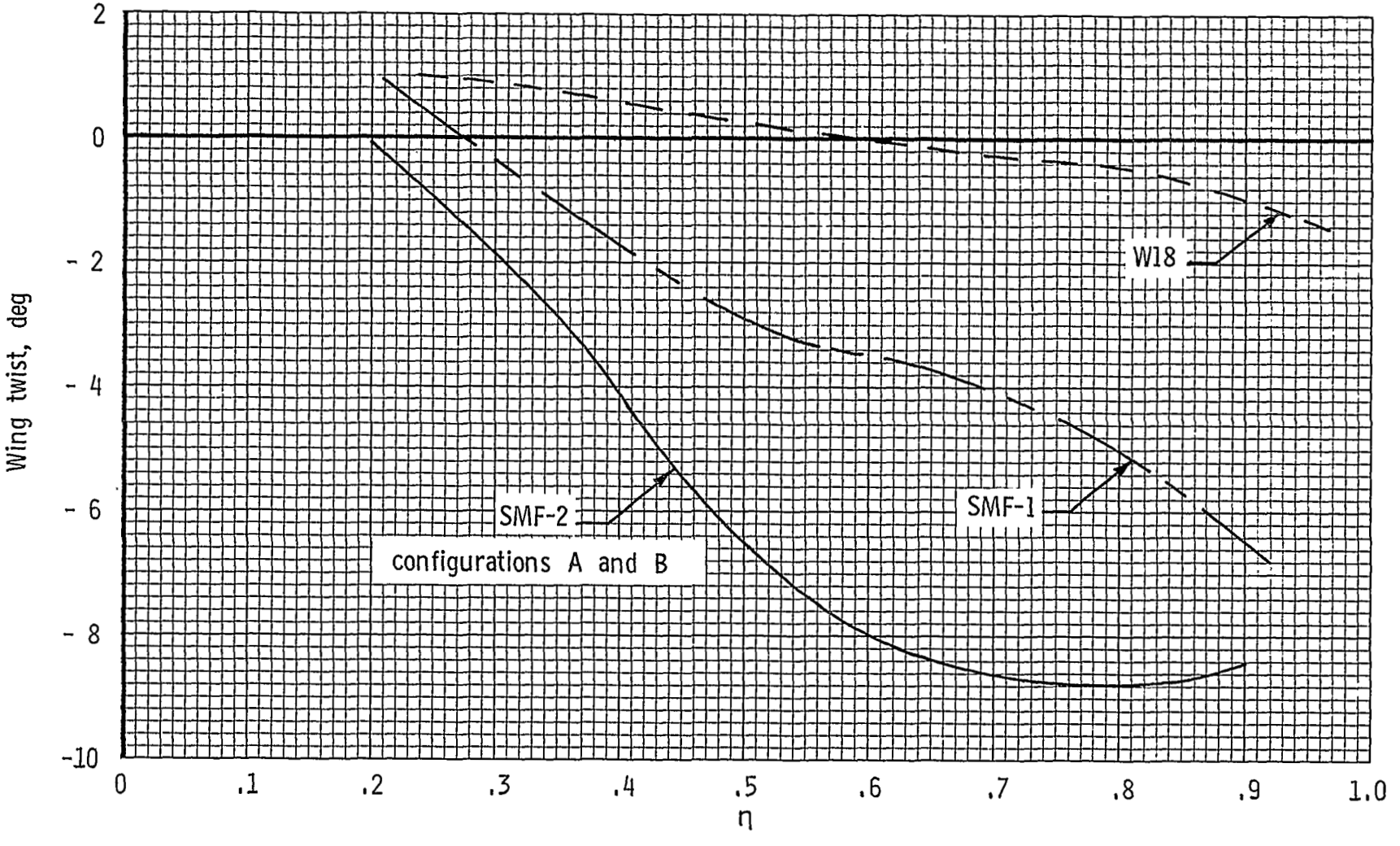

(f) Twist distribution for all wings.

Figure 1.- Continued.

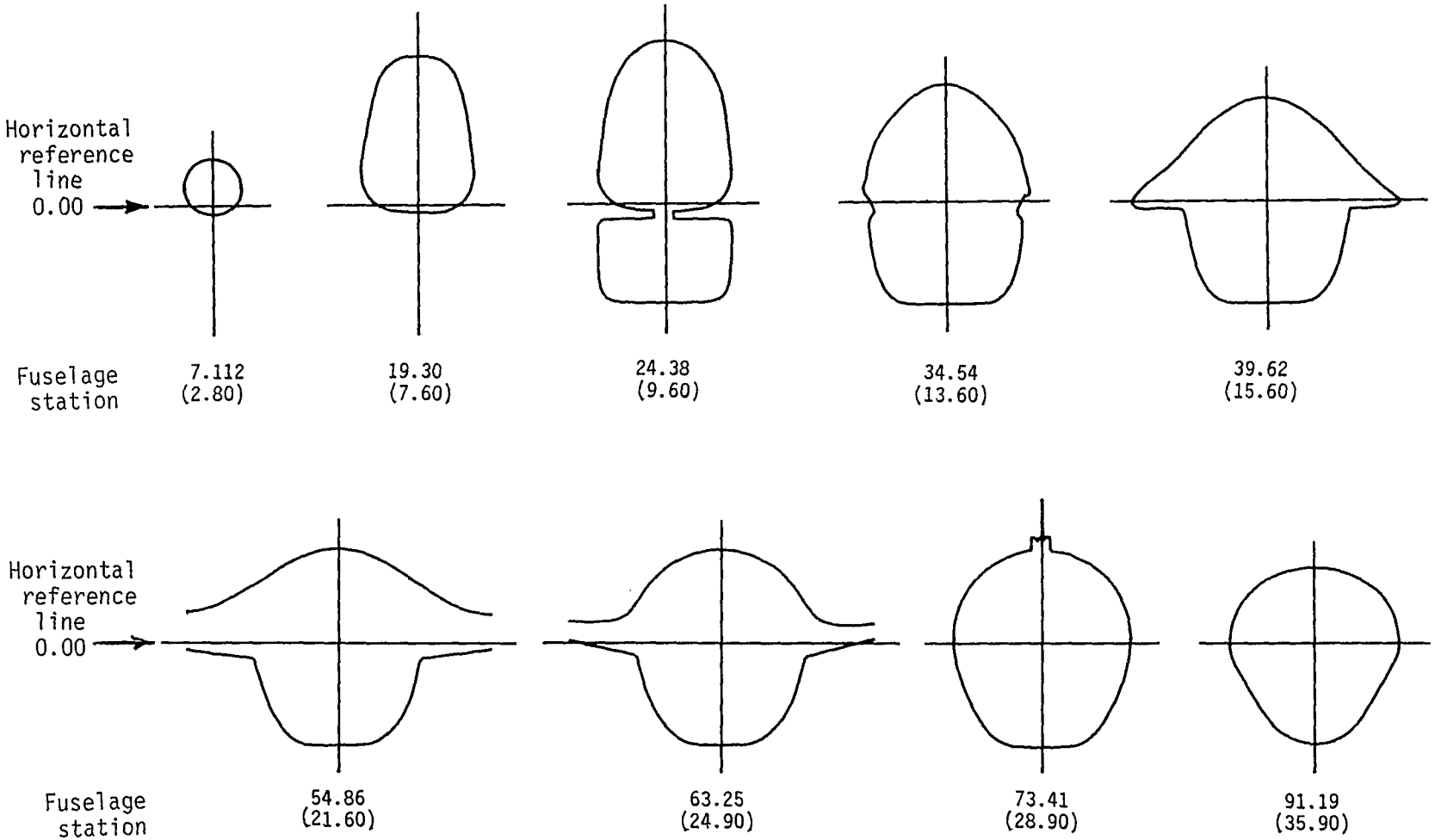

(g) Fuselage external contours.

Figure 1.- Concluded.

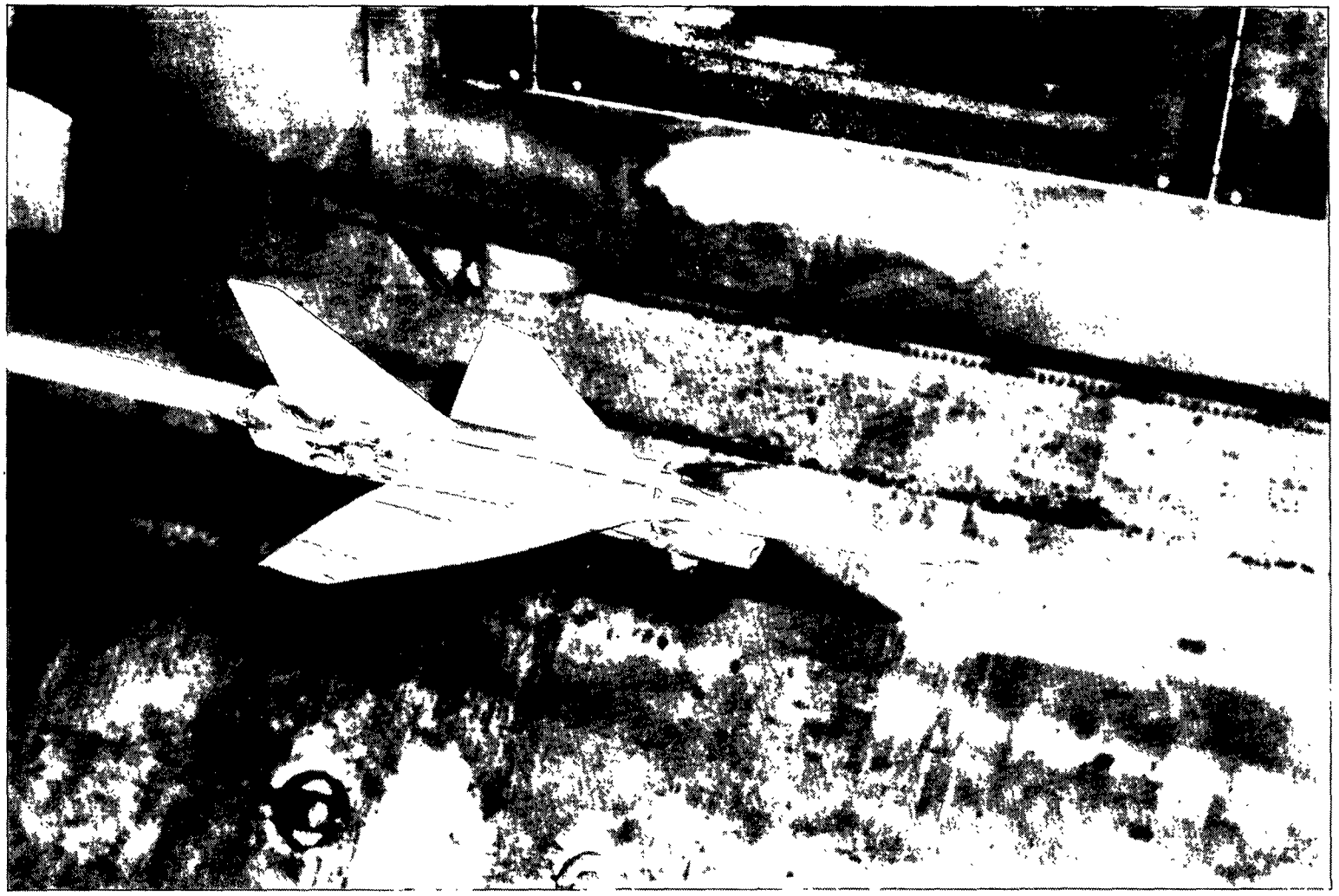

L-81-10,141

(a) Three-quarter front top view.

Figure 2.- Model with SMF-2 configuration B wing mounted in Langley 16-Foot Transonic Tunnel.

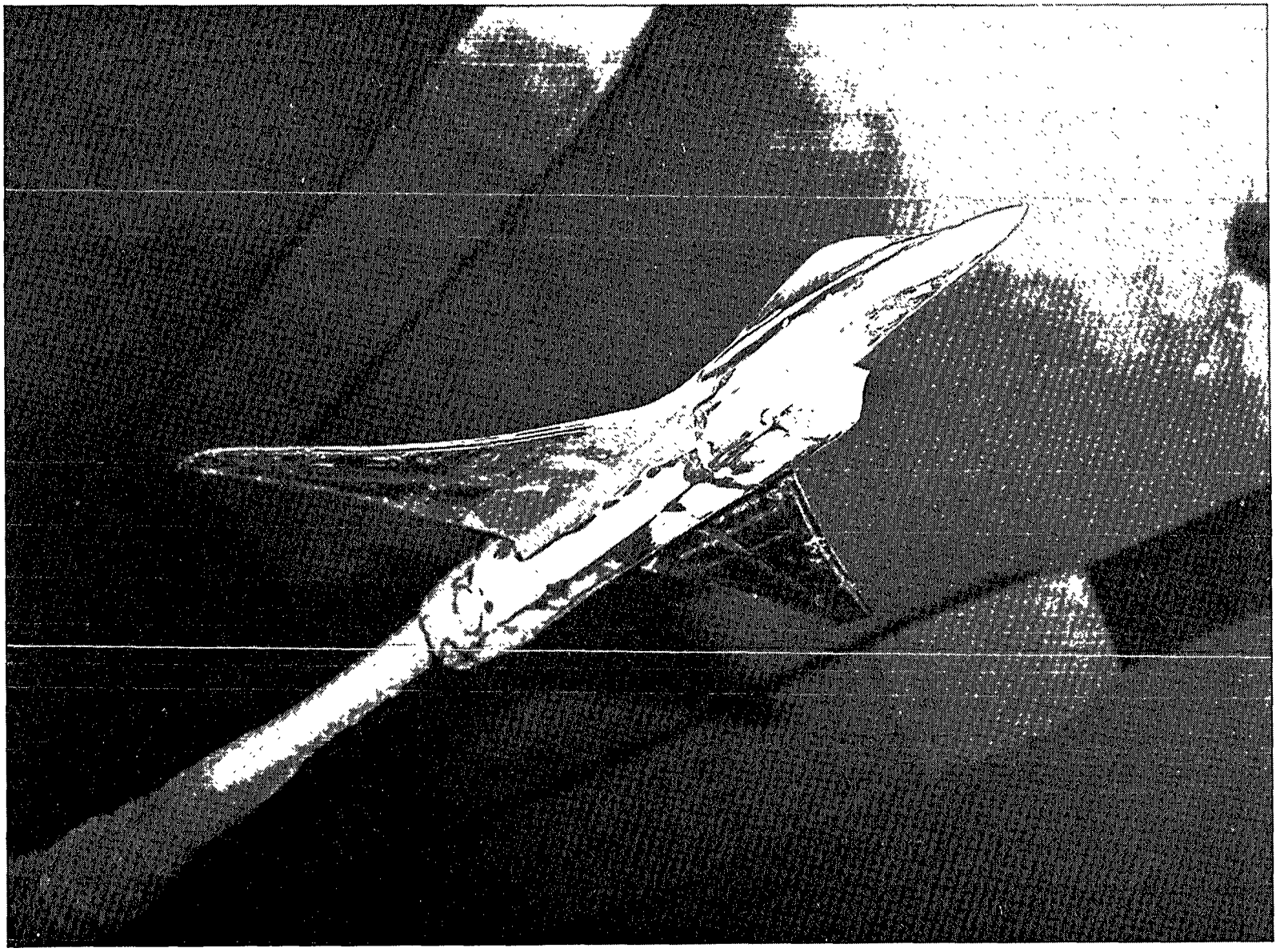

L-80-10,877

(b) Three-quarter front bottom view.

Figure 2.- Concluded.

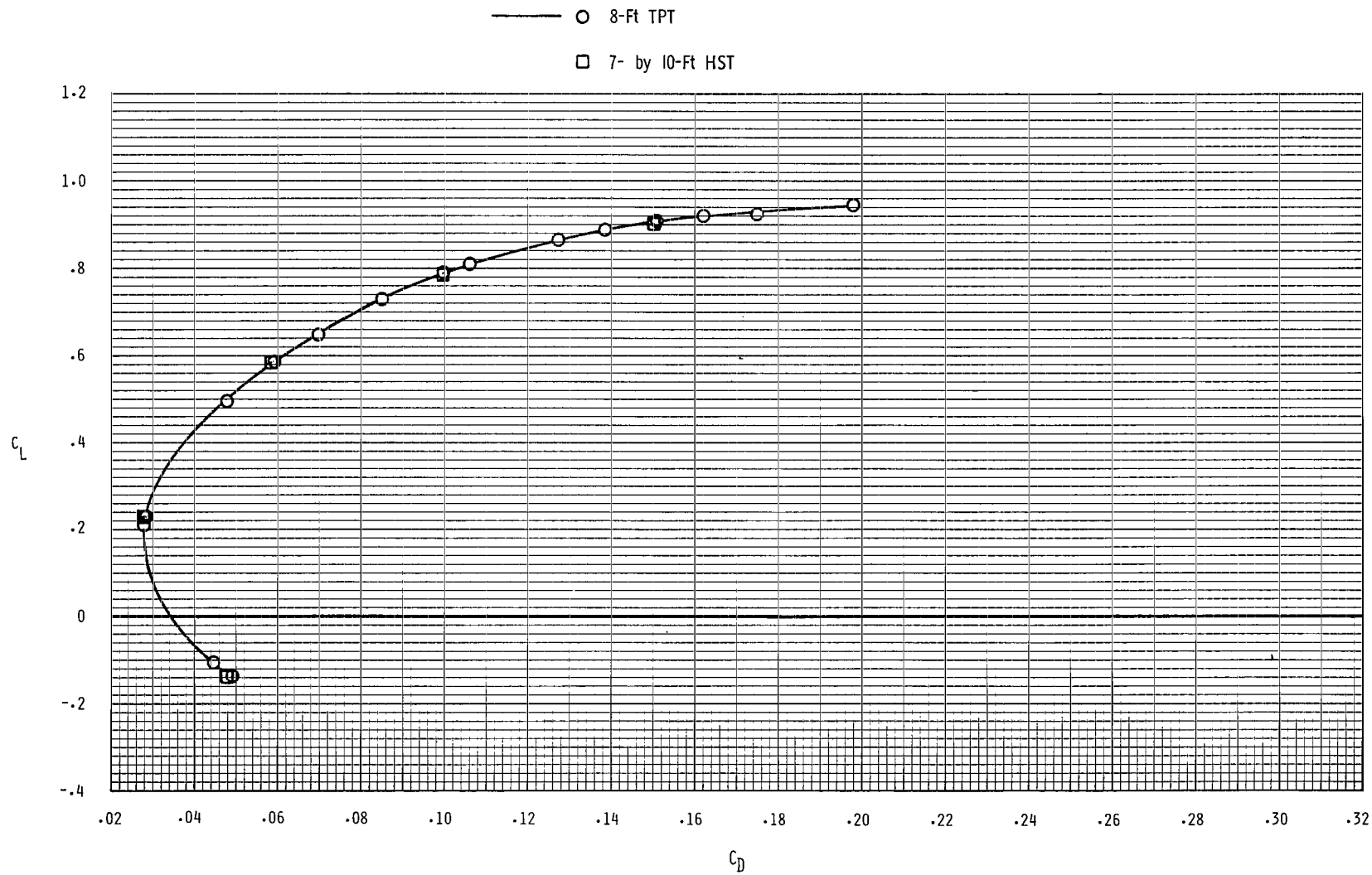

(a) 8-Ft TPT and 7- by 10-Ft HST. SMF-2 model.

Figure 3.- Comparison of lift and drag data for three Langley wind tunnels. M = 0.85.

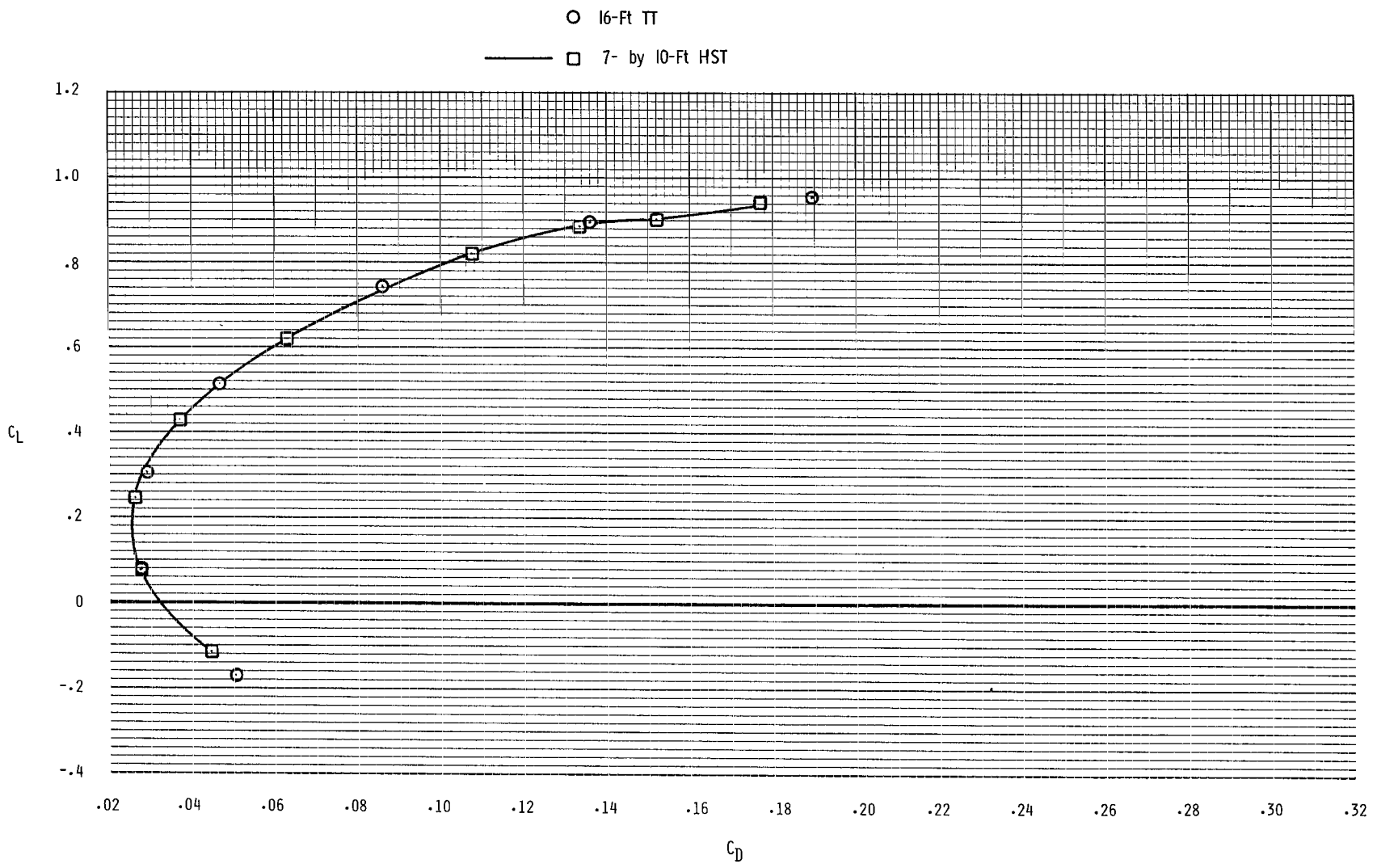

(b) 16-Ft TT and 7- by 10-Ft HST. SMF-2 configuration A.

Figure 3.- Concluded.

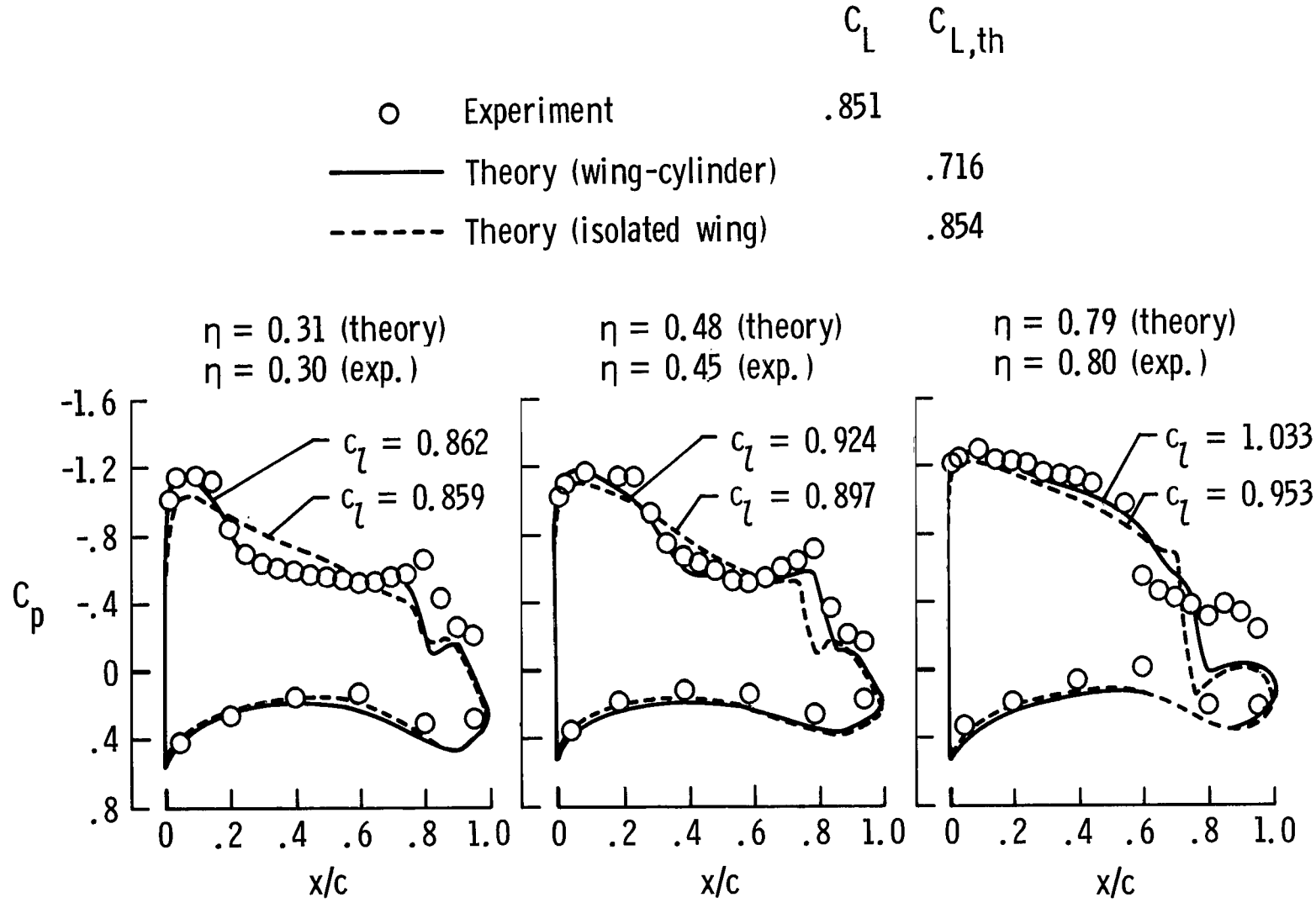

Figure 4.- Effects of a cylindrical fuselage on theoretical wing pressure distributions and correlation with experiment for SMF-2 at M = 0.90.

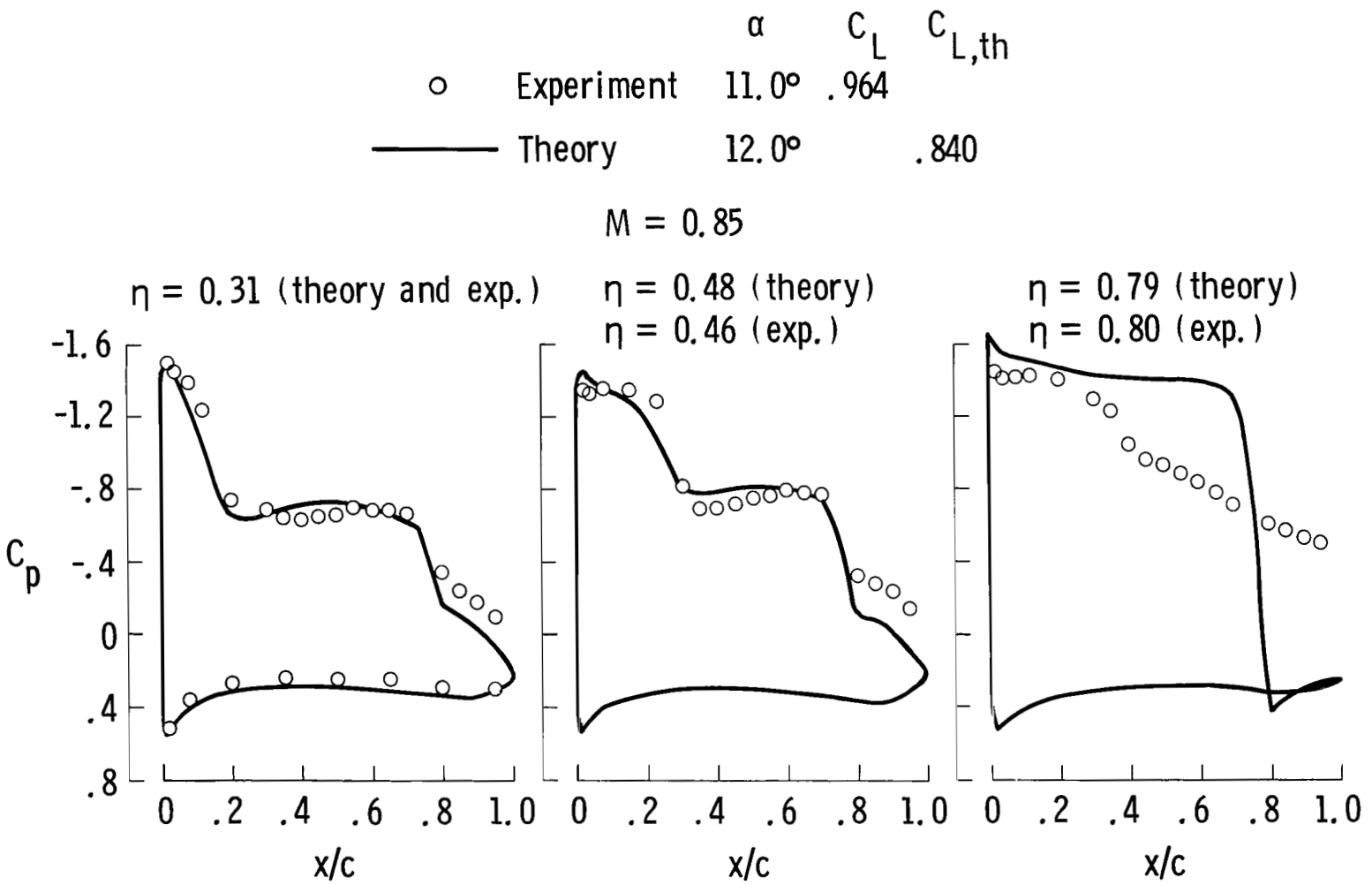

(a) SMF-1.

Figure 5.- Correlation of theoretical and experimental wing pressure distributions for SMF-1 and configurations A and B of SMF-2.

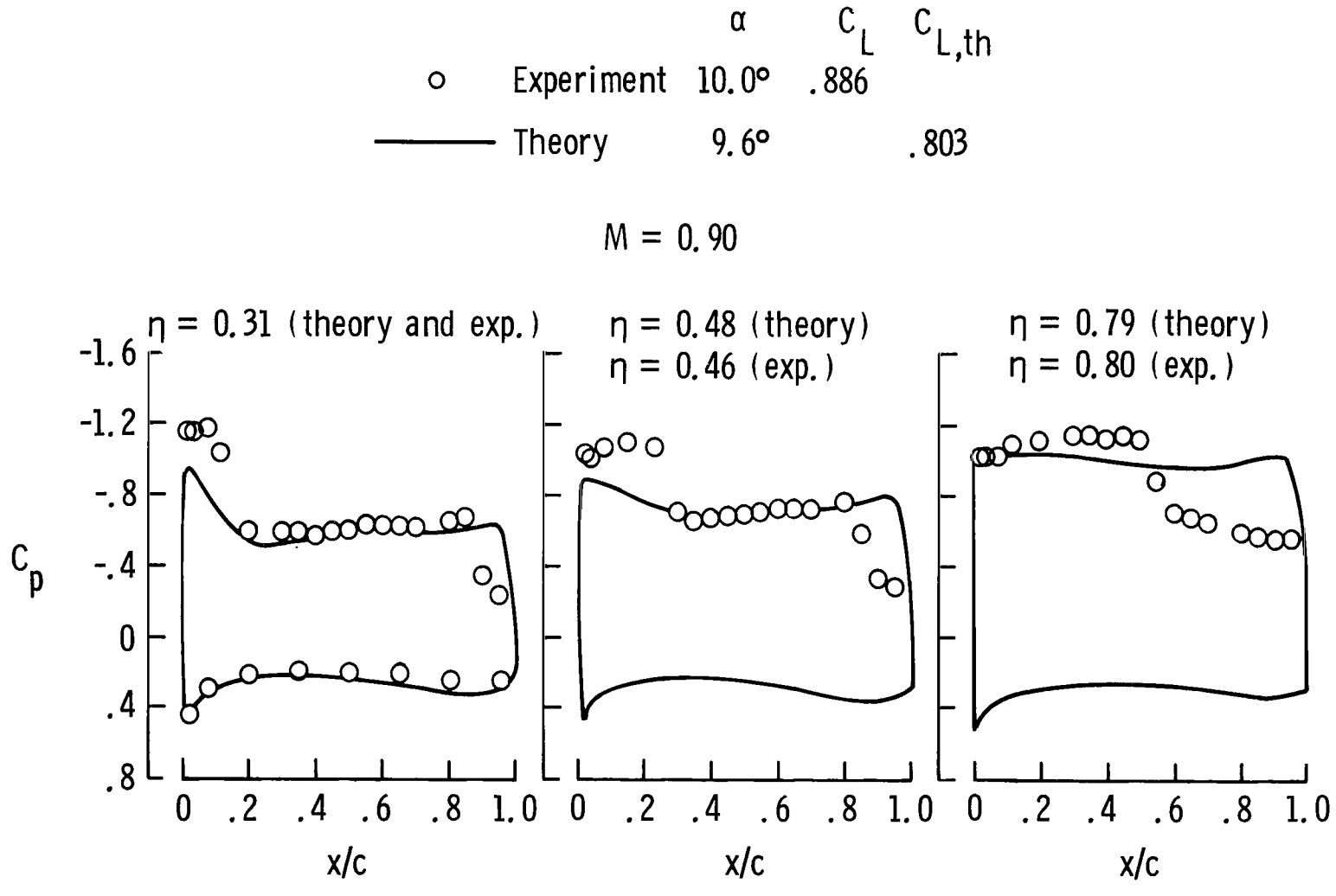

(a) Continued.

Figure 5.- Continued.

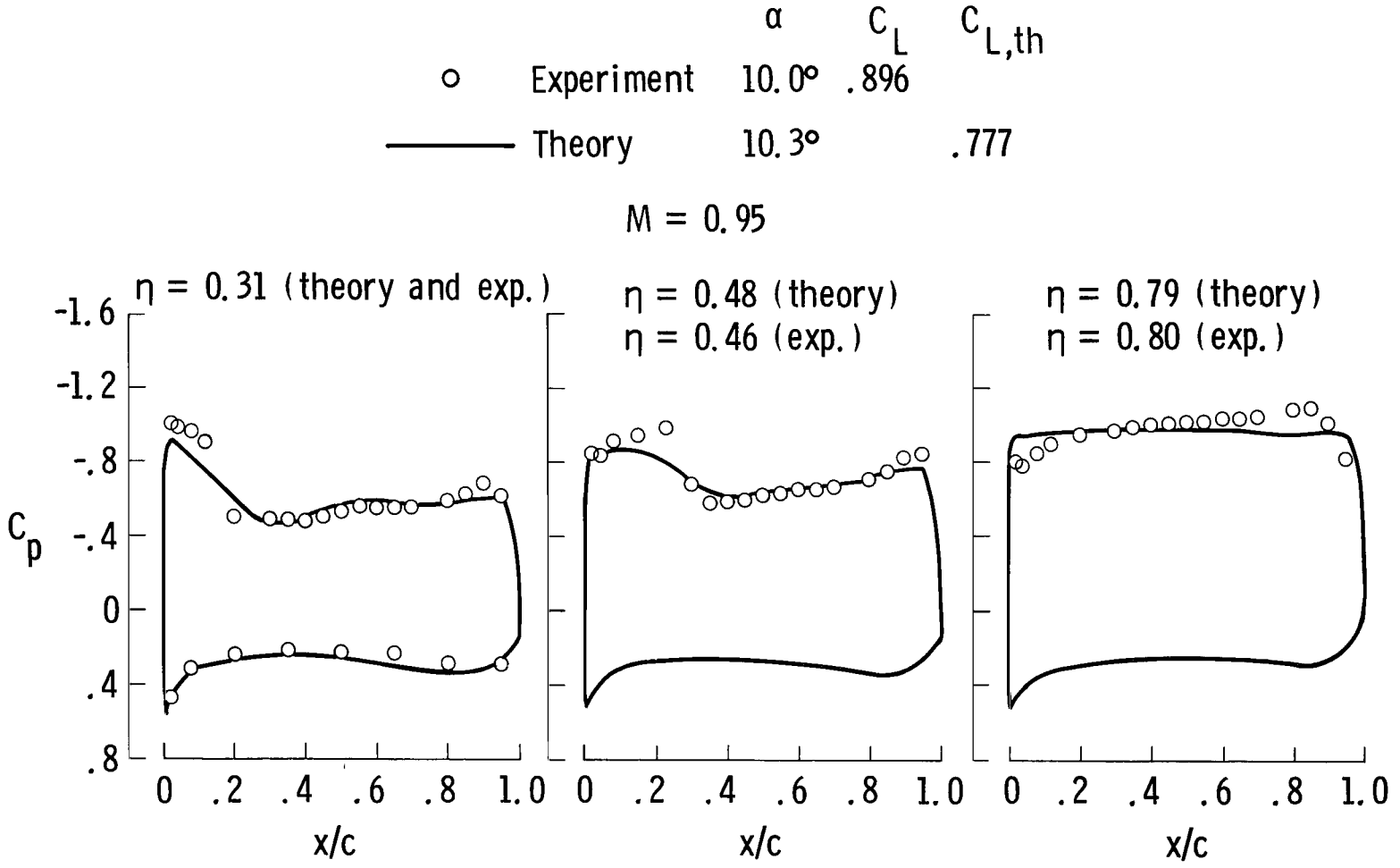

(a) Concluded.

Figure 5.- Continued.

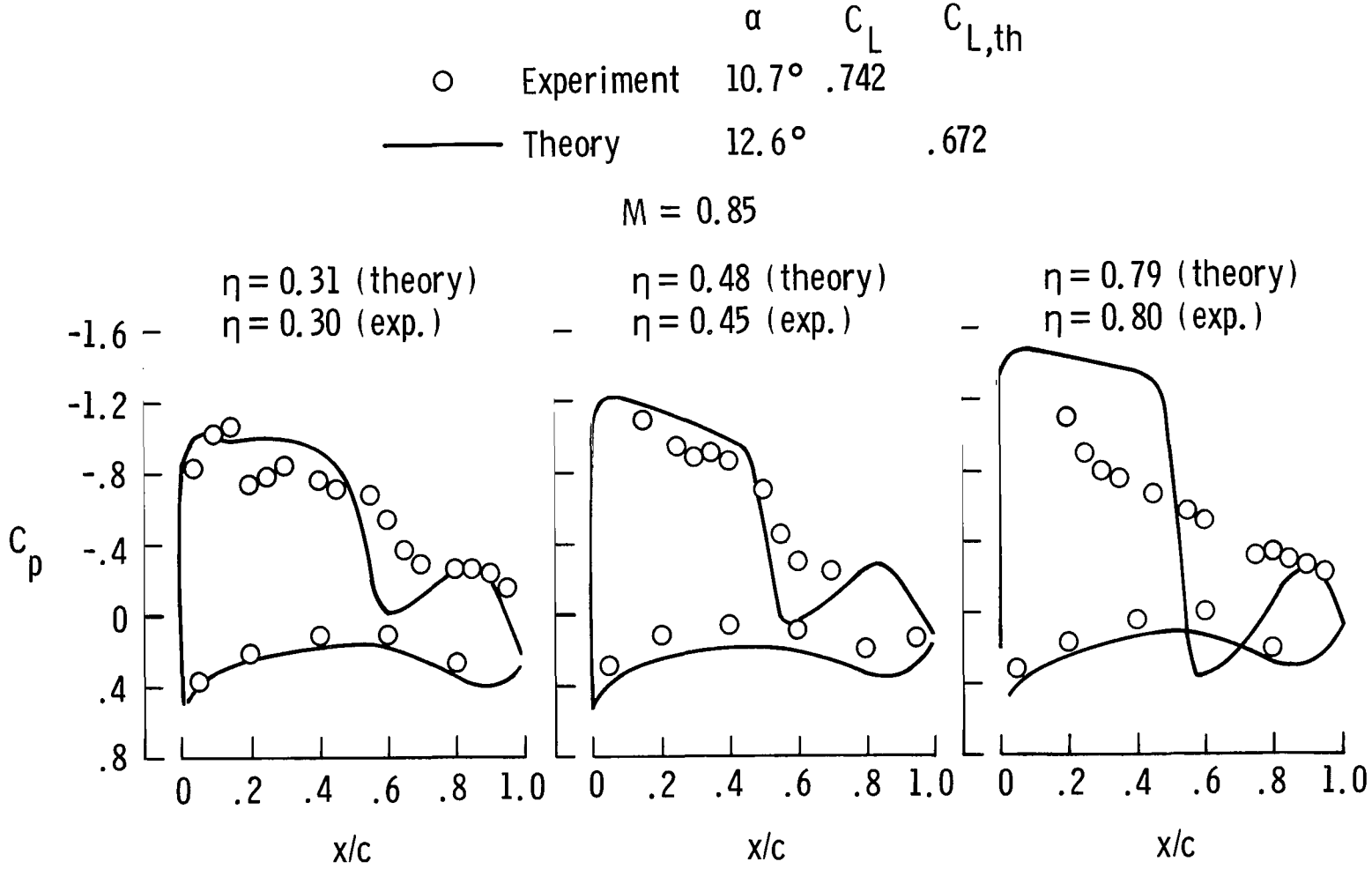

(b) SMF-2 configuration A.

Figure 5.- Continued.

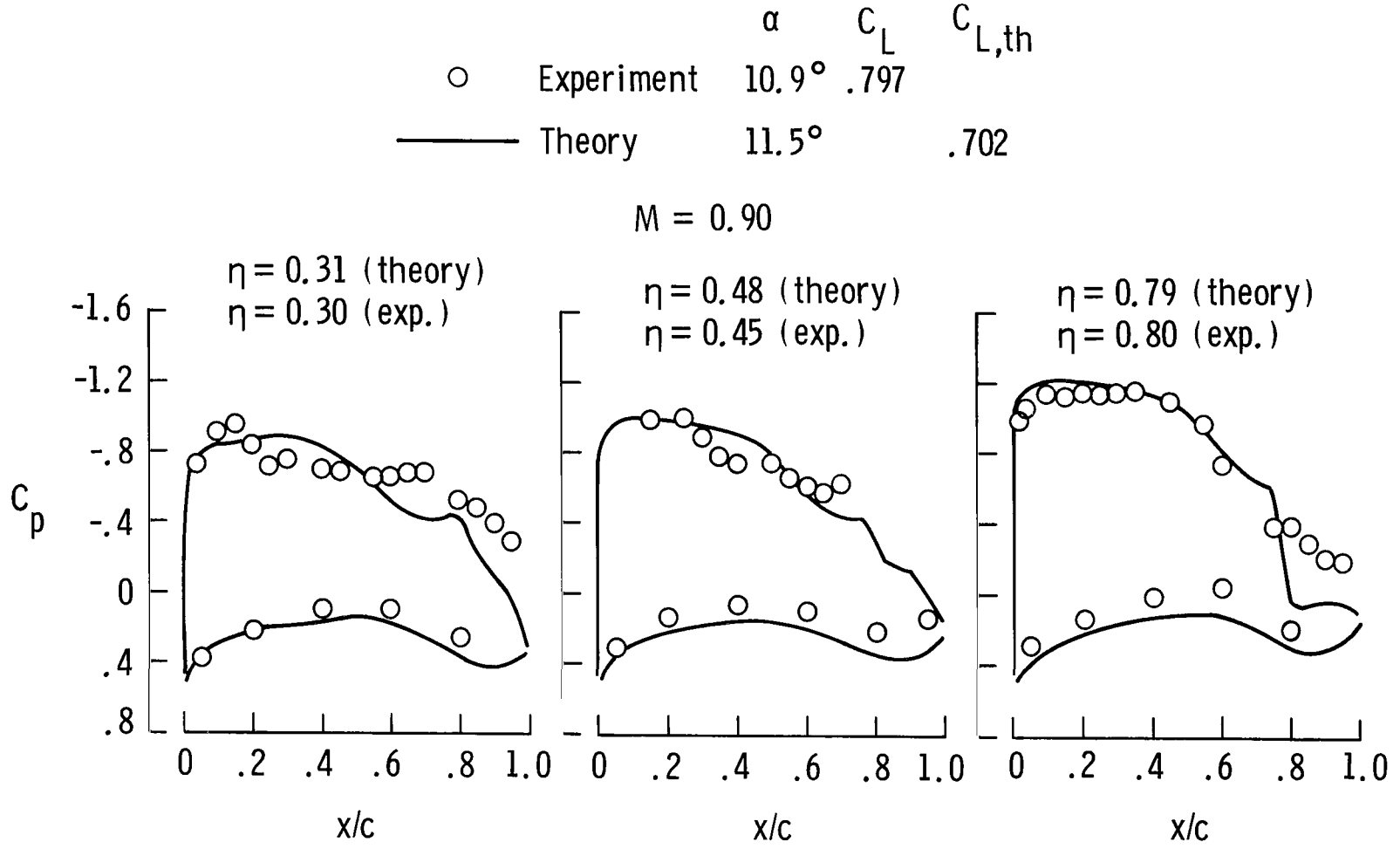

(b) Continued.

Figure 5.- Continued.

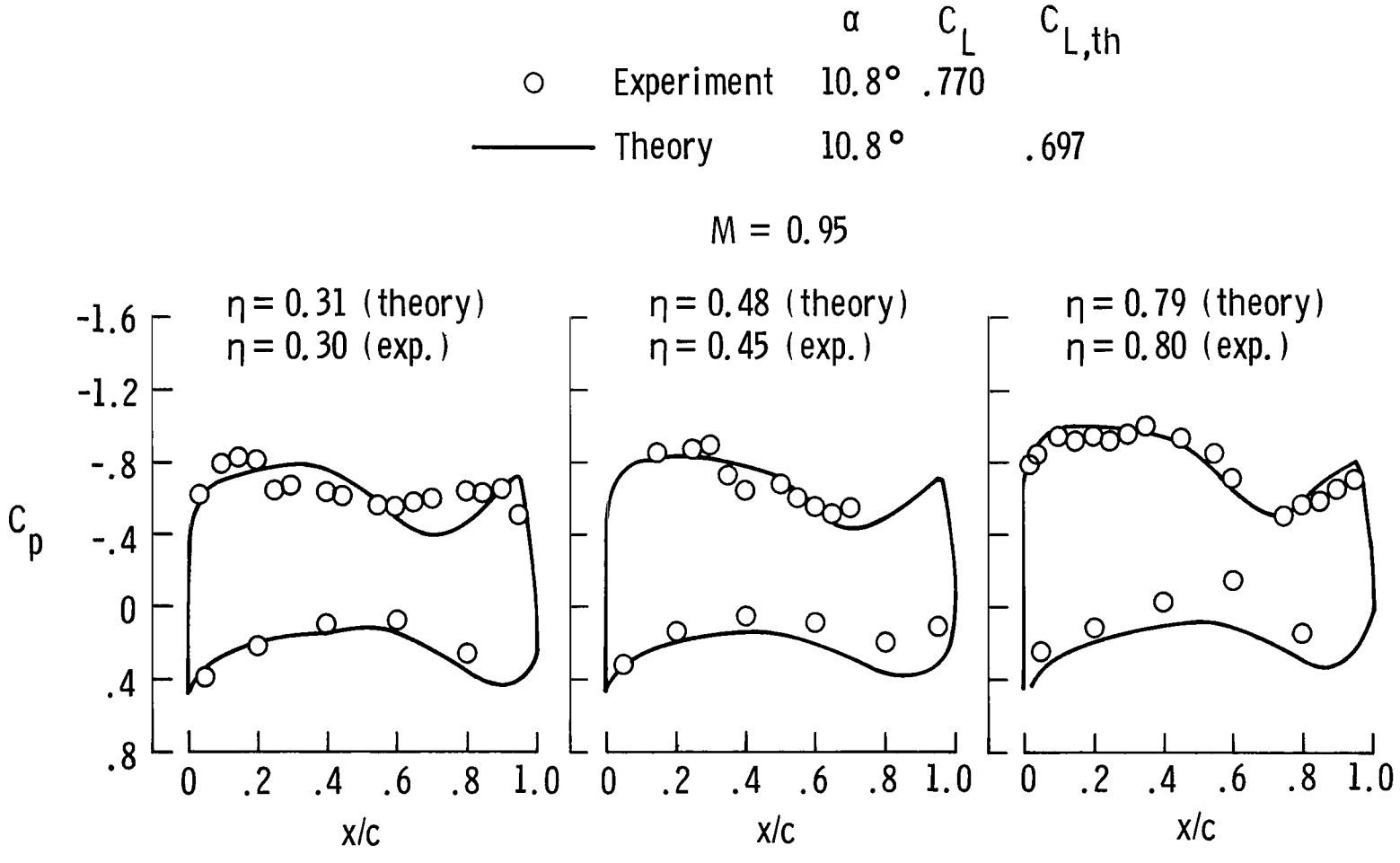

(b) Concluded.

Figure 5.- Continued.

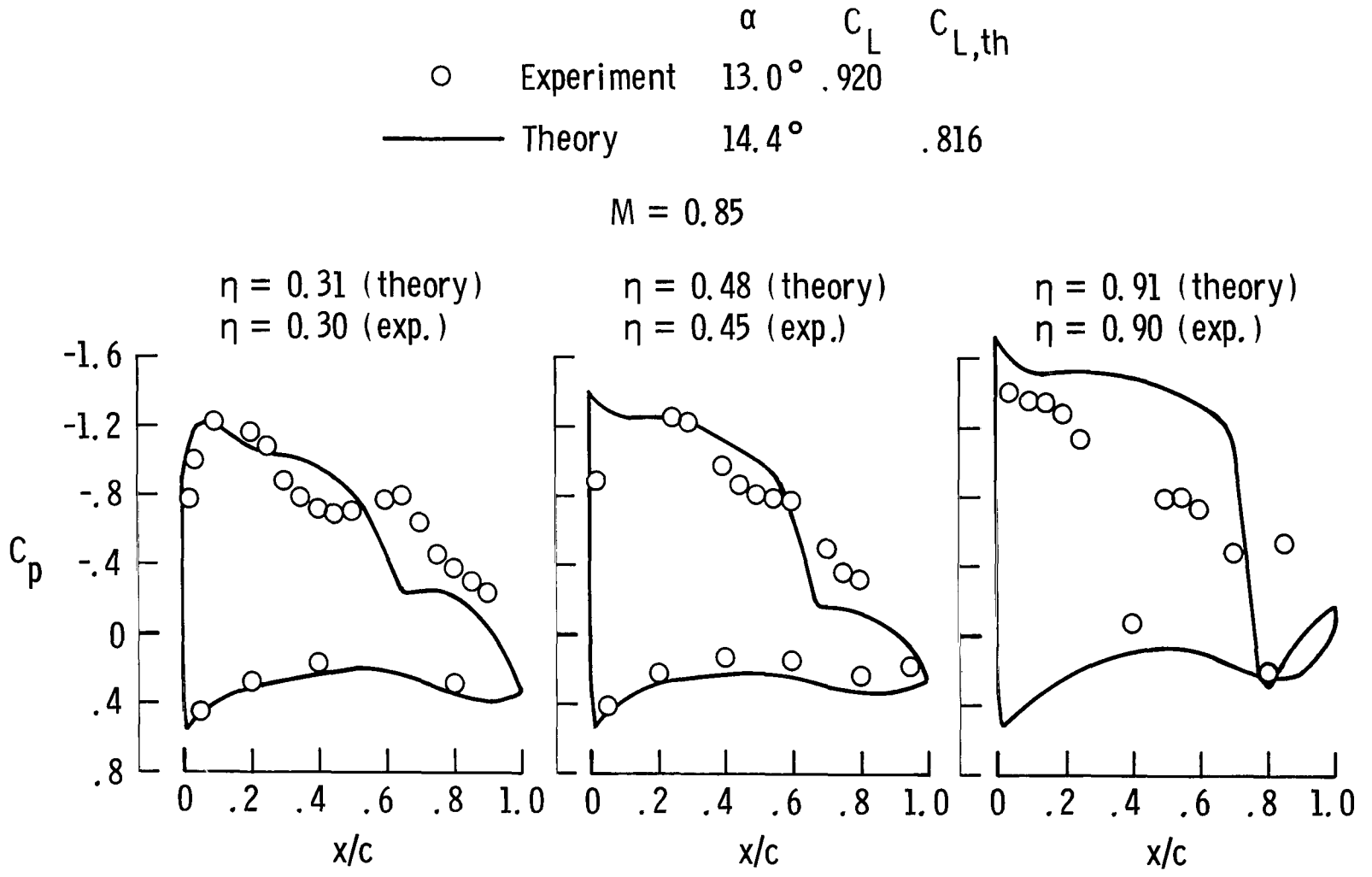

(c) SMF-2 configuration B.

Figure 5.- Continued.

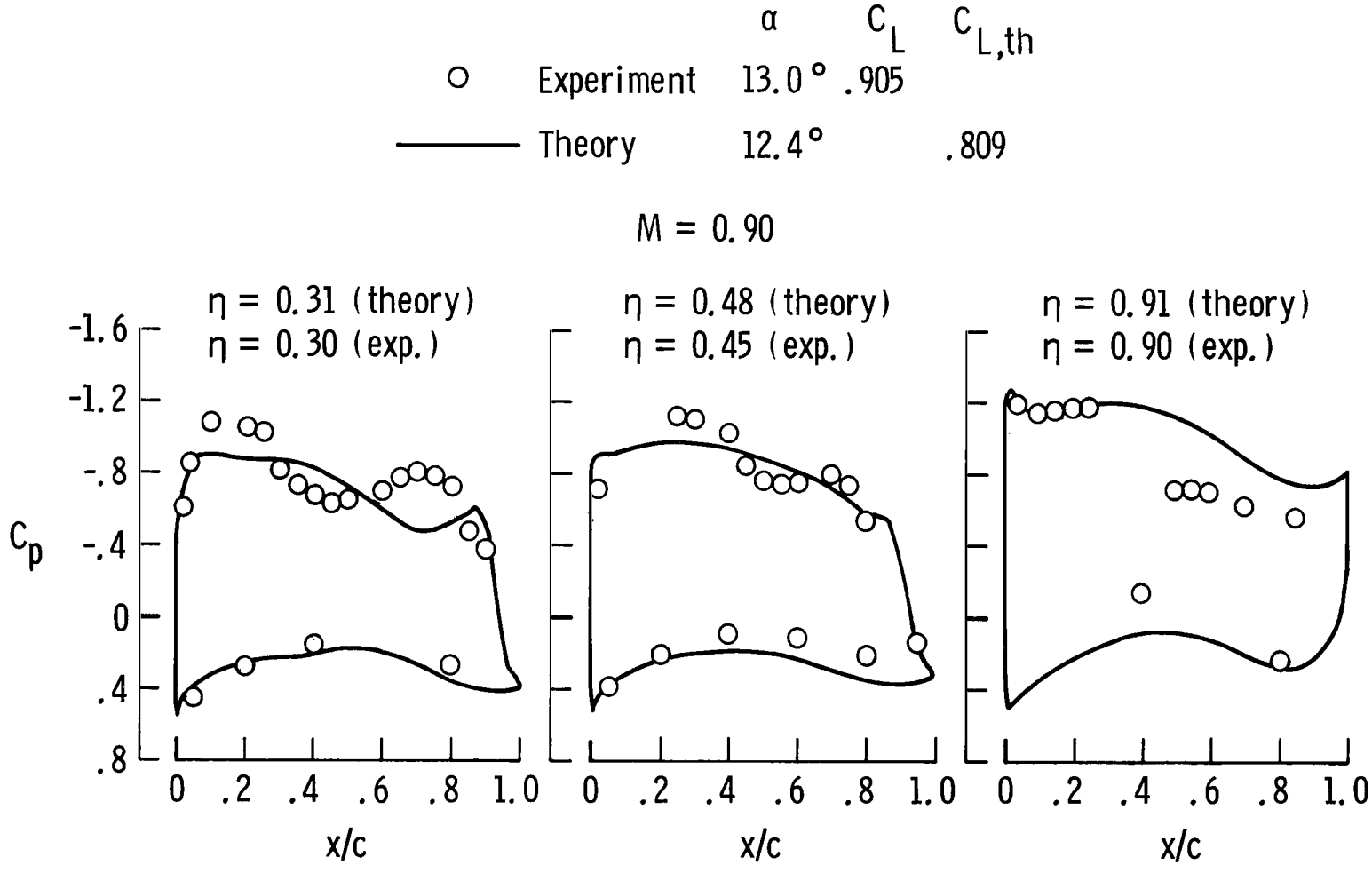

(c) Continued.

Figure 5.- Continued.

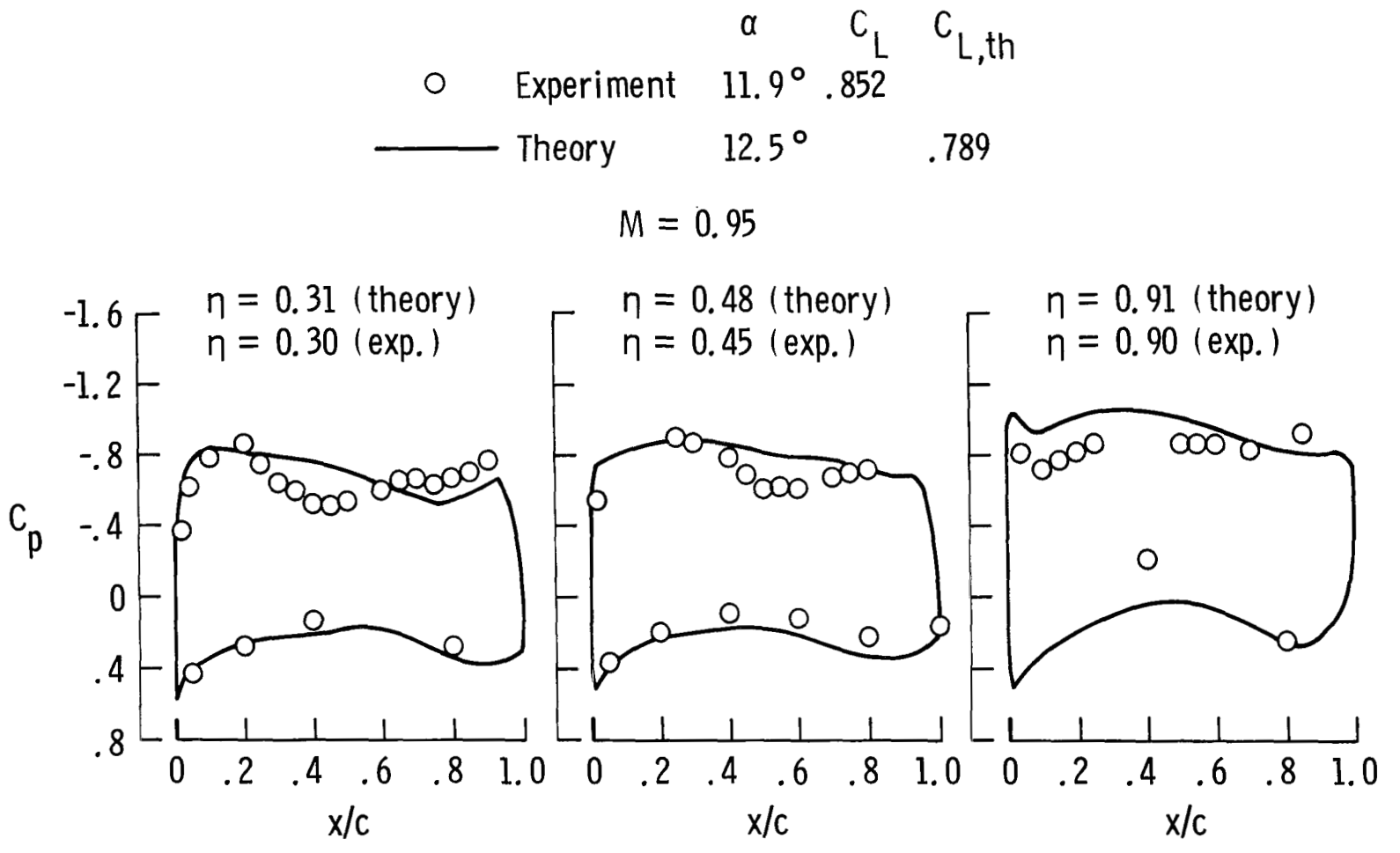

(c) Concluded.

Figure 5.- Concluded.

Configuration	α	$C_{L,th}$
A	14.2°	.817
B	14.4°	.816

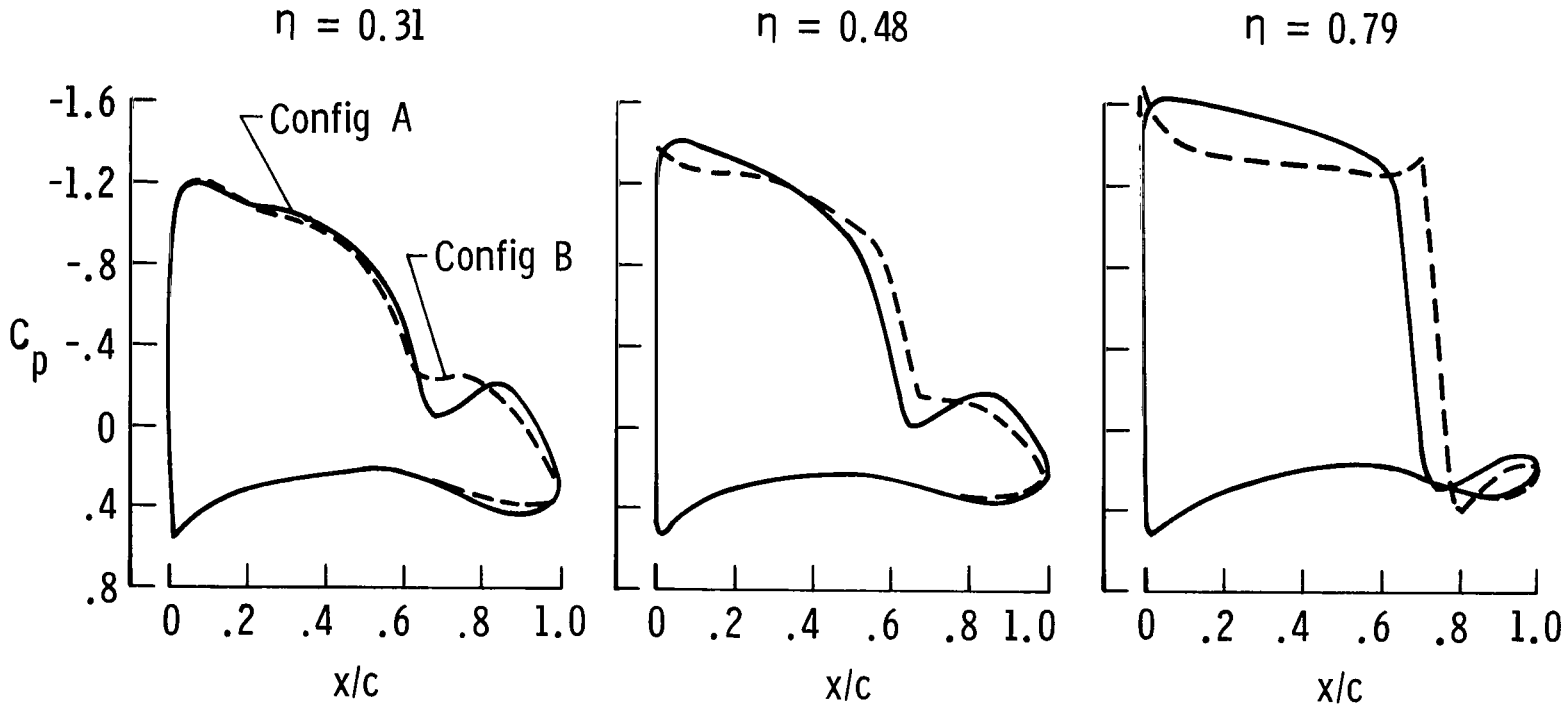

(a) M = 0.85.

Figure 6.- Comparison of theoretical wing pressure distributions for configurations A and B of SMF-2.

Configuration	α	$C_{L,th}$
A	12.6°	.816
B	12.4°	.809

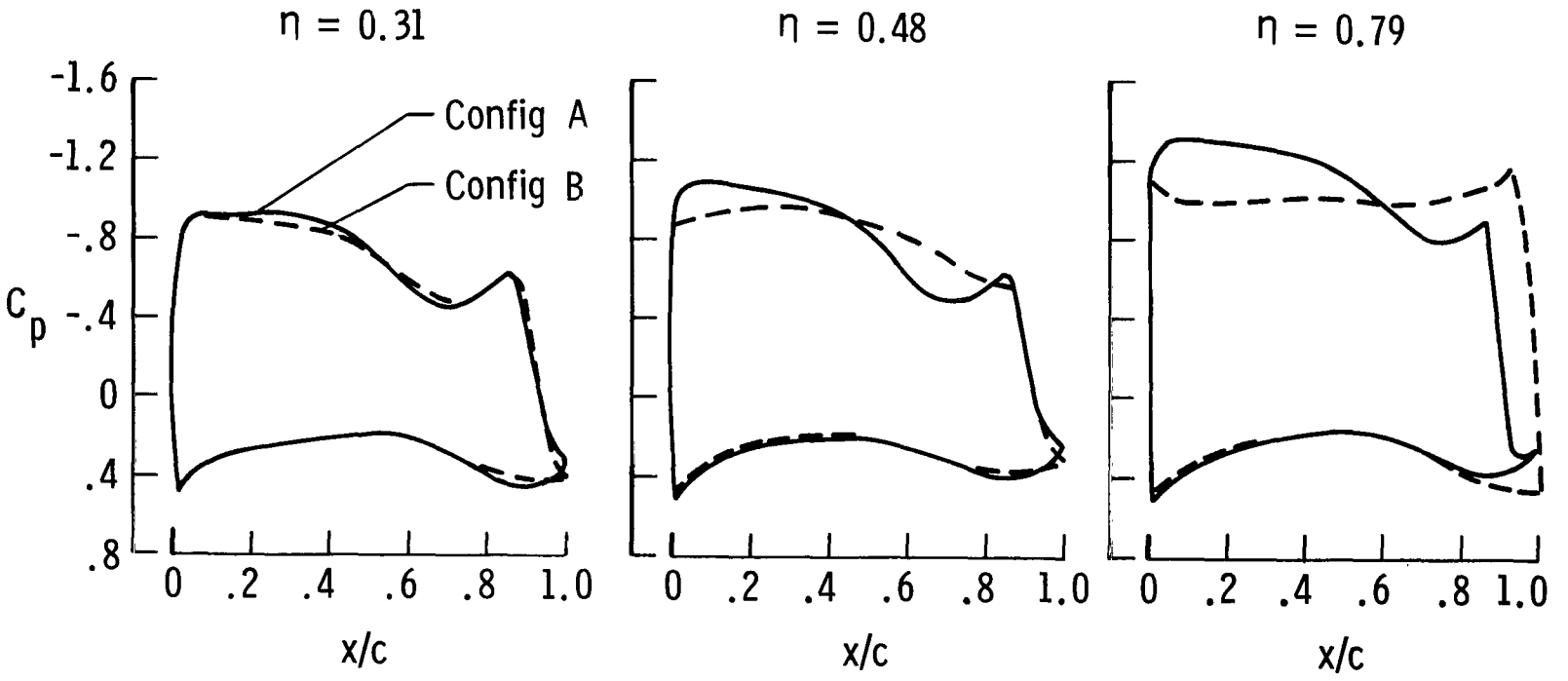

(b) M = 0.90.

Figure 6.- Continued.

Configuration	α	$C_{L,th}$
A	12.2°	.774
B	12.5°	.789

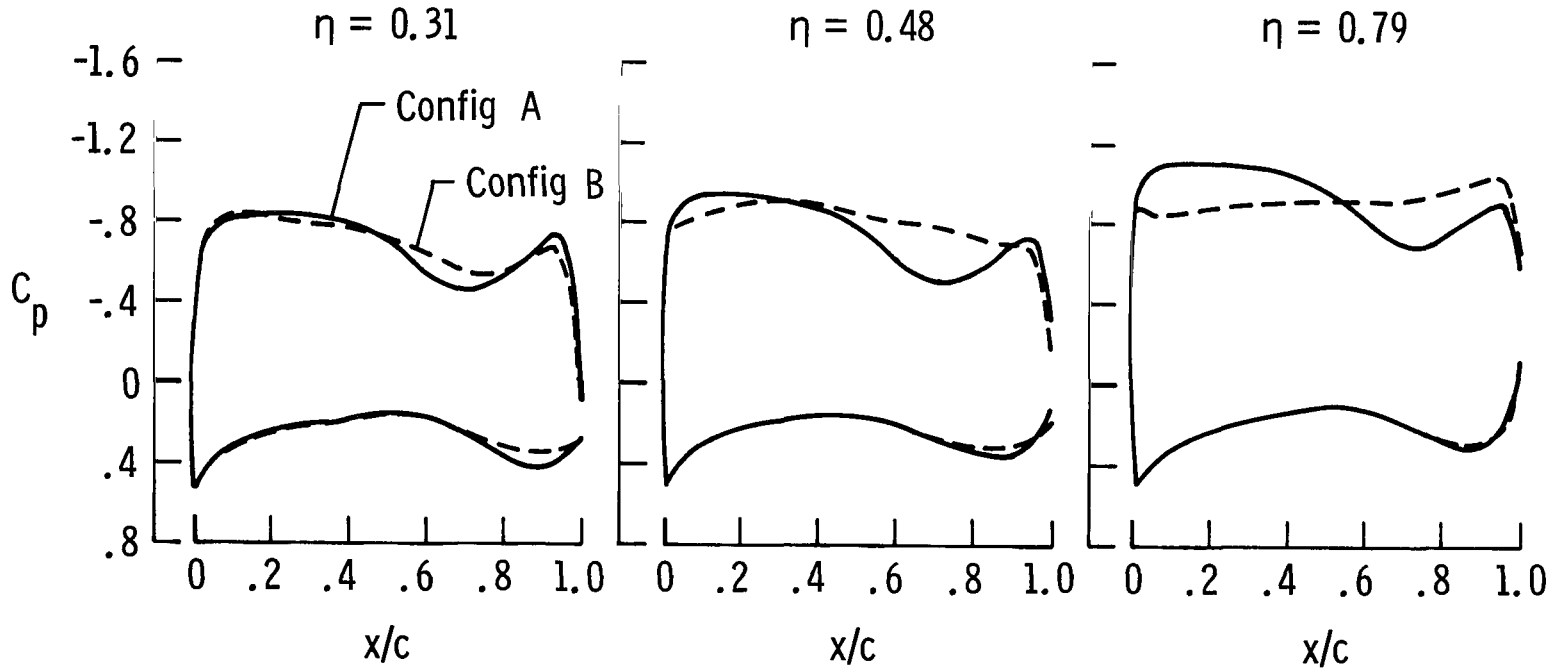

(c) M = 0.95.

Figure 6.- Concluded.

Configuration	α	$C_{L,th}$
W18	7.0°	.826
SMF-1	12.0°	.840
SMF-2 config B	14.4°	.816

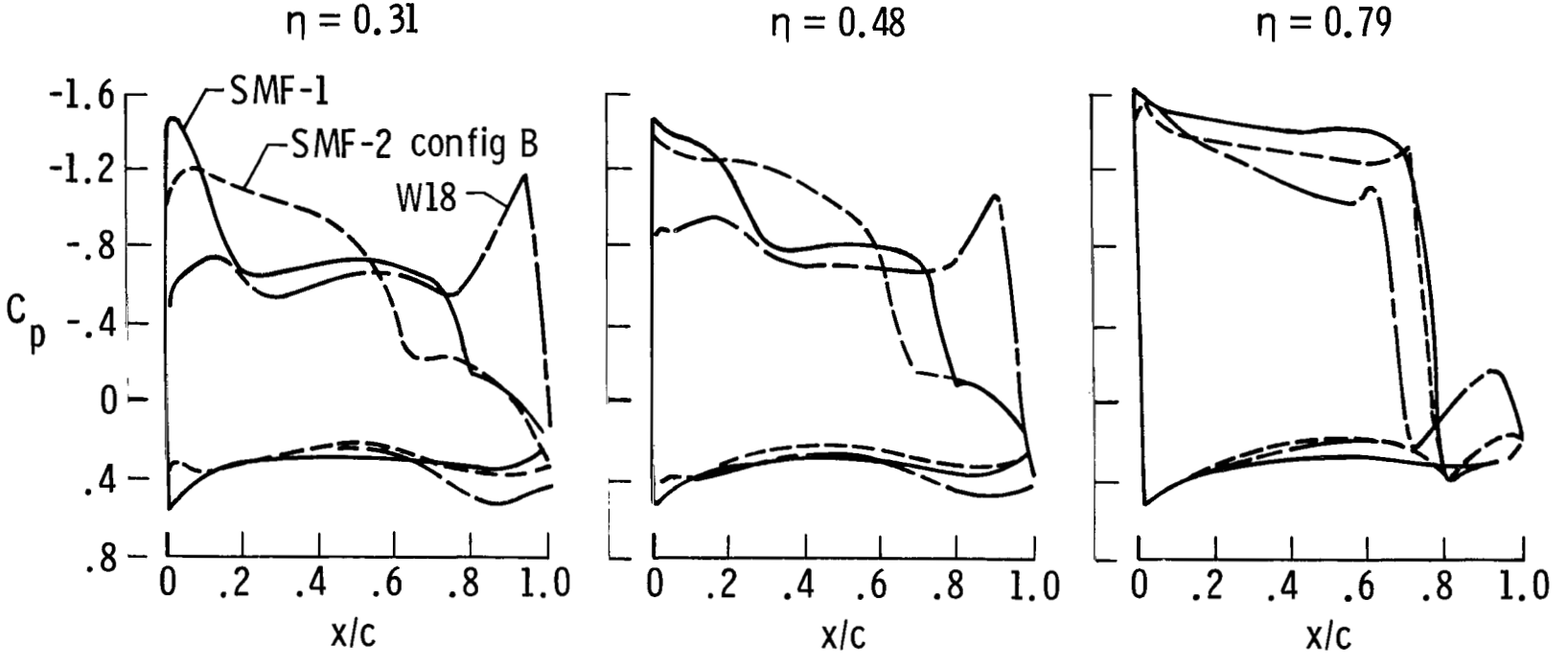

(a) M = 0.85.

Figure 7.- Comparison of theoretical wing pressure distributions for W18, SMF-1, and configuration B of SMF-2.

Configuration		α	$C_{L,th}$
W18		6.7°	.812
SMF-1		9.6°	.803
SMF-2	config B	12.4°	.809

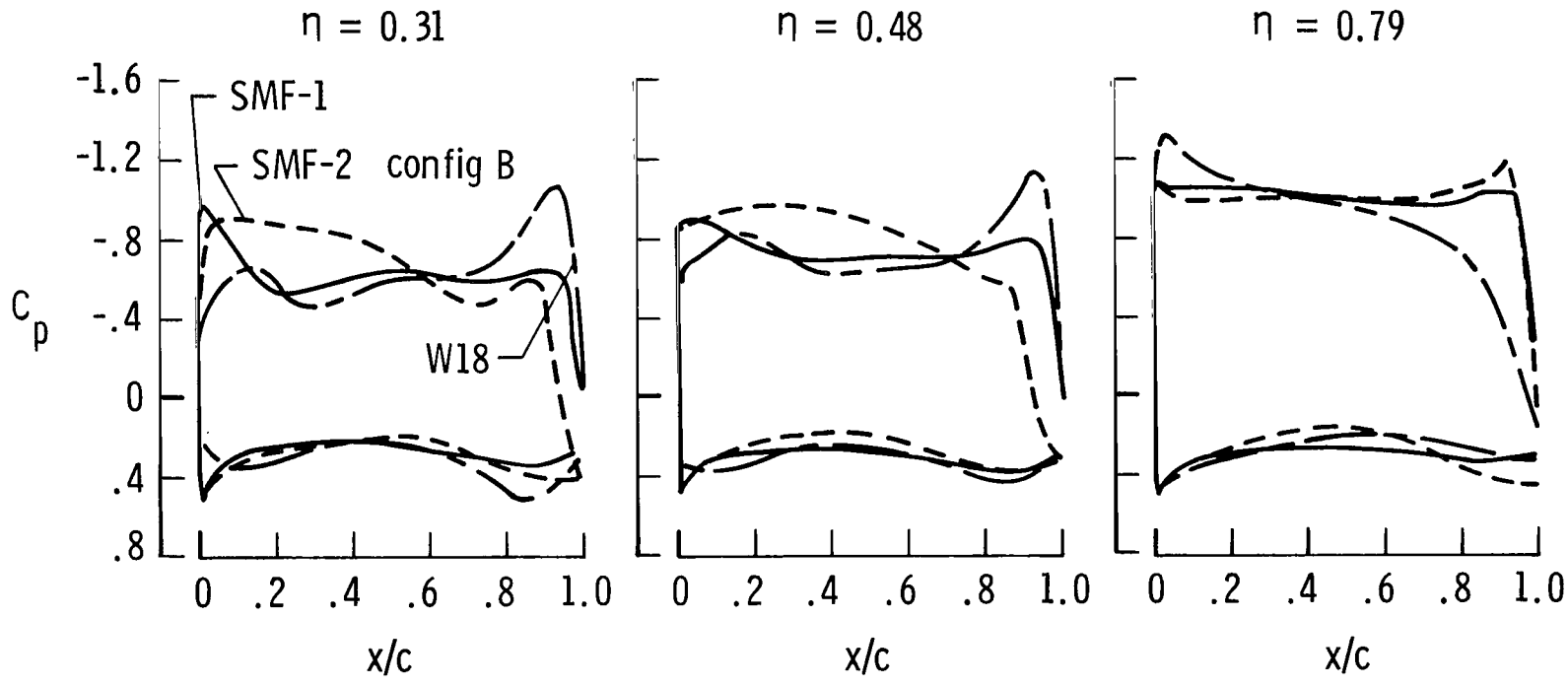

(b) M = 0.90.

Figure 7.- Continued.

Configuration		α	$C_{L,th}$
W18		7.3°	.788
SMF-1		10.3°	.777
SMF-2	config B	12.5°	.789

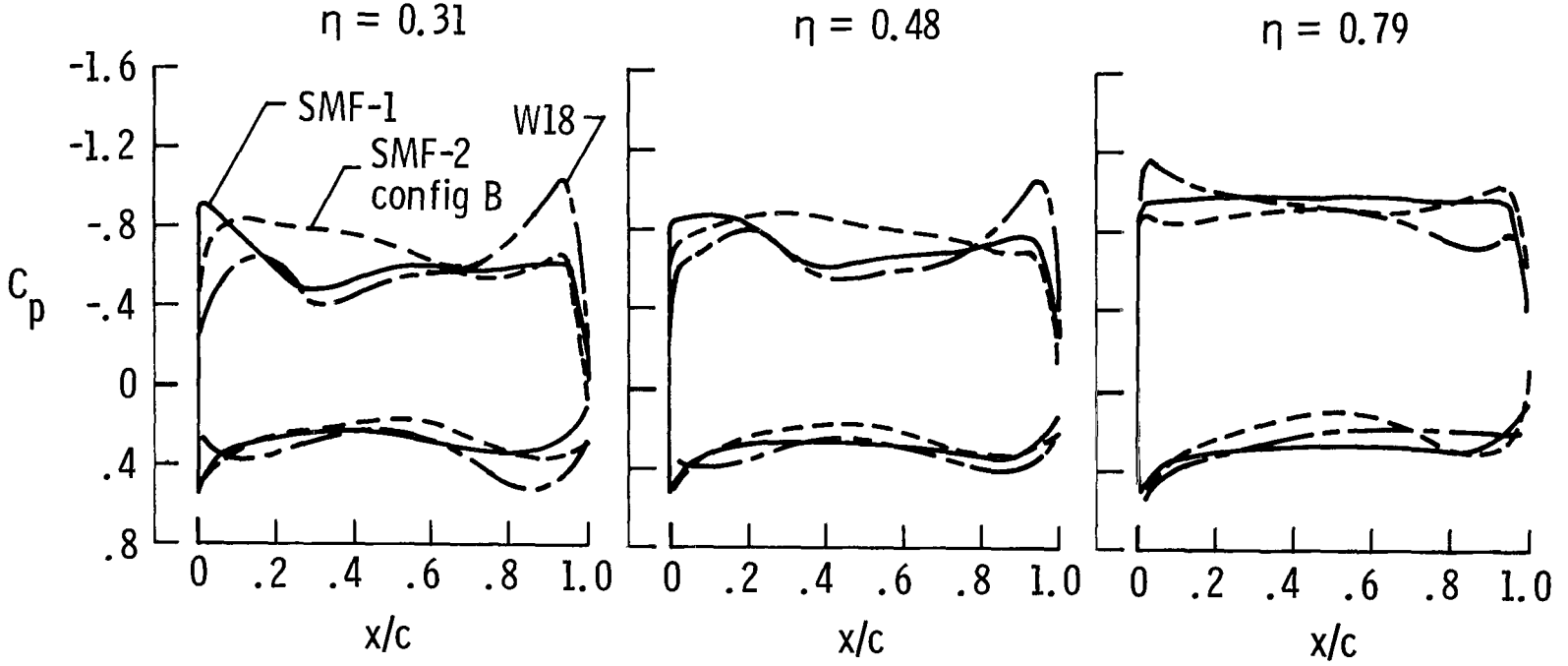

(c) M = 0.95.

Figure 7.- Concluded.

Twist	α	$C_{L,th}$	$C_{D,th}$
SMF-1 twist	9.1^{o}	.815	.1021
W18 twist	6.7^{o}	.812	.1055

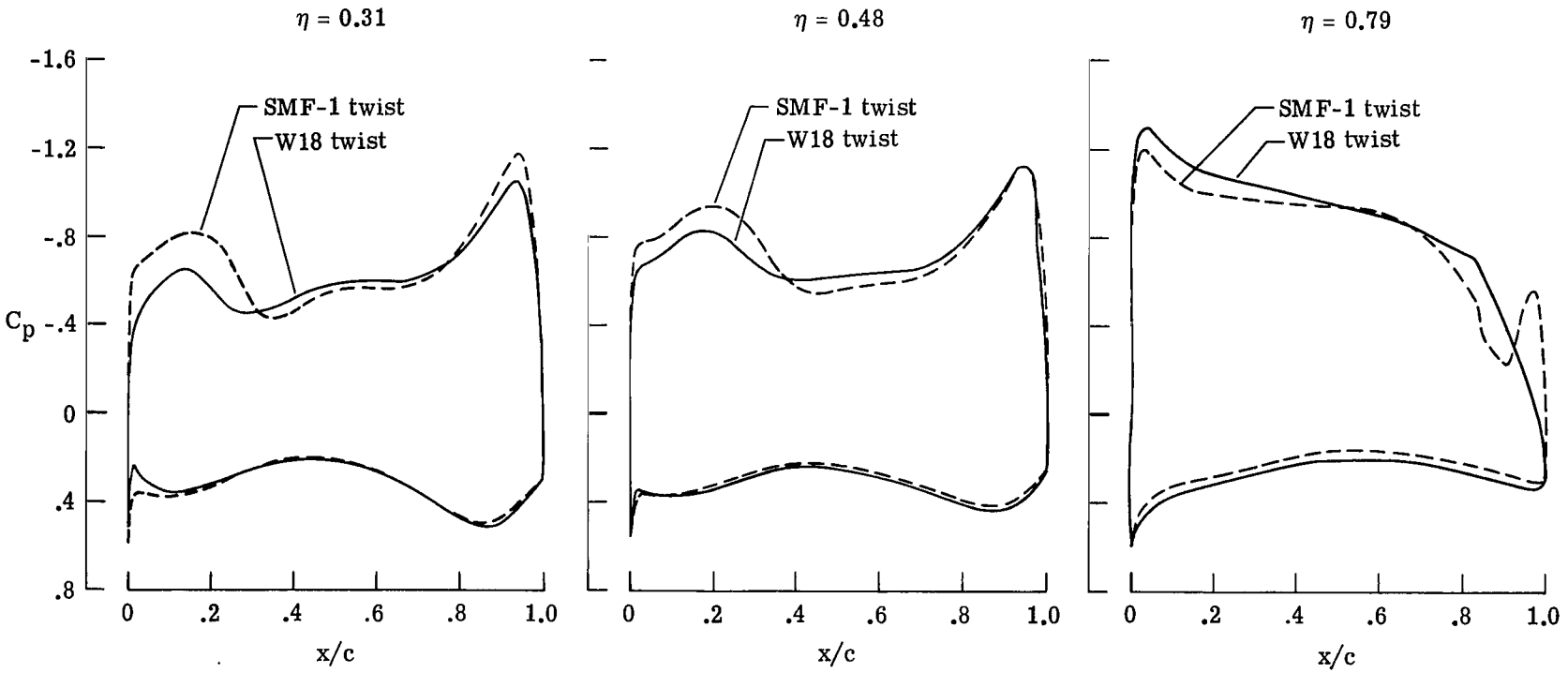

Figure 8.- Effect of SMF-1 twist distribution on theoretical wing pressure distribution of W18. M = 0.90.

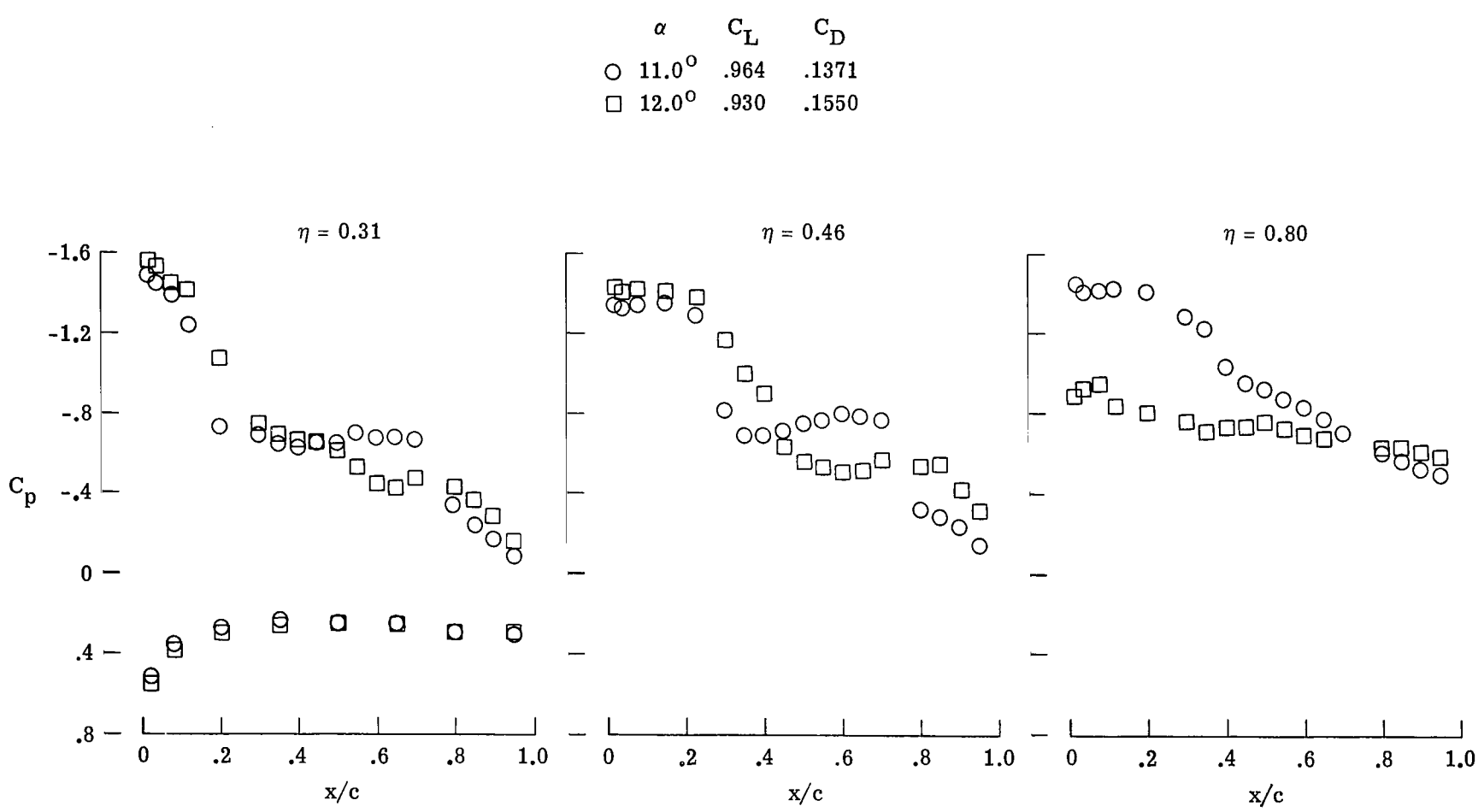

(a) M = 0.85.

Figure 9.- Experimental wing pressure distributions on SMF-1 in regions of breaks in the drag polars.

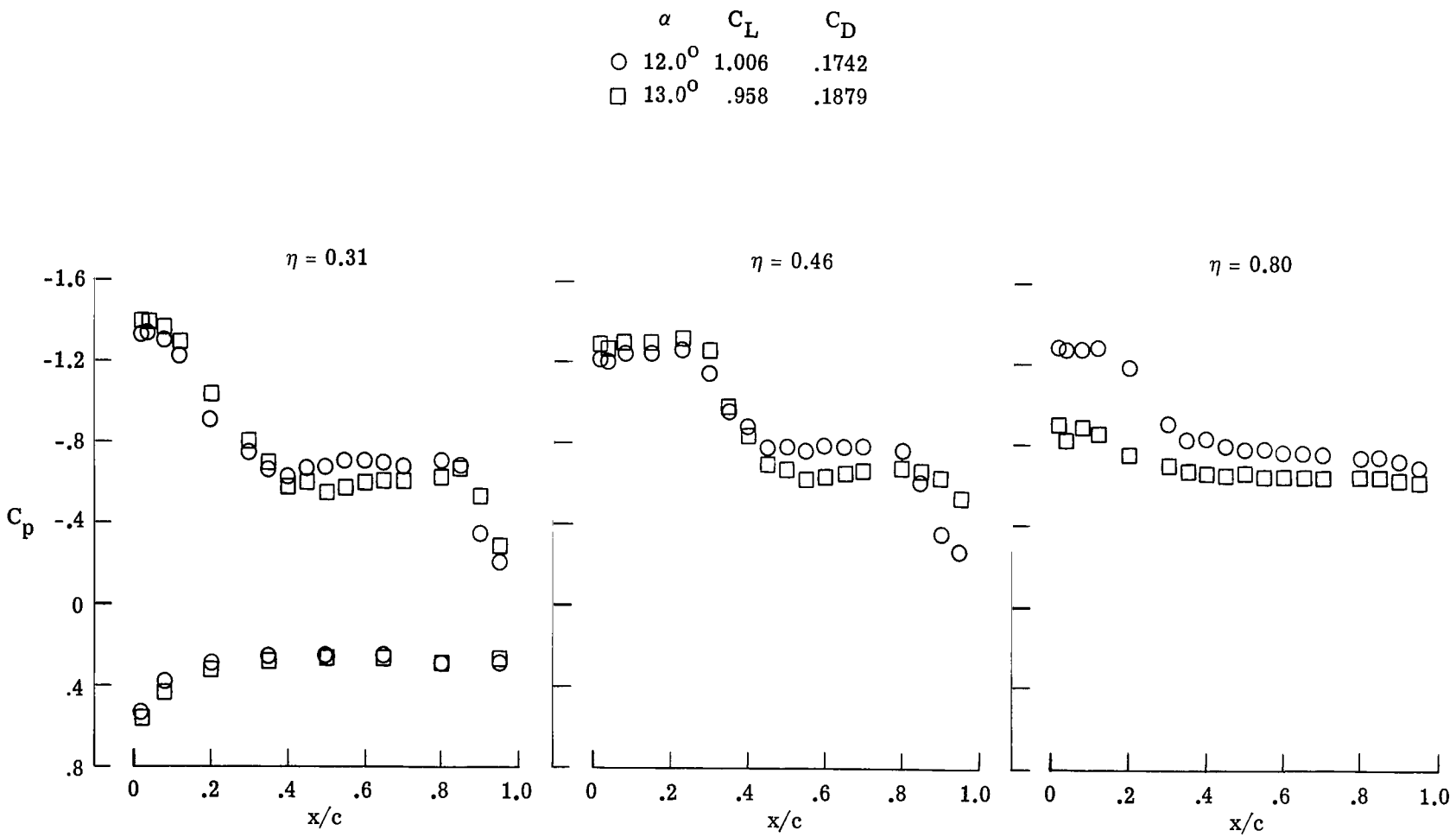

(b) M = 0.90.

Figure 9.- Concluded.

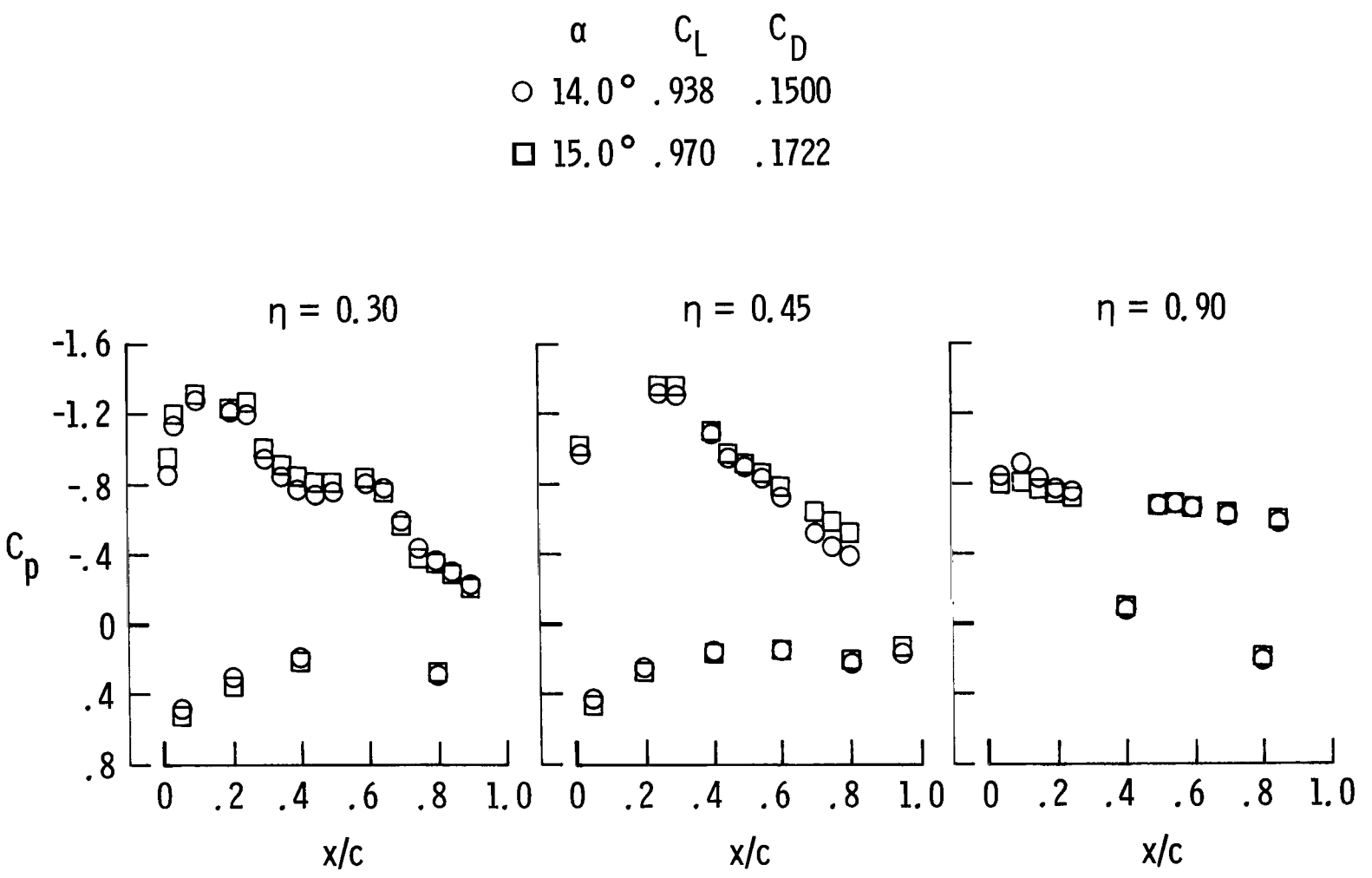

(a) M = 0.85.

Figure 10.- Experimental wing pressure distributions on configuration B of SMF-2 in regions of breaks in the SMF-1 drag polars.

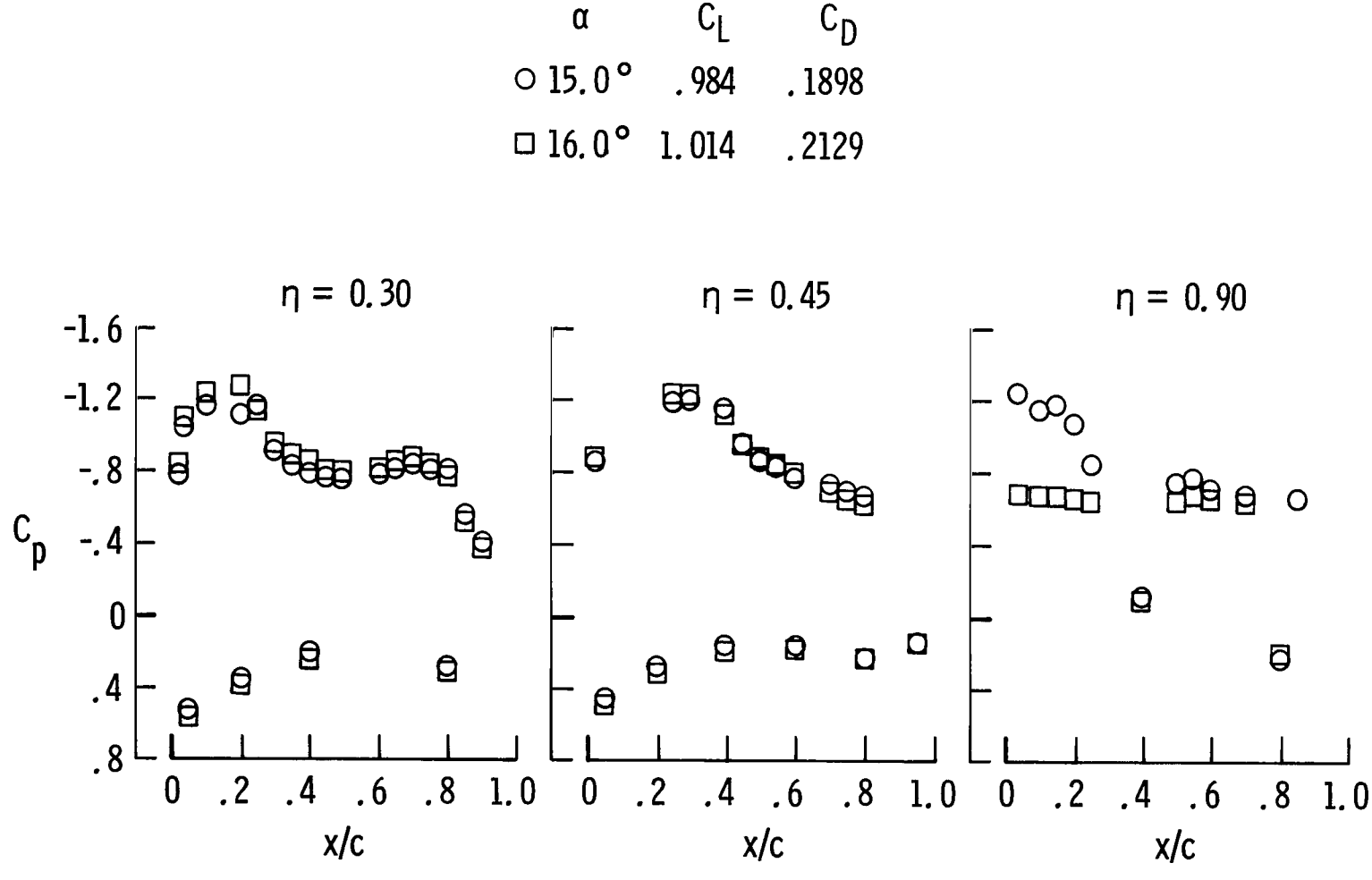

(b) M = 0.90.

Figure 10.- Concluded.

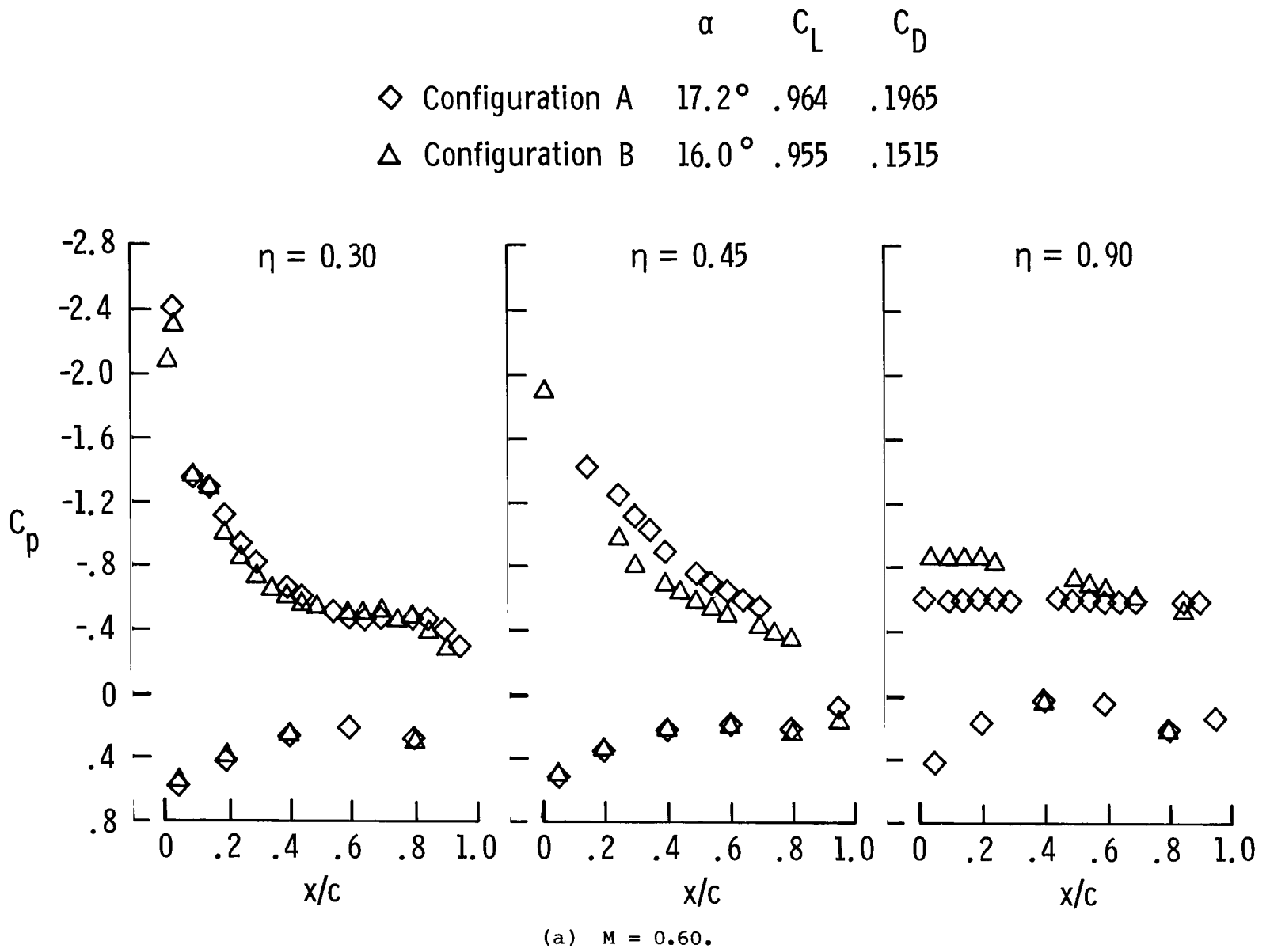

(a) M = 0.60.

Figure 11.- Comparison of experimental wing pressure distributions for configurations A and B of SMF-2.

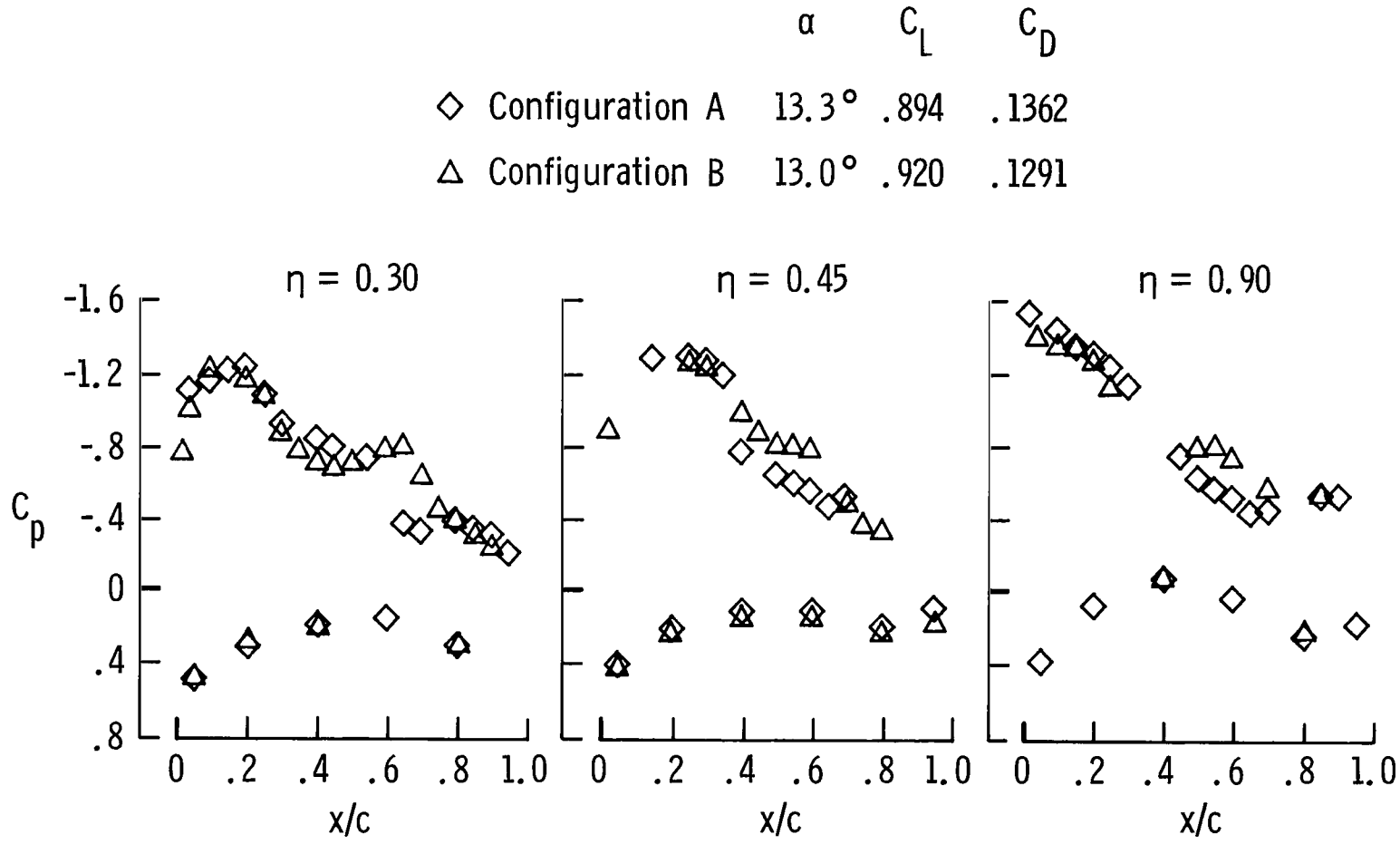

(b) M = 0.85.

Figure 11.- Continued.

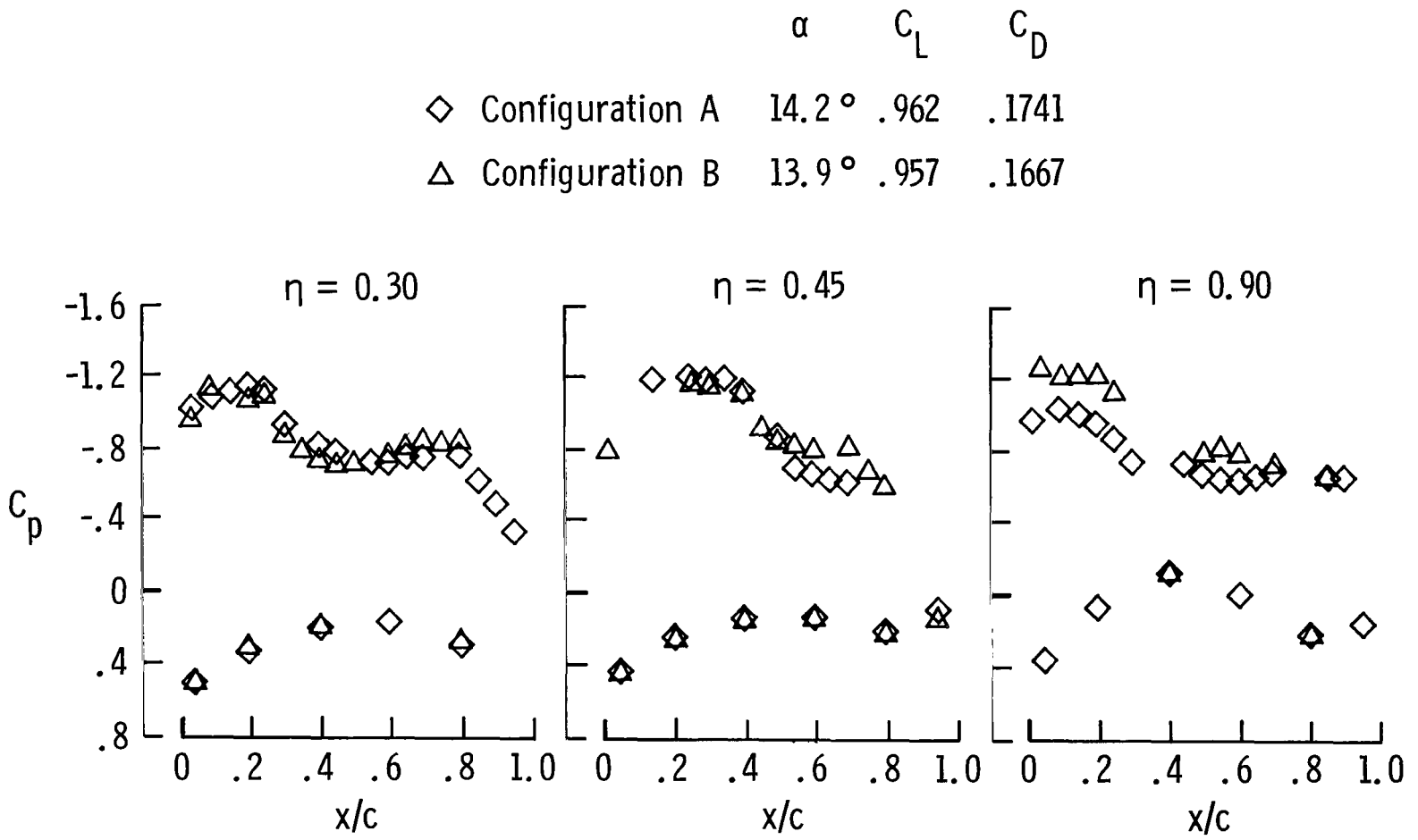

(c) M = 0.90.

Figure 11.- Continued.

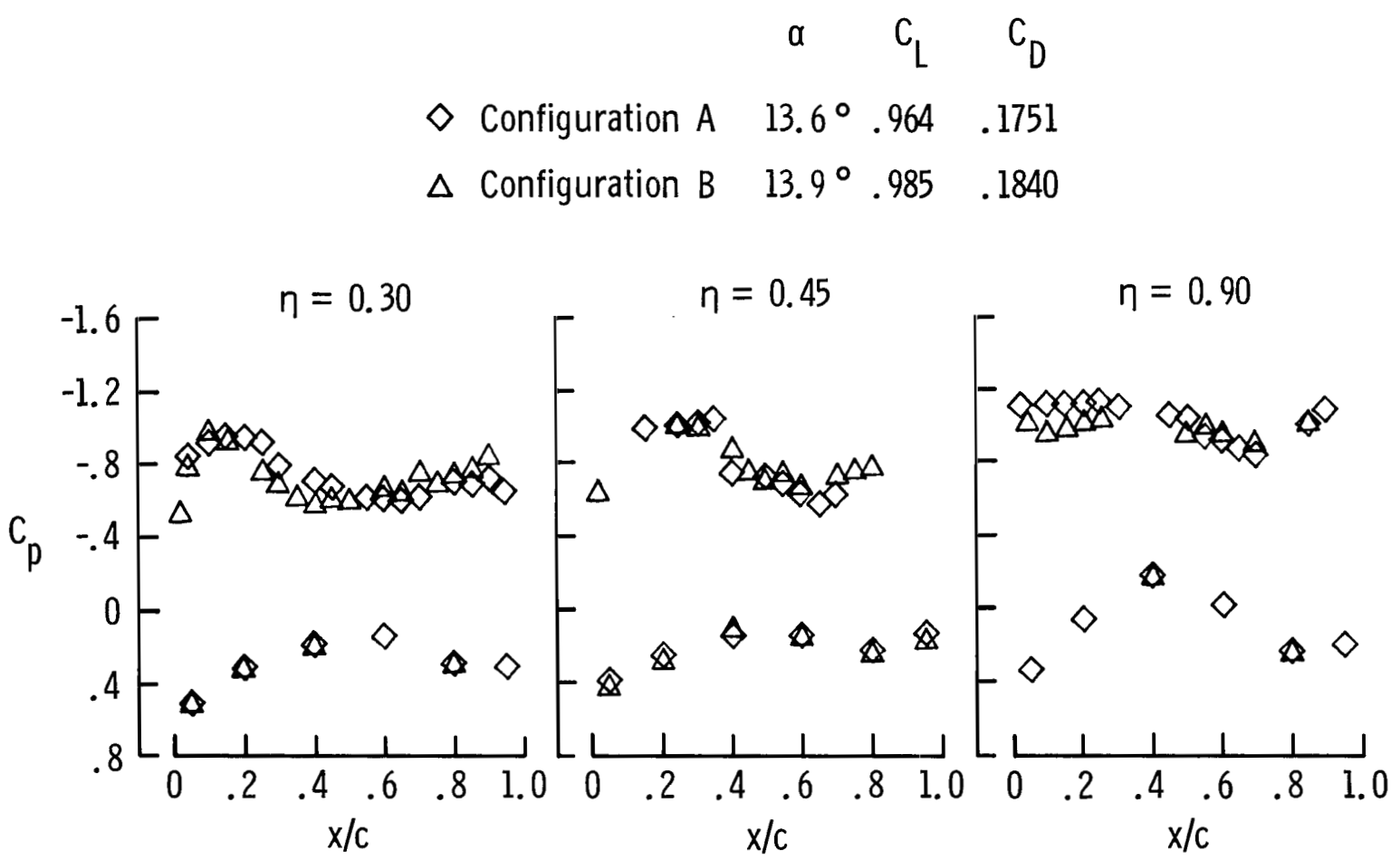

(d) M = 0.95.

Figure 11.- Concluded.

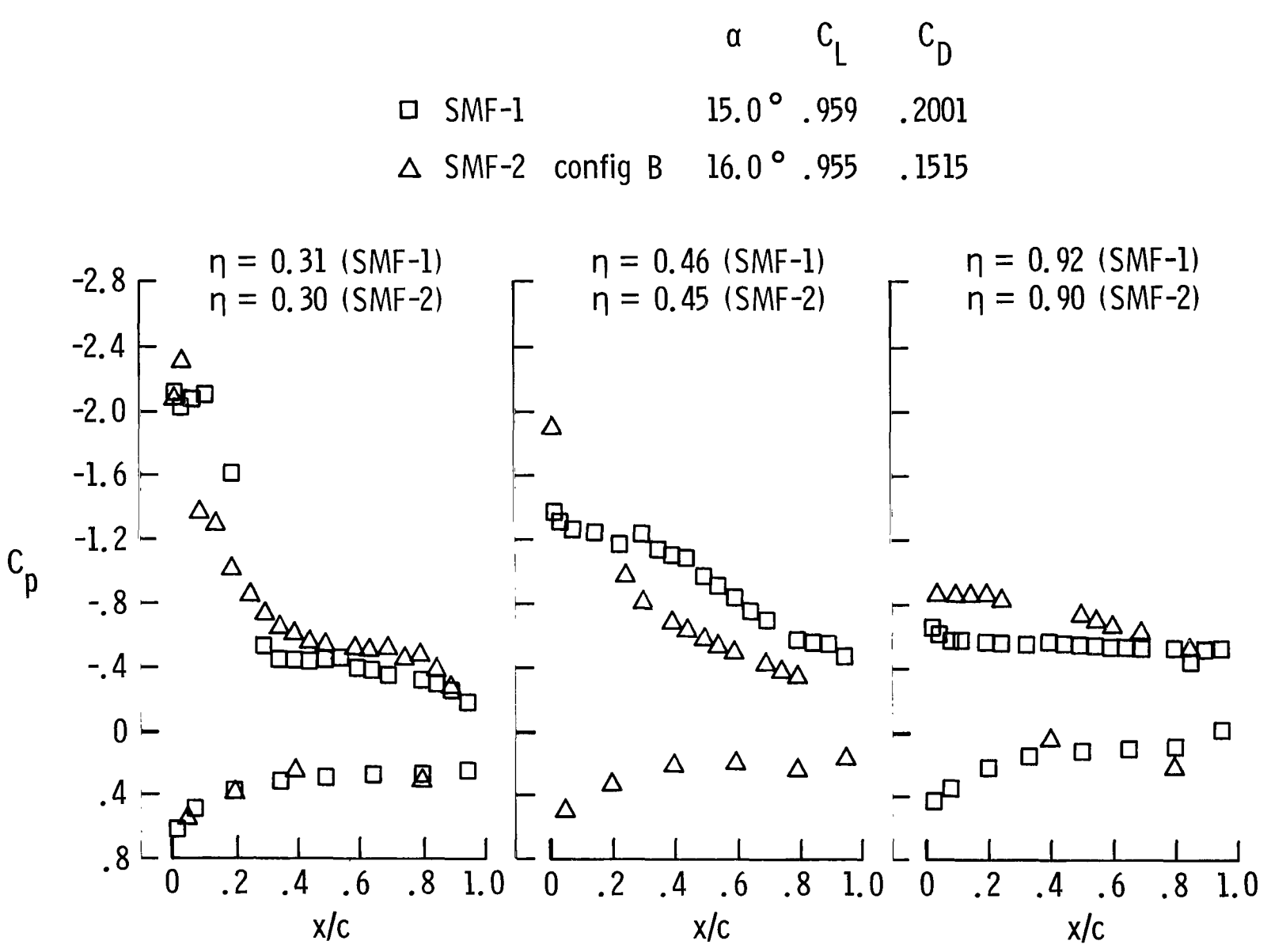

(a) M = 0.60.

Figure 12.- Comparison of experimental wing pressure distributions for SMF-1 and configuration B of SMF-2.

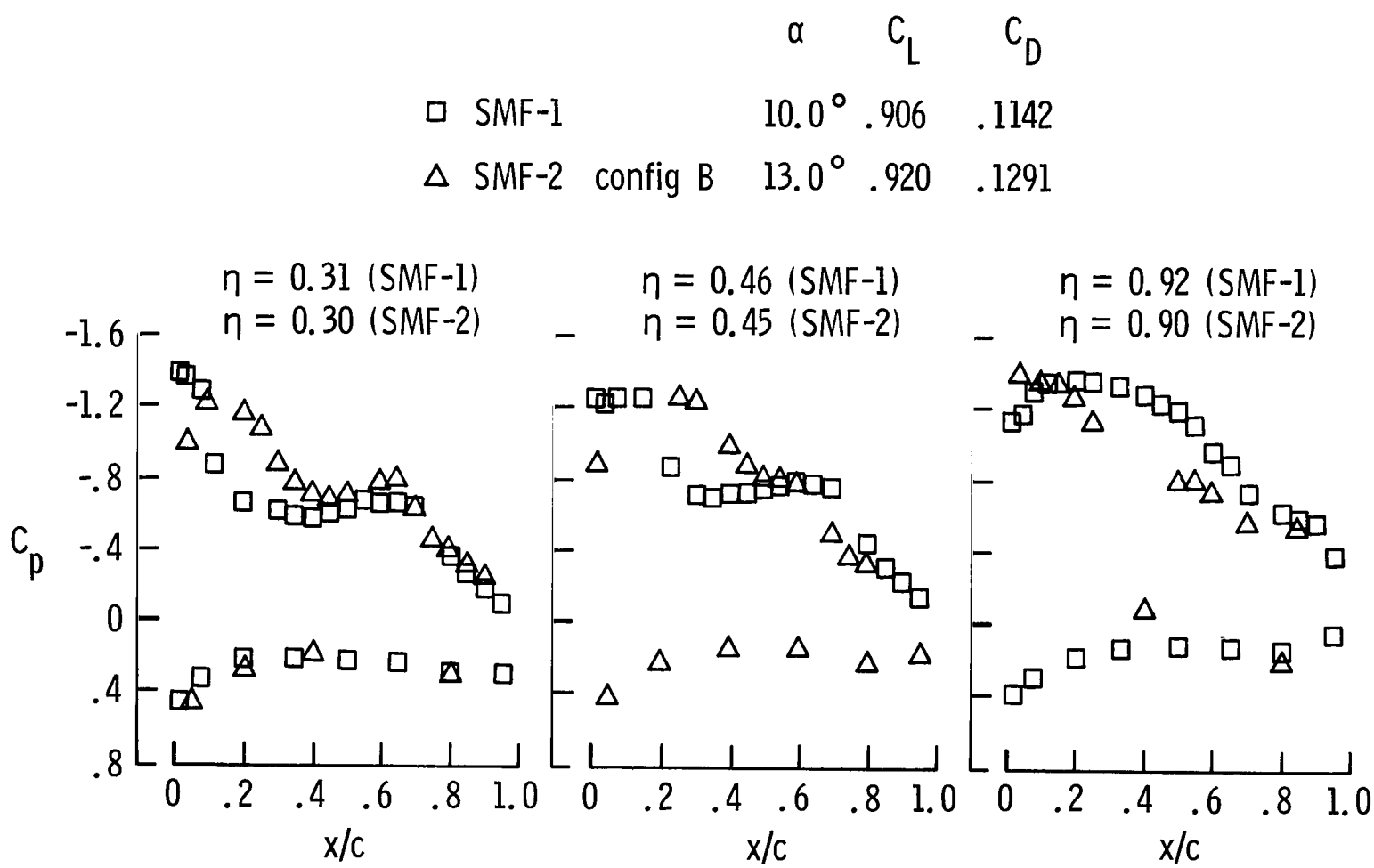

(b) M = 0.85.

Figure 12.- Continued.

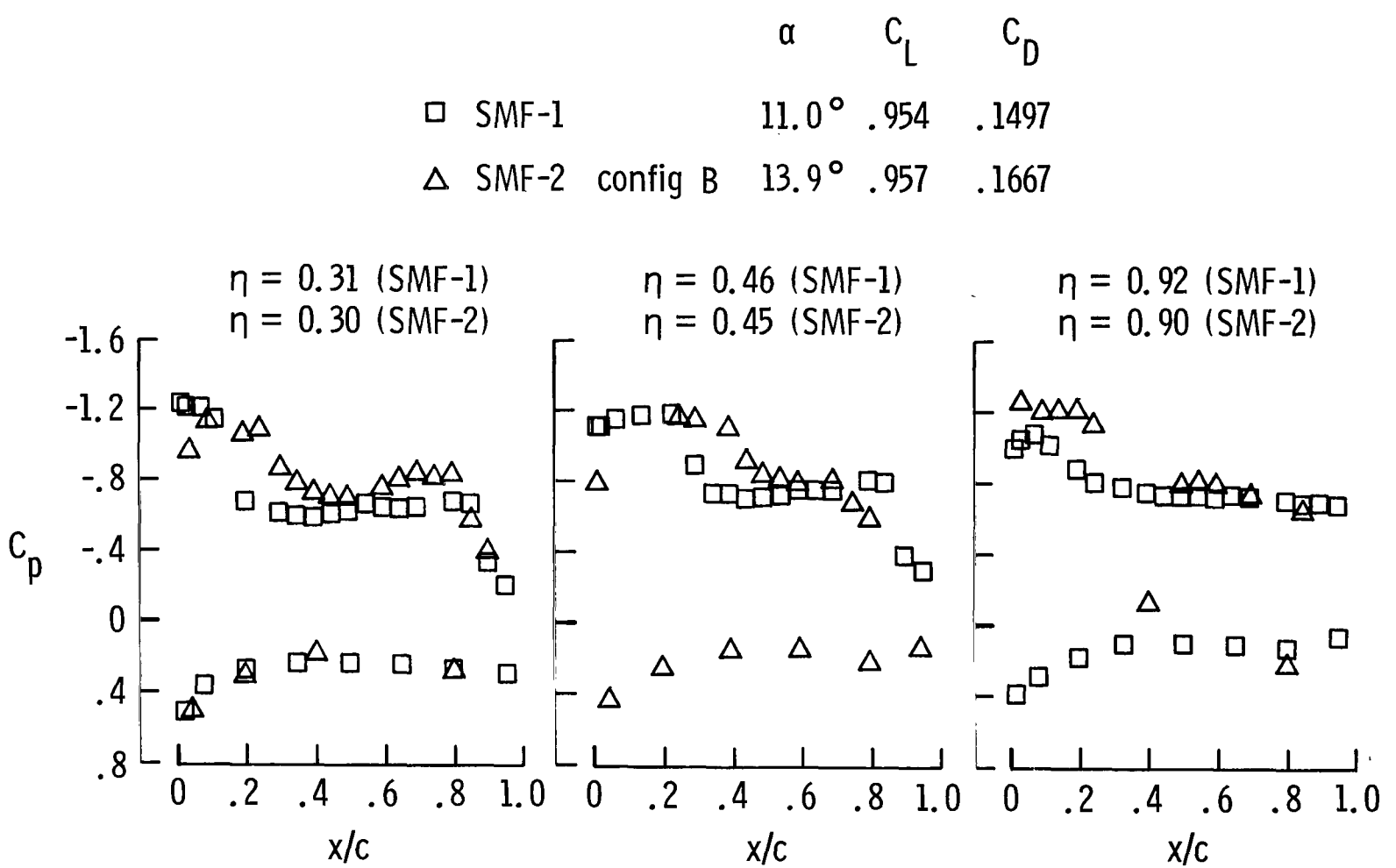

(c) M = 0.90.

Figure 12.- Continued.

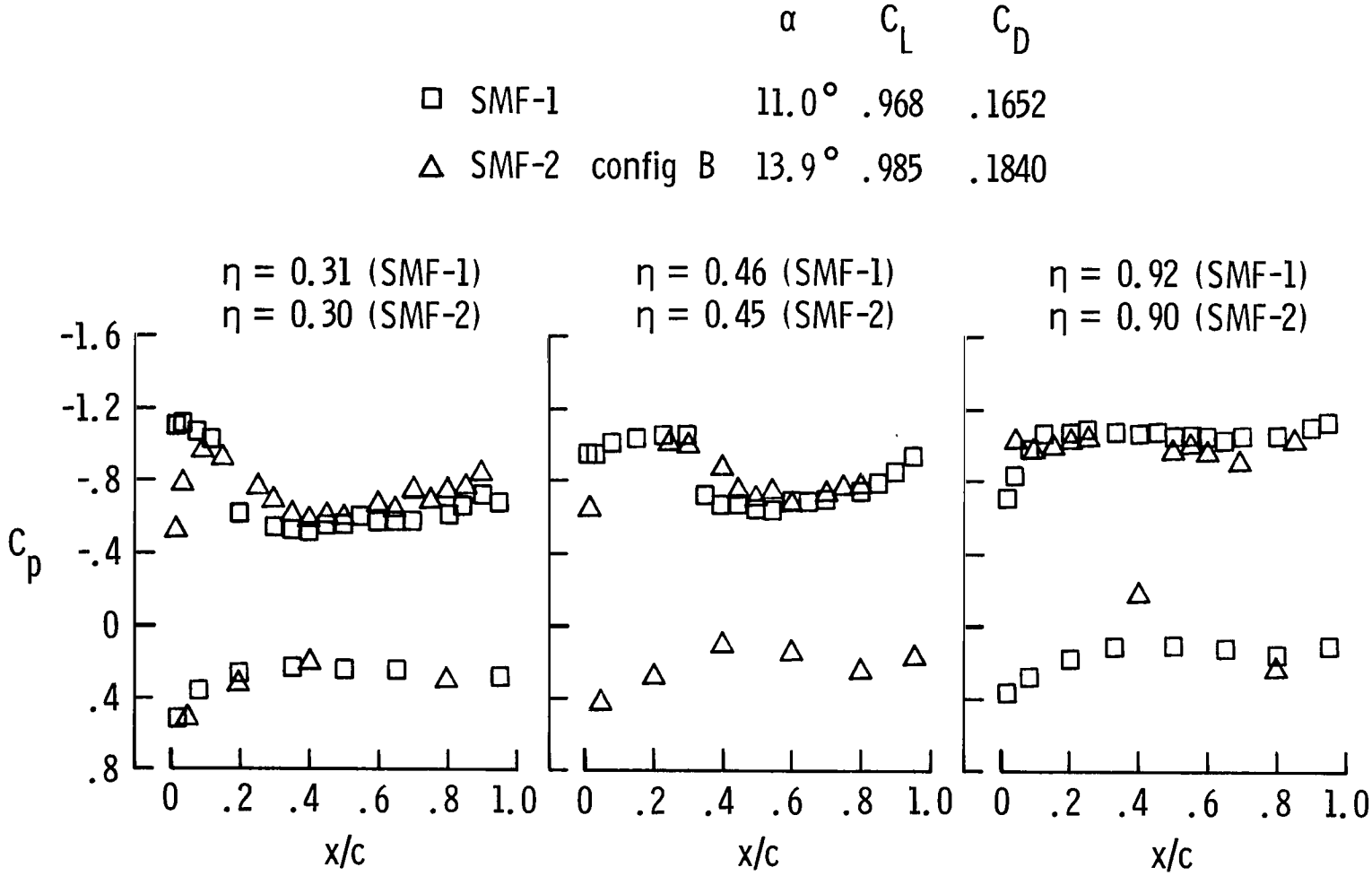

(d) M = 0.95.

Figure 12.- Concluded.

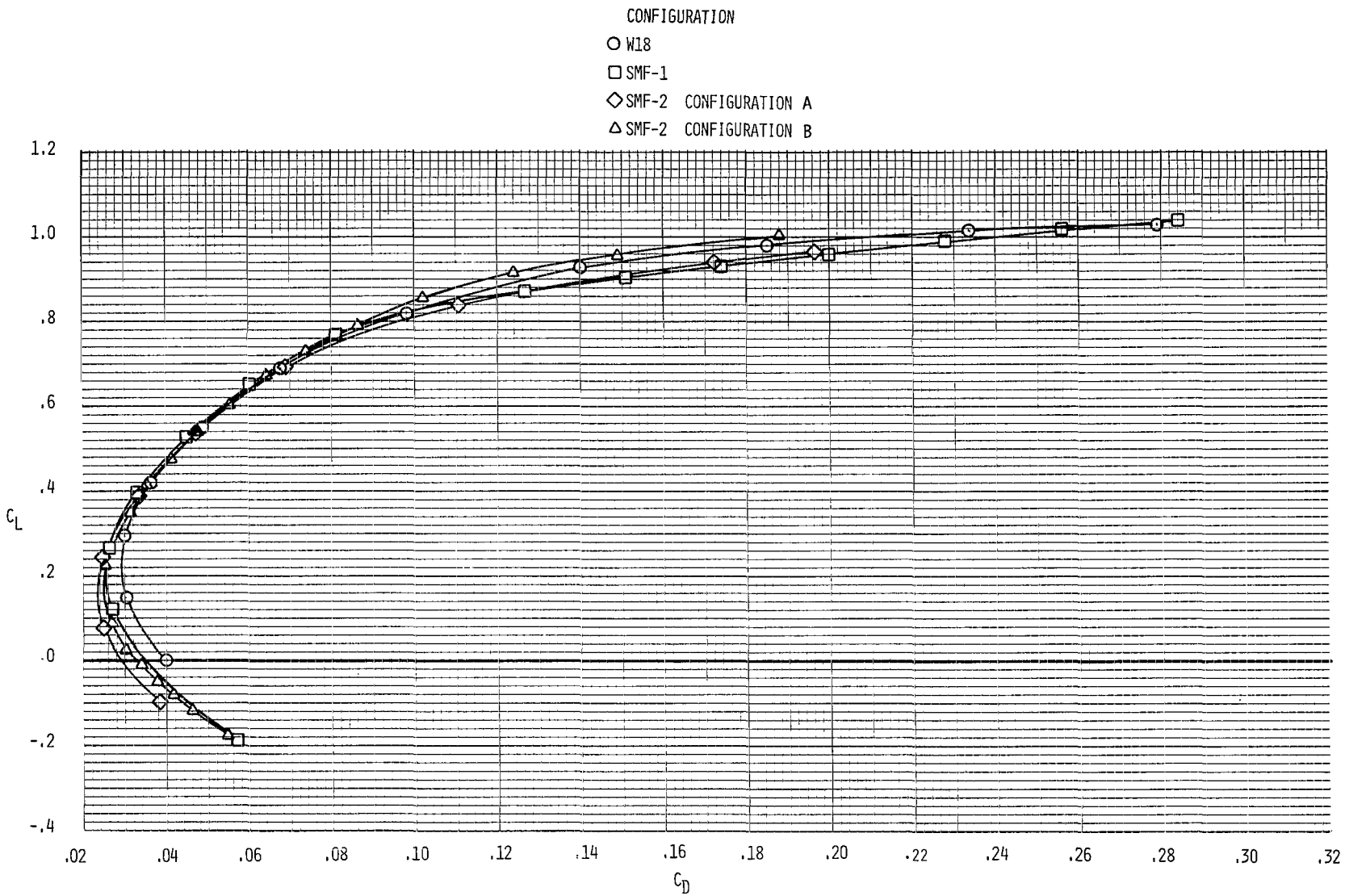

(a) M = 0.60.

Figure 13.- Effect of supercritical wing geometry on experimental lift and drag characteristics.

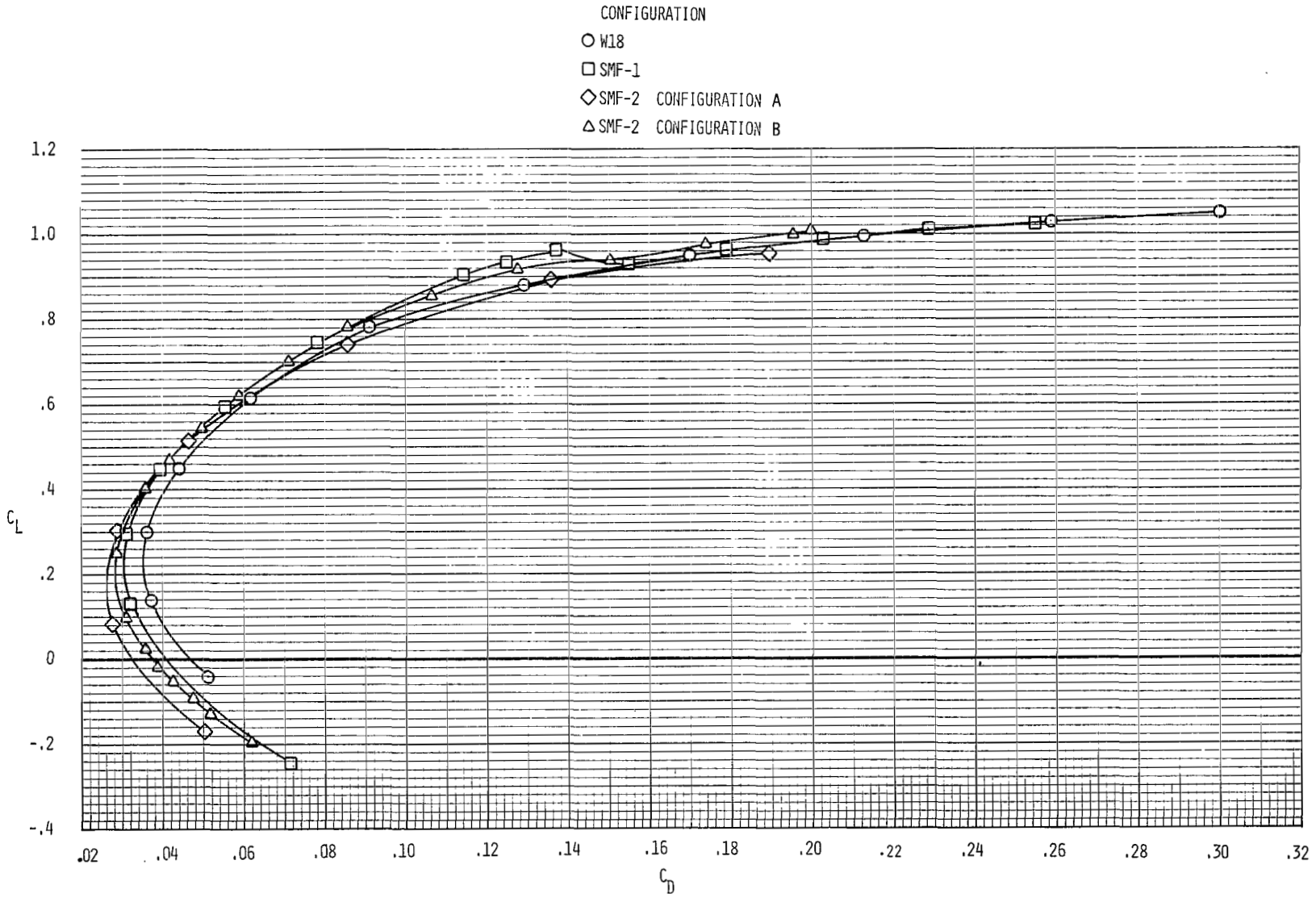

(b) M = 0.85.

Figure 13.- Continued.

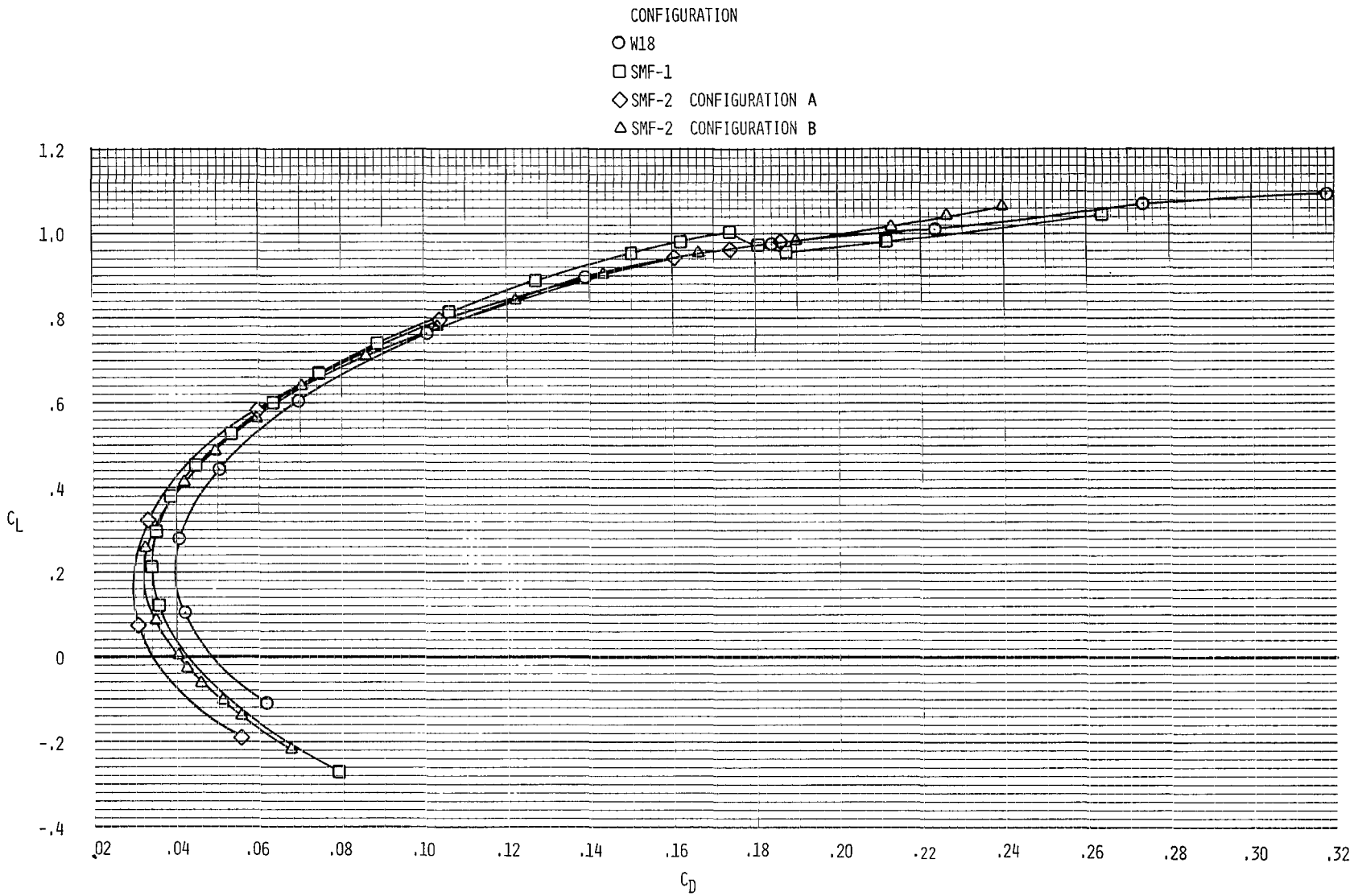

(c) M = 0.90.

Figure 13.- Continued.

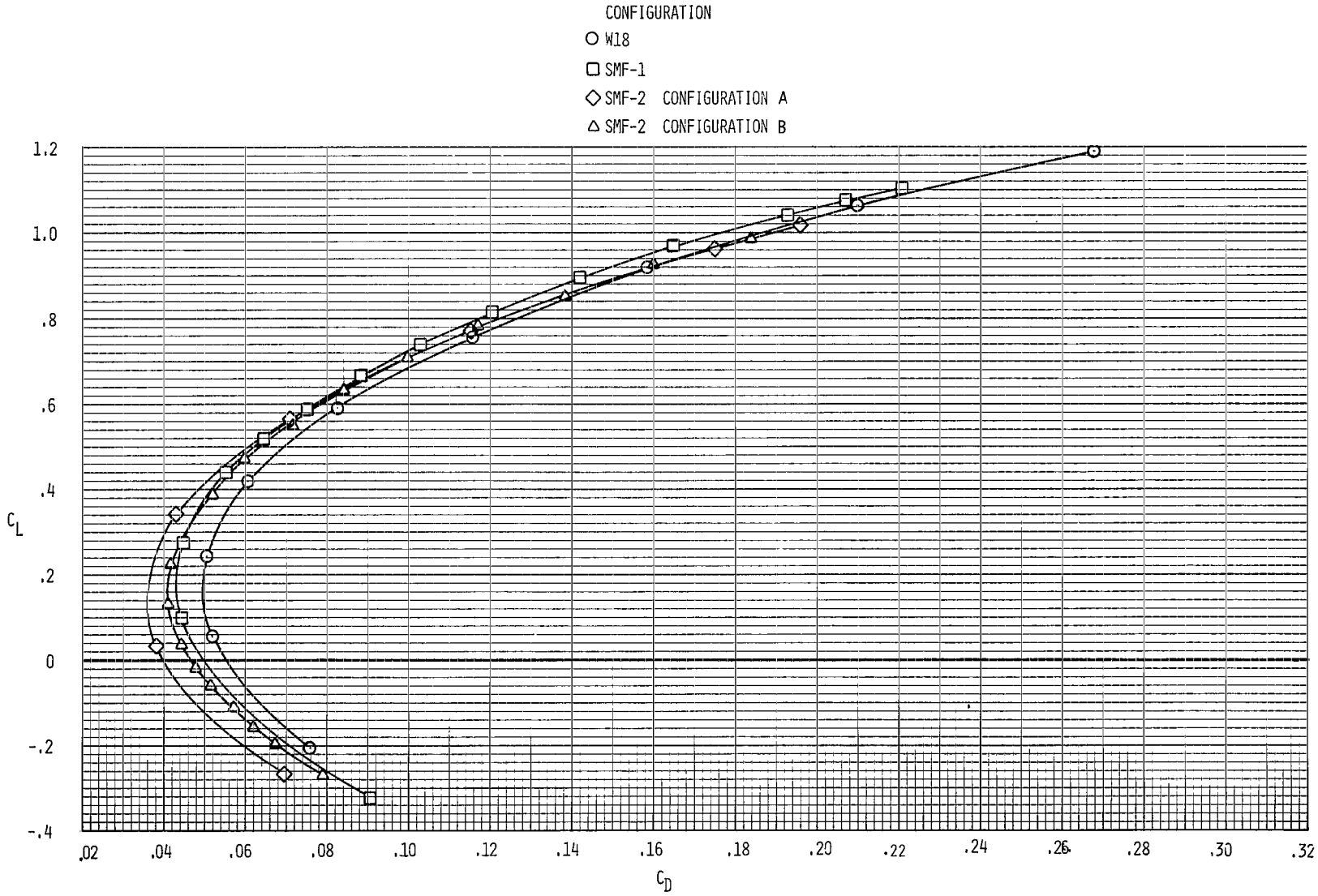

(d) M = 0.95.

Figure 13.- Concluded.

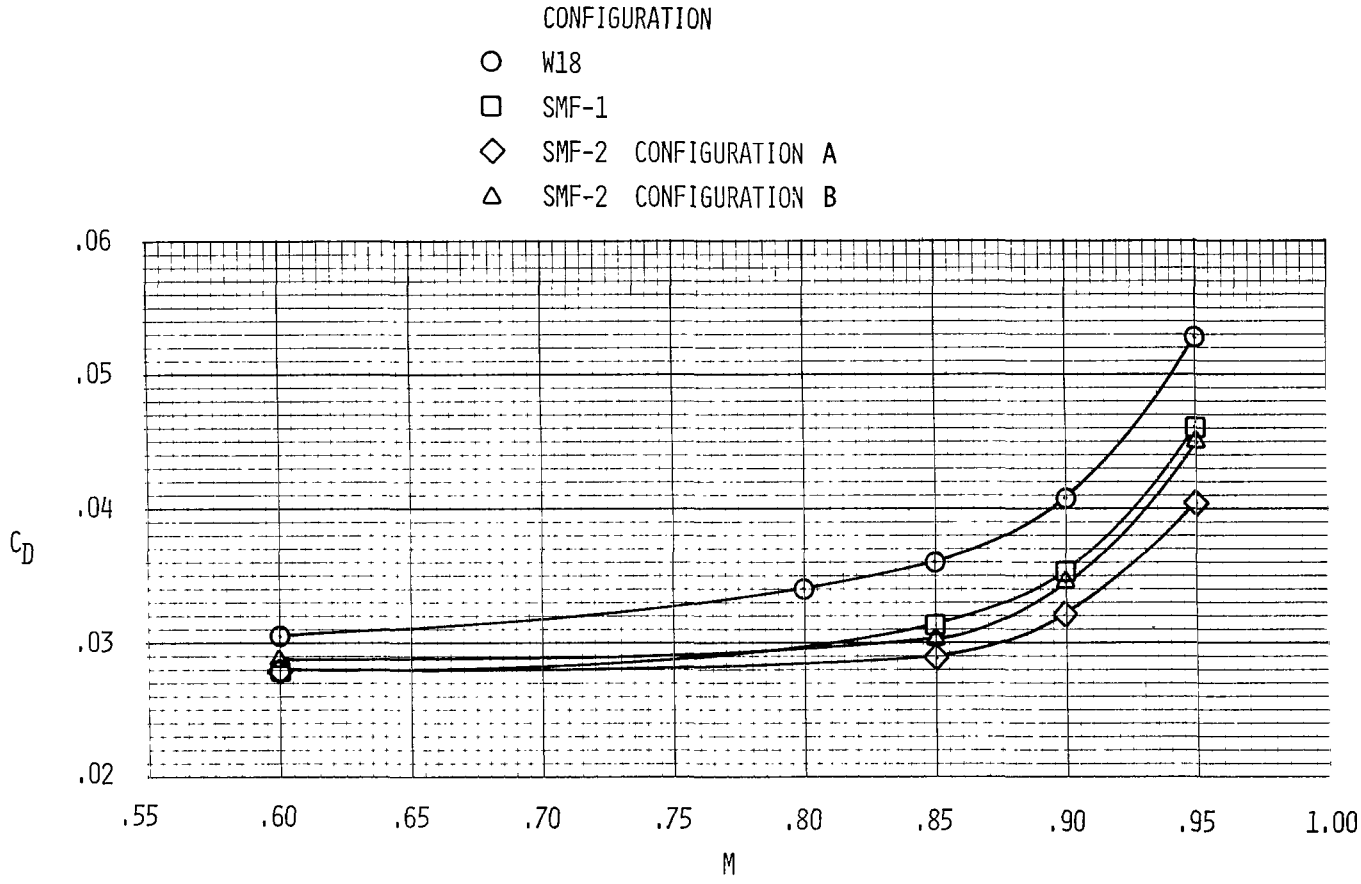

(a) $C_L = 0.30$.

Figure 14.- Effect of supercritical wing geometry on experimental drag variation with Mach number at fixed C_L.

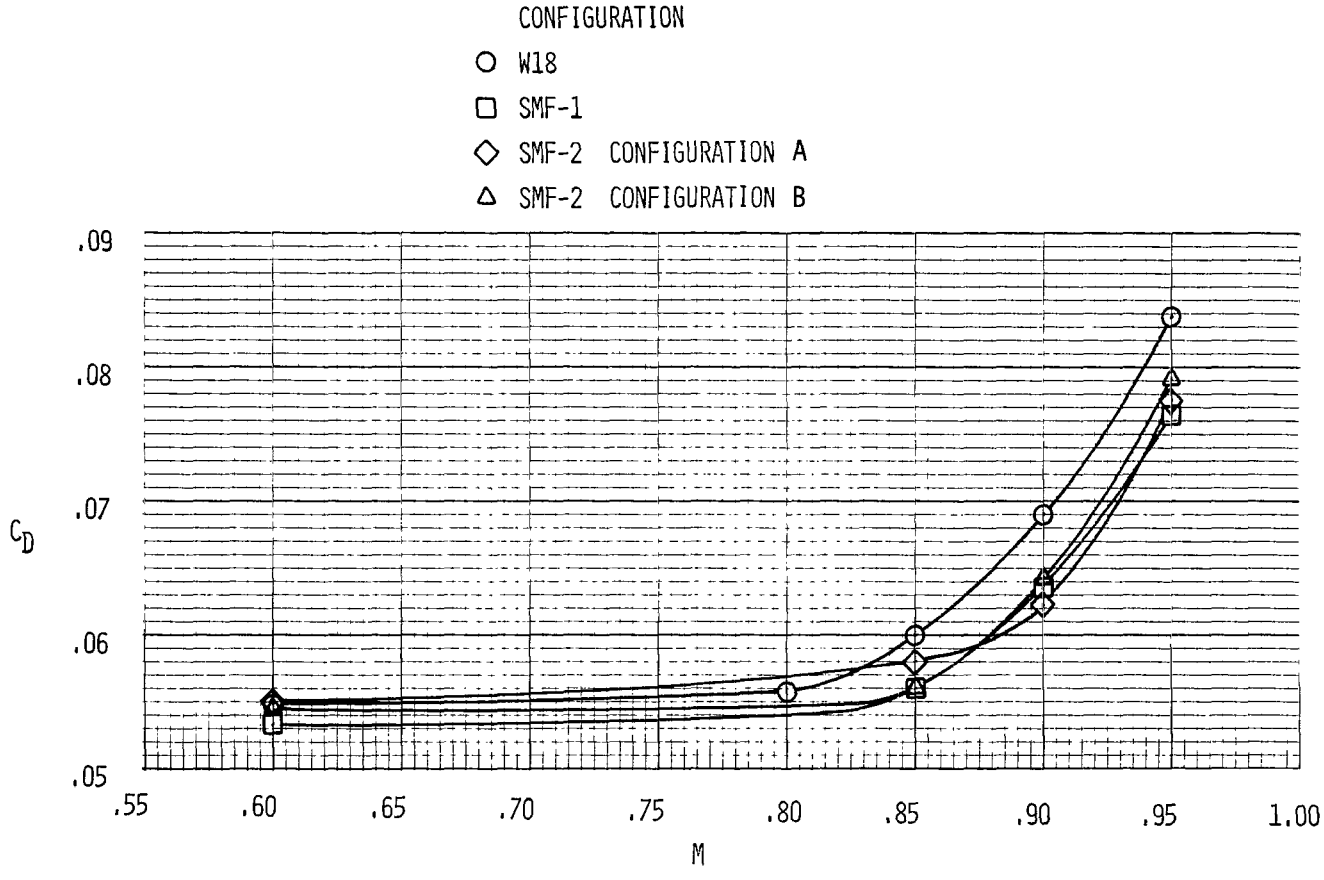

(b) C_L = 0.60.

Figure 14.- Continued.

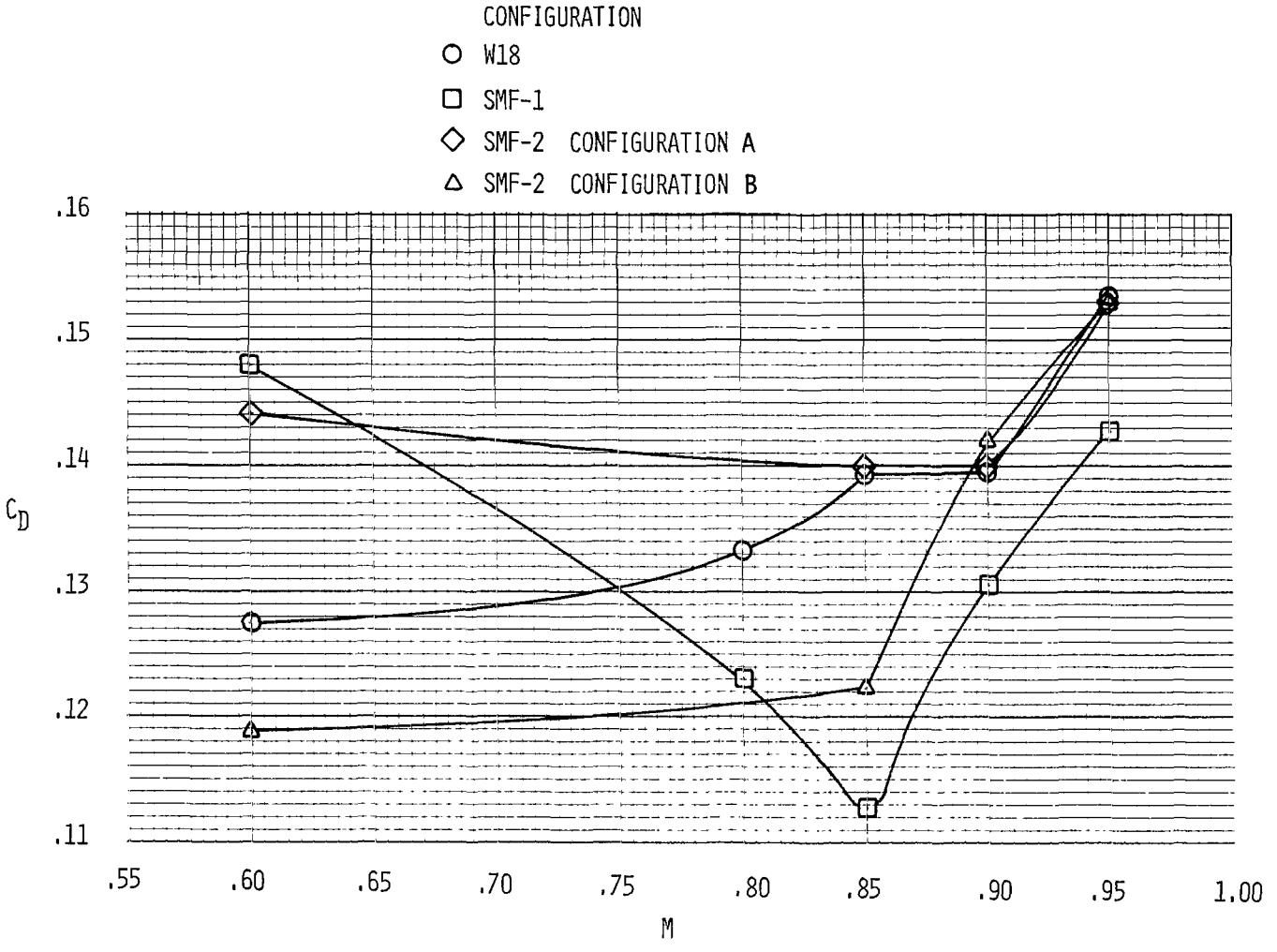

(c) $C_L = 0.90$.

Figure 14.- Continued.

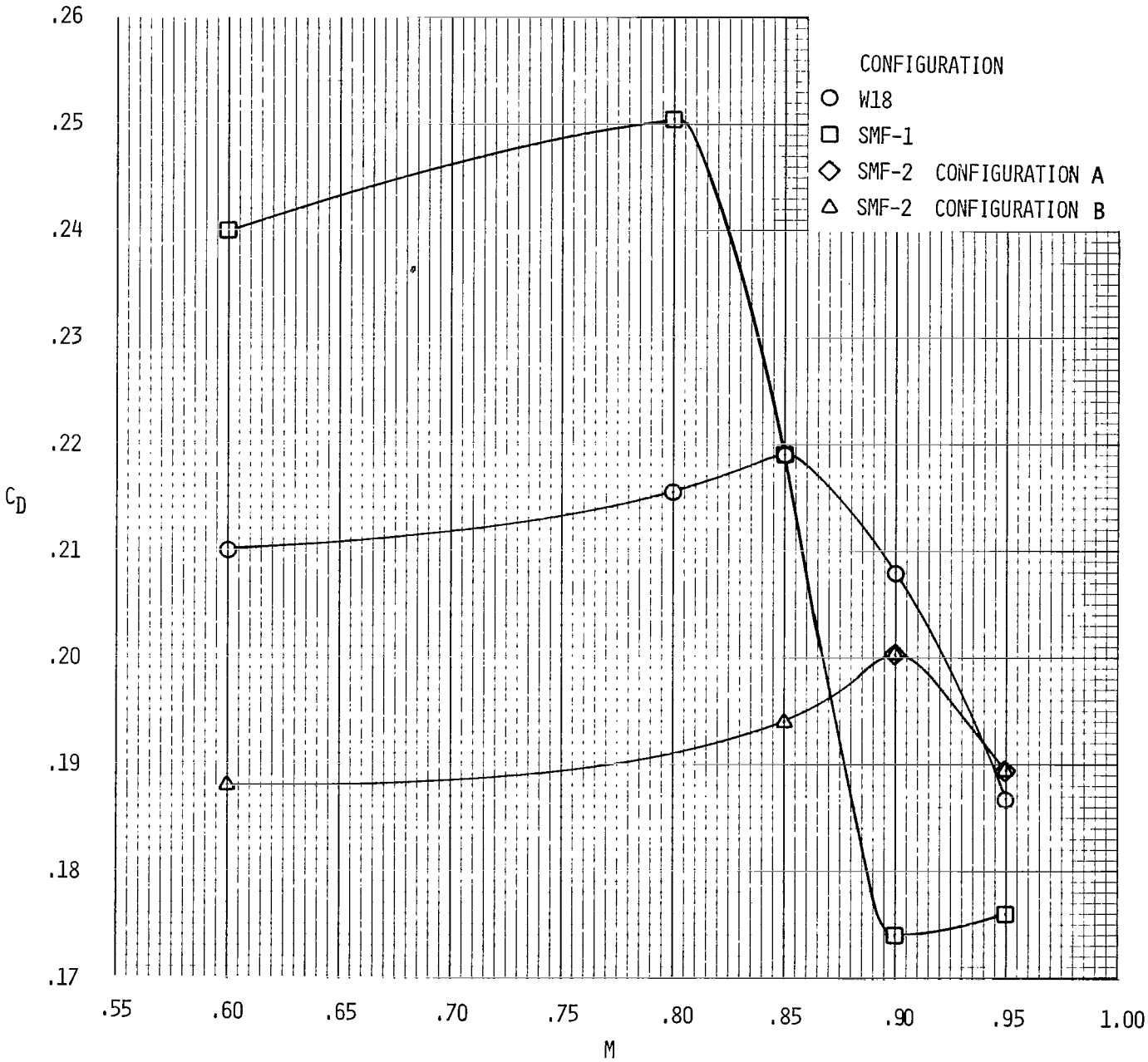

(d) $C_L = 1.00$.

Figure 14.- Concluded.

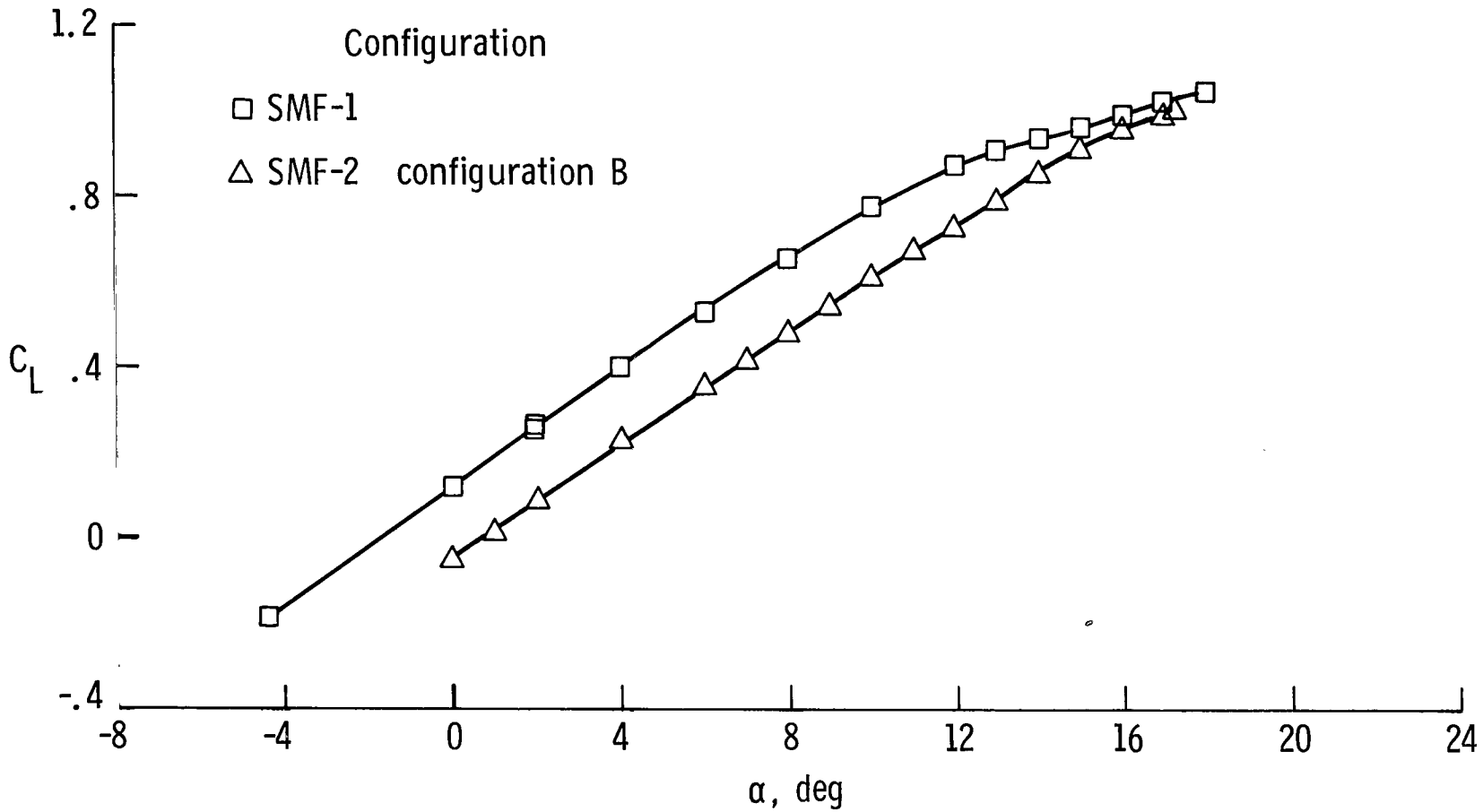

(a) M = 0.60.

Figure 15.- Experimental lift characteristics of SMF-1 and configuration B of SMF-2.

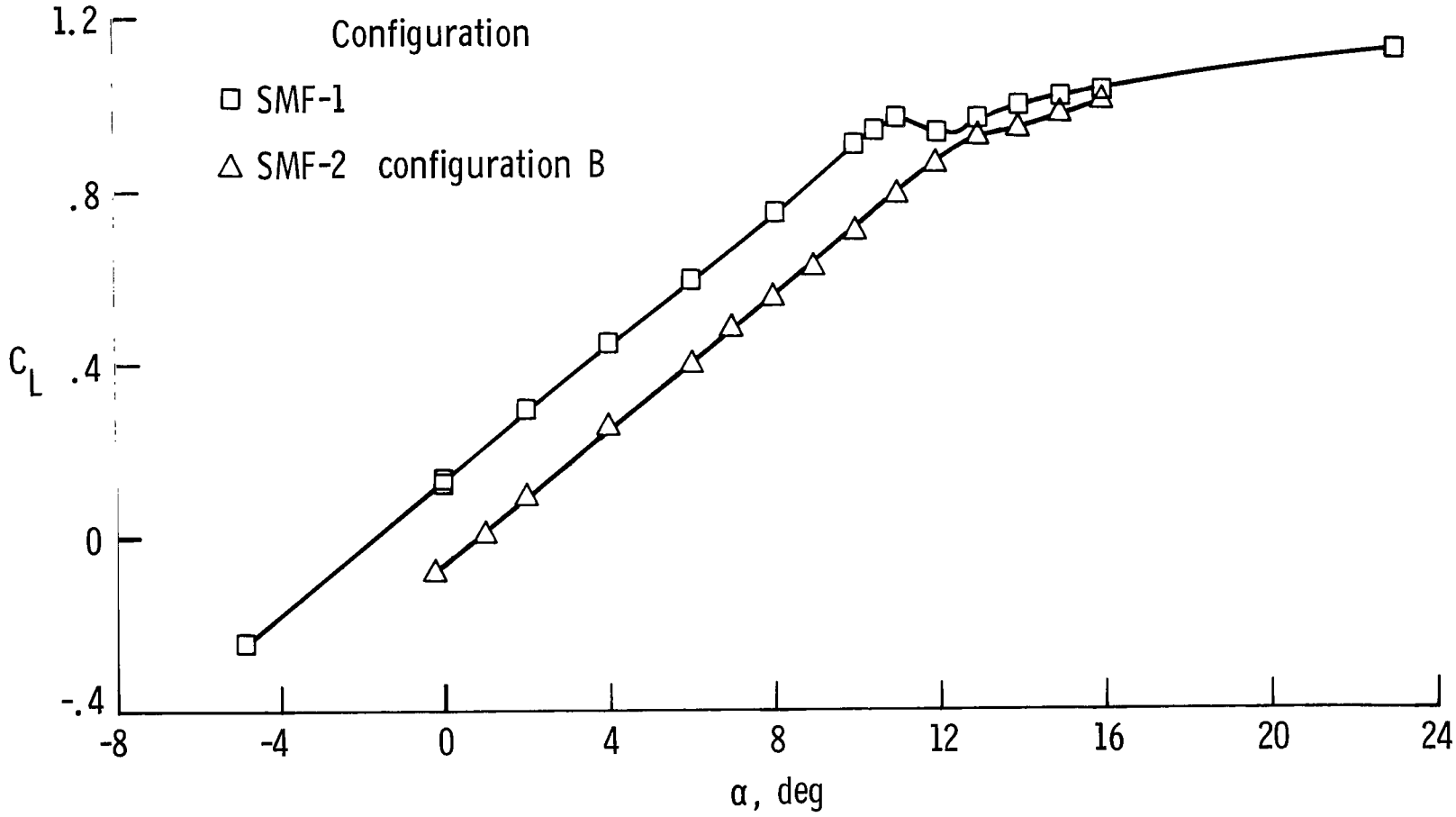

(b) M = 0.85.

Figure 15.- Continued.

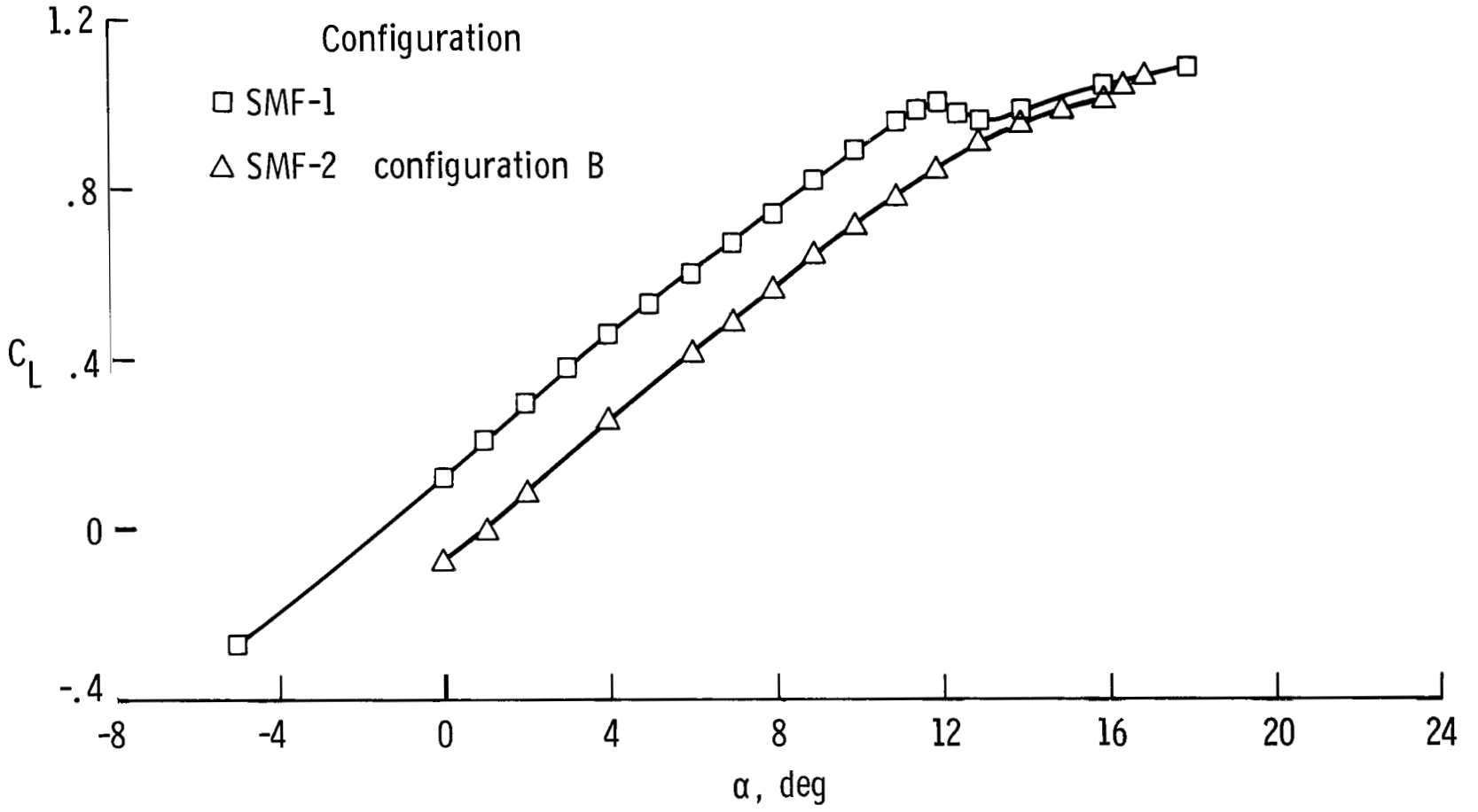

(c) M = 0.90.

Figure 15.- Continued.

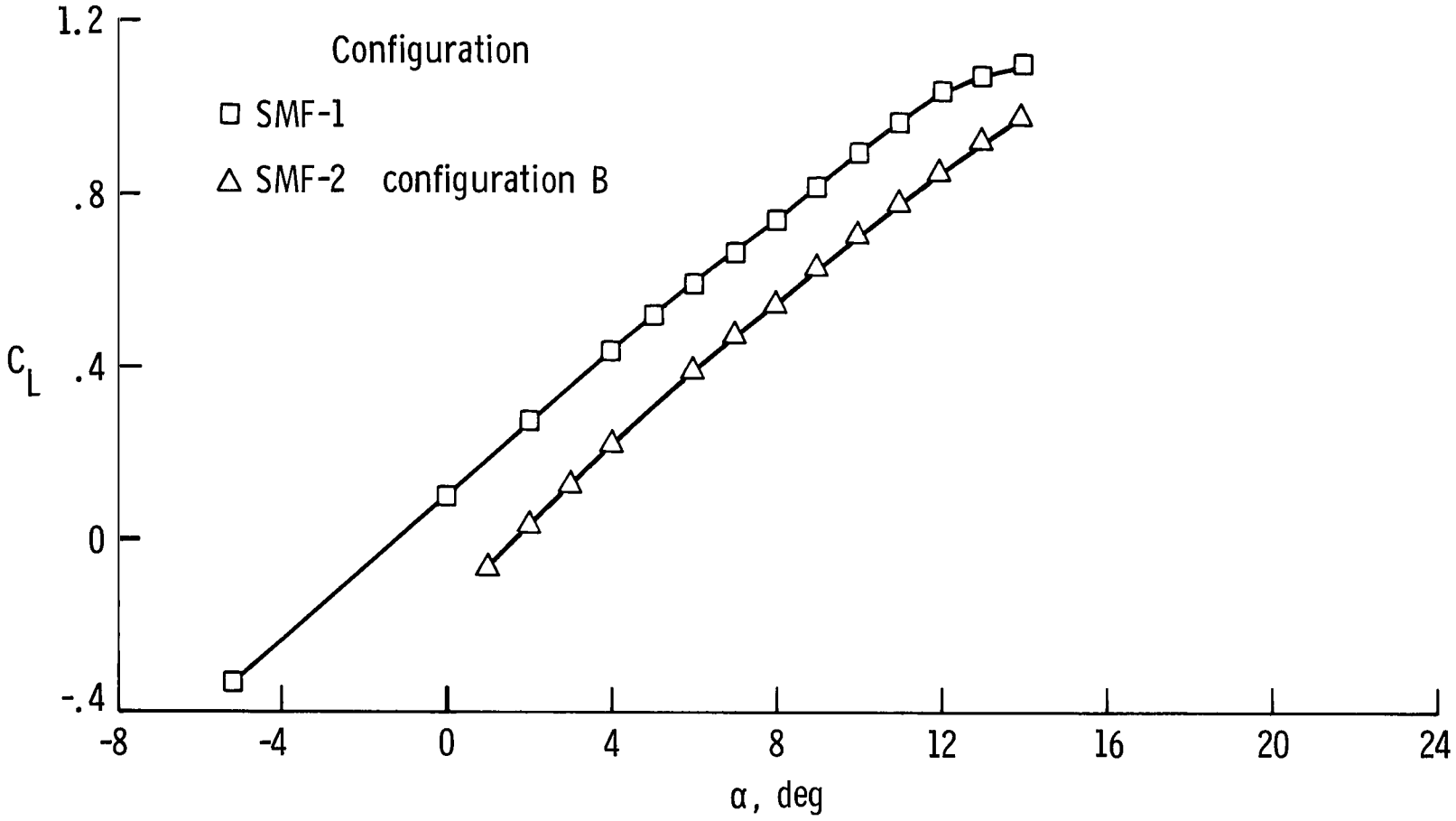

(d) M = 0.95.

Figure 15.- Concluded.

1. Report No.	2. Government Accession No.	3. Recipient's Catalog No.
NASA TP-2282		

4. Title and Subtitle	5. Report Date
AERODYNAMIC DESIGN FOR IMPROVED MANEUVERABILITY BY USE OF THREE-DIMENSIONAL TRANSONIC THEORY	February 1984
	6. Performing Organization Code: 505-43-23-06
7. Author(s): Michael J. Mann, Richard L. Campbell, and James C. Ferris	8. Performing Organization Report No.: L-15681
	10. Work Unit No.
9. Performing Organization Name and Address: NASA Langley Research Center, Hampton, VA 23665	11. Contract or Grant No.
	13. Type of Report and Period Covered: Technical Paper
12. Sponsoring Agency Name and Address: National Aeronautics and Space Administration, Washington, DC 20546	14. Sponsoring Agency Code

15. Supplementary Notes

16. Abstract

Improvements in transonic maneuver performance by the use of three-dimensional transonic theory and a transonic design procedure were examined in this study. The FLO-27 code of Jameson and Caughey was used to design a new wing for a fighter configuration with lower drag at transonic maneuver conditions. The wing airfoil sections were altered to reduce the upper-surface shock strength by means of a design procedure which is based on the iterative application of the FLO-27 code. The planform of the fighter configuration was fixed and had a leading-edge sweep of 45° and an aspect ratio of 3.28. Wind-tunnel tests were conducted on this configuration at Mach numbers from 0.60 to 0.95 and angles of attack from -2° to 17°. The transonic maneuver performance of this configuration was evaluated by comparison with a wing designed by empirical methods and a wing designed primarily by two-dimensional transonic theory. The configuration designed by the use of FLO-27 had the same or lower drag than the empirical wing and, for some conditions, lower drag than the two-dimensional design. For some maneuver conditions, the drag of the two-dimensional design was somewhat lower.

17. Key Words (Suggested by Author(s)): Transonic aerodynamics; Computational wing design; Fighter aircraft; Maneuvering aerodynamics; Transonic wing design; Maneuvering aircraft

18. Distribution Statement: Unclassified - Unlimited

Subject Category 02

19. Security Classif. (of this report)	20. Security Classif. (of this page)	21. No. of Pages	22. Price
Unclassified	Unclassified	70	A04

For sale by the National Technical Information Service, Springfield, Virginia 22161 NASA-Langley, 1984

National Aeronautics and
Space Administration

Washington, D.C.
20546

Official Business
Penalty for Private Use, $300

THIRD-CLASS BULK RATE

Postage and Fees Paid
National Aeronautics and
Space Administration
NASA-451

2 1 1U,A, 840216 S00903DS
DEPT OF THE AIR FORCE
AF WEAPONS LABORATORY
ATTN: TECHNICAL LIBRARY (SUL)
KIRTLAND AFB NM 87117

NASA

POSTMASTER: If Undeliverable (Section 158 Postal Manual) Do Not Return